Zwitterionic Polymer-based Platforms for Biotherapeutics and Implants

Caroline Tsao

A dissertation

submitted in partial fulfillment of the

requirements for the degree of

Doctor of Philosophy

University of Washington

2020

Reading Committee:

Shaoyi Jiang, Chair

Buddy D. Ratner

Elizabeth Nance

Program Authorized to Offer Degree:

Chemical Engineering

University of Washington

Abstract

Zwitterionic polymer-based platforms for Biotherapeutics and Implants

Caroline Tsao

Chair of the Supervisory Committee:
Professor Shaoyi Jiang
Chemical Engineering

Novel biotherapeutics and advanced implantable devices have greatly improved the quality of life for many patients. Biotherapeutics offer great advantages of high specificity towards difficult diseases, yet biotherapeutics are often physiochemically unstable and immunogenic; implantable devices with multiple functionalities create effective solutions to medical situations, yet they often suffer from reduced longevity due to the foreign body reaction triggered. Many biomaterials have been developed to tackle these issues. However, few biomaterials have been transferred from benchtop to clinical treatments, and biocompatibility issues of biomaterials have started to draw concerns. Thus, the development of new biomaterials is essential for the realization of contemporary medical treatments.

In this dissertation, we discuss the development of zwitterionic polymer-based platforms for peptide therapeutics, non-invasive drug delivery, and implants. We first investigate how

zwitterionic polymers would enhance the performance of peptides therapeutics. The native glucagon-like peptide-1 (GLP-1) no longer suffers from rapid renal clearance and degradation after the conjugation of a zwitterionic polymer and provides glycemic control in mice for up to 6 days, demonstrating its potential as a diabetes treatment. We next develop a non-invasive pulmonary systemic delivery platform for large protein drugs. The zwitterionic polymers significantly improved the bioavailability of organophosphate hydrolase (OPH) and the prevention of organophosphate poisoning through the non-invasive delivery of the conjugated OPH shows significant potential for protecting our warfighters in threat of nerve agents. In addition, we also design high-strength, pure zwitterionic-elastomeric-networked (ZEN) hydrogels through the mechanisms of swellability and the locking effect. The ZEN hydrogels can be considered highly biocompatible as no fibrotic capsule was formed after one year of implantation, which showed great potential for implantable devices.

In these studies, we explore and expand the capacity of using zwitterionic polymers for protein/peptide drug delivery and long-term implantation. The new findings could provide new solutions and advance the field of biotherapeutics development, non-invasive drug delivery system, and implantable devices.

TABLE OF CONTENTS

LIST OF FIGURES

LIST OF TABLES

ACKNOWLEDGEMENTS

For all the studies presented here, the author would like to thank her advisor, Dr. Shaoyi Jiang for support and inspiration. The author would like to next thank committee members, Dr. Buddy Ratner, Dr. Elizabeth Nance, and Dr. Marjorie Olmstead, for their support and insightful inputs. The author also would like to thank Dr. Peng Zhang, Dr. Hsiang-Chieh (Roger) Hung, Dr. Dianyu Dong, Dr. Zhefan Yuan, Kan Wu, and all the other members in Prof. Jiang's research group for their kind help and patience. The author would also like to thank all friends she met at the Husky Badminton Club. Lastly, the author would especially thank her family and Jason Hung for continuous support along this long journey.

DEDICATION

This dissertation is dedicated to Mom and Dad, whose passion for science is what inspired me.

Chapter 1. Introduction

Novel biological therapeutics and advanced implantable devices have greatly improved the quality of life for many patients. The development of new peptide- or protein-based biotherapies for various difficult-to-treat diseases is at a breakneck pace[1–4]. Designs of novel implantable devices with unprecedented functionalities create effective solutions to challenging medical situations[5–11]. Yet, biological therapeutics are often physiochemically unstable in complex environments and immunogenic[12–16], while implantable devices often suffer from reduced longevity due to the foreign body reaction triggered[17–20]. Biomaterials, defined as substances that are in contact with biological tissues, have demonstrated their unlimited potentials in enhancing and evolving ideas for various medical applications, such as drug delivery systems and regenerative medicine[21–26]. However, few biomaterials have been transferred from benchtop to clinical treatments, and biocompatibility issues of biomaterials have started to draw concerns[27–30]. Thus, the search and development of unique biomaterials that can tackle these issues are an ongoing quest for researchers to realize innovative healthcare solutions[31–33].

Since the discovery of insulin in 1922, it is now a required treatment for over 150 million patients worldwide[34]. Biological therapeutics, or biotherapeutics, have always been an enticing idea due to their specificity towards an explicit disease owing to their complex nature[35,36]. To this date, there are more than 240 biotherapeutics, including peptides, proteins, enzymes, monoclonal antibodies, and antibody-drug conjugates, that have been approved by the U.S. Food and Drug Administration (FDA)[37]. However, biotherapeutics generally suffer from three major issues: physiochemical instability in complex environments, suboptimal circulation half-life due to rapid renal clearance, and their inherent immunogenicity due to the foreignness to humans[38–41]. These

issues have radically limited their efficacy and possible delivery routes, and have caused concerns towards their safety of usage[42–44]. One of the most commonly used methods is through conjugating polyethylene glycol (PEG) to proteins, known as PEGylation[45–48]. This is thus far the most straight-forward tactic used to modify therapeutic proteins, as 15 PEGylated biotherapeutics that have been approved by the FDA to this date[48–52]. PEGylation provides biological products increased hydrodynamic volume to prevent renal clearance, improved stabilization in complex biological environments, and reduced immunogenicity due to "stealth" shielding. However, major issues with PEGylation have surfaced in recent years: the loss of activity and presences of anti-PEG antibodies. In the case of Pegasys® (pegylated interferon alfa-2a), its activity was greatly reduced from 100% to 7% after the conjugation of a single chain of PEG[53]. Anti-PEG antibodies were detected in patients administered with Krystexxa® (Pegloticase) and Oncaspar® (Pegaspargase). More than 40% of the patients receiving Pegloticase became responders after four months of treatments due to the generation of anti-PEG antibodies[54]; Around 20% of the patients developed anti-PEG antibodies just after a single injection of Pegaspargase[55]. The discovery of pre-existing anti-PEG antibody found in at least 25% of the population further brings concerns[56–59]. An RNA aptamer, pegnivacogin (RB006), terminated its clinical trial phase III early due to the unusually high percentage of patients experiencing severe allergic reactions after the first injection caused by anti-PEG antibody[60,61]. These results have demonstrated that the presence of anti-PEG antibodies in the bloodstreams could potentially trigger anaphylaxis and infusion reactions that are fatal. Therefore, an alternative to this 'gold standard' is urgently needed to supplement or replace the use of PEGylation.

The field of implantable devices, on the other hand, has a different set of challenges to tackle. Implantable devices, such as tissue adhesives[62–64], tissue engineering scaffolds[65–67], drug

delivery carriers[68–70], biosensors and electronic components[71–73], have offered new treatments and monitoring abilities. Hydrogels have long been attractive for many biomedical applications as they resemble the extracellular matrix (ECM) in biological tissues due to their high water content and diverse compositions and structures[74–76]. However, classic hydrogels are often weak which are mechanically unsuitable for some biomedical applications[77–79]. Furthermore, these hydrogel-based implantable devices often lose their functionality within the first couple of months as a result of eliciting the foreign body reaction towards the materials[18–20], demonstrating the lacking of biocompatibility. Thus, the development of both highly-biocompatible and tough hydrogels is critical for the biomedical field.

Poly(carboxybetaine) (pCB) is a class of zwitterionic polymers designed based on a natural osmolyte, glycine betaine[80]. With both the positively-charged and negatively-charged functional groups presented on the same monomer, zwitterionic polymers are net-neutral, but can achieve a strong, electrostatically induced-hydration around themselves[81–83]. Therefore, pCB polymers are considered to be super-hydrophilic. It has been previously demonstrated that pCB polymer-coatings resist non-specific protein adsorption from undiluted blood plasma and serum to an undetectable level (< 0.3 ng/cm^2)[84], demonstrating the expectational non-fouling properties of pCB polymers. The "water-loving" nature of pCB polymers brings potentials to biomedical applications such as biotherapeutics modifications and implants[85]. The conjugation of pCB polymers was first demonstrated to be able to facilitate the stabilization of chymotrypsin at high temperatures, and also maintain or even increase its enzymatic activity[86]. This study opened up various applications of pCB polymer-modified biotherapeutics. It was further revealed that pCB polymers can help eliminate protein immunogenicity and are low-immunogenic themselves[87–92]. Furthermore, pCB hydrogels were able to resist fibrotic capsule formation induced by the foreign body reaction when

implanted subcutaneously in mice for up to three months[93], again demonstrating the excellent biocompatibility of pCB polymers.

In this dissertation, novel platforms for drug delivery and implantable device utilizing zwitterionic pCB polymers are developed. In Chapter 2, we first investigate how pCB polymers would aid the efficacy of small peptides. Our previous studies have focused on large biotherapeutics, such as enzymes and cytokines, which have illustrated enhanced efficacy after the conjugation of pCB polymers. Small biotherapeutics, mainly peptides, suffer from rapid renal clearance due to their low molecular weights. Some peptides also suffer from fast enzymatic degradation once entered the bloodstream, such as the case for glucagon-like peptide-1 (GLP-1)[94]. While the conjugation of macromolecules, such as PEG, polysaccharides, and bovine serum albumin (BSA), has demonstrated to improve the circulation half-lives of the peptides, the activities of the peptides are often greatly sacrificed[95,96]. Thus, it remains an important goal to develop materials that can improve the pharmacokinetics of the peptide without reducing its activity. We set out to develop a long-lasting GLP-1 construct for the treatment of type 2 diabetes mellitus (T2DM) utilizing a pCB polymer. GLP-1 potentiates insulin secretion in a glucose-dependent fashion, which contributes to the reduced risk of hypoglycemia when compared with other glucose-lowering agents[97,98]. However, native GLP-1 is subjected to fast renal clearance due to its low molecular weight and is degraded rapidly by peptidase such as Dipeptidyl peptidase IV (DDP-IV)[94]. Therefore, limited studies have been done on studying the therapeutic effect of the native GLP-1 peptide due to its short half-life of 2 to 3 minutes. In this study, we conjugated a pCB polymer with a molecular weight of 66 kDa onto the native GLP-1 in order to prolong its circulation half-life and protect it from the degradation of enzymes without losing much its potency in mice.

In Chapter 3, we developed a non-invasive pulmonary systemic delivery platform for large biotherapeutics. Non-invasive systemic biological drug delivery *via* the pulmonary route has always been fantasized since the 1950s owing to the large surface area of the lung for absorption, high epithelial permeability, and a more favorable environment for biologicals[99]. However, large proteins (molecular weight > 40 kDa) having an average bioavailability of 1% to 5% *via* pulmonary route administration remains a primary constraint[100,101]. Organophosphorus hydrolase (OPH) is an enzymatic protein that has received much attention as an advanced prophylactic against organophosphate (OP) nerve agents or insecticides due to its catalytic activity and broad substrate specificity when compared to other OP bioscavengers[102–104]. Moreover, because of the unpredictable and urgent needs for the protection of warfighters at the frontline, bioscavengers delivery methods that are easy, quick, and efficacious are much desired. Moreover, OPH is a rather hydrophobic dimer protein that requires protection in physiological environments as it is unstable. Therefore, the goal of this study is to improve the bioavailability of pulmonary systemic delivery of large biotherapeutics utilizing pCB polymers and OPH as a model protein.

In addition to improving the pharmacokinetics and efficacy of biotherapeutics, we last explore the possibility of developing a high-strength, pure zwitterionic hydrogel for future implantable devices in Chapter 4. Using a class of the biomaterials, synthetic hydrogels, as implantable devices for tissue engineering or biosensors, have been an attractive idea[105–107]. However, unlike naturally-occurring ECM that can withstand large deformations, classic covalent single network hydrogels are generally considered weak and are not mechanically suitable for long term implantation[74–76]. Many efforts have been made to improve the mechanical properties of the hydrogels, including non-covalent bonds (e.g., hydrogen bonds[108], hydrophobic associations[109], and ionic interactions[110]) toughened hydrogels, hydrogels with highly stretchable networks[111], and

double-network hydrogels[77,78,112–114]. However, the biocompatibility of these biomaterials remains a major challenge. The majority of synthetic materials are unable to prevent the triggering of the foreign body reaction, resulting in the formation of fibrotic capsules within the first few months after its implantation in living tissues[115–117]. Zwitterionic hydrogels developed previously have demonstrated their high biocompatibility, yet the mechanical strengths of such are too weak for any implant applications[93,118,119]. While many studies have implemented zwitterionic materials into hydrogels to enhance the biocompatibility, the amphiphilic or hydrophobic constituents still are able to induce the foreign body reaction[120,121]. Herein, we aim to design a pure zwitterionic-elastomeric-networked (ZEN) hydrogel which has significantly improved mechanical properties without sacrificing its excellent biocompatibility.

To summarize, the goal of this dissertation is to (1) investigate the conjugation of zwitterionic pCB polymer to the GLP-1 peptide as potential T2DM treatment., (2) design non-invasive pulmonary systemic drug delivery for large biotherapeutics utilizing zwitterionic pCB polymers, and (3) develop pure, high-strength, and highly biocompatible zwitterionic-elastomeric-networked hydrogel. The new findings from these studies could advance the field of biotherapeutics development, non-invasive drug delivery system, and implantable devices, which have the potential to realize healthcare solutions and further improve our quality of life.

Chapter 2. Zwitterionic Polymer Conjugated Glucagon-Like Peptide-1 For Prolonged Glycemic Control

Glucagon-like peptide-1 (GLP-1) is of particular interest for treating type 2 diabetes mellitus (T2DM) as it induces insulin secretion in a glucose-dependent fashion and has the potential to facilitate weight control. However, native GLP-1 is a short incretin peptide that is susceptible to fast proteolytic inactivation and rapid clearance from the circulation. Various GLP-1 analogs and bioconjugation of GLP-1 analogs have been developed to counter these issues, but these modifications are frequently accompanied by the sacrifice of potency and the induction of immunogenicity. Here, we demonstrated that with the conjugation of a zwitterionic polymer, poly(carboxybetaine) (pCB), the pharmacokinetic properties of native GLP-1 were greatly enhanced without serious negative effects on its potency and secondary structure. The pCB conjugated GLP-1 further provided glycemic control for up to 6 days in a mouse study. These results illustrate that the conjugation of pCB could realize the potential of using native GLP-1 for prolonged glycemic control in treating T2DM.

2.1 INTRODUCTION

Type 2 diabetes mellitus (T2DM) is a long-term progressive metabolic disease characterized by high blood glucose (hyperglycemia) due to the dysfunction of pancreatic β-cells and insulin resistance[122,123]. The incidence of diabetes is expected to increase as it has affected 463 million people worldwide in 2019, in which T2DM is accounting for ~90% of all cases. The number of people affected by diabetes is expected to reach 700 million by 2045, estimated by the International Diabetes Federation[124]. Native glucagon-like peptide-1 (GLP-1(7-36), abbreviated to

GLP-1) is an incretin peptide secreted from intestinal L-cells in response to meal intake, in order to induce insulin secretion from pancreatic β-cells and suppress glucagon release in a glucose-dependent fashion[97,98,125]. While overweight and obesity are now considered as the major risk factor of noninsulin-dependent diabetes mellitus, continuous subcutaneous infusion of GLP-1 has resulted in a sustained weight loss over a period of at least six weeks in a human study[126]. Therefore, GLP-1 shows great potential use in the treatment of T2DM and obesity. However, native GLP-1 has its limitation for clinical use due to the rapid proteolytic inactivation and degradation by dipeptidyl peptidase IV (DPP-IV) enzyme[127–129]. The peptide bond in Ala^8-Glu^9 is cleaved by DDP-IV which results in a metabolite of GLP-1(9-36) that has a 100-fold lower binding affinity compared to the native intact peptide[130,131]. To overcome this shortcoming, two possible approaches have been considered: (1) utilize natural analogs or synthetic analogs by modifying the residues vulnerable to DPP-IV, and (2) "shield" the native peptide with synthetic materials to protect it from proteolytic inactivation.

A number of GLP-1 analogs, mainly GLP-1 receptor agonists (GLP-1 RAs), have been developed based on the first approach, including exenatide, a lizard-derived analog; tapsoglutide, an analog with α-aminoisobutyric acid (Aib) substitutions; and liraglutide, an acylated derivative[132–134]. Unfortunately, these GLP-1 analogs have raised undesired immune responses: anti-drug antibodies (ADA) towards GLP-1 RAs due to the foreignness introduced upon residue modifications. The incidences of antibody formation in clinical were 45.4% of the patients treated with exenatide, 49% with tapsoglutide, 69.8% with lixisenatide, and 8.6% with liraglutide[135–137]. The generation of ADA could lead to a compromise of therapeutic efficacy of GLP-1 RAs and an increase in hypersensitivity reactions after administration[13,138,139]. Thus, the delivery of native GLP-1 for treating T2DM is still an attractive idea as there is low risk of ADA generation, which

is desirable for long-term treatments. On the other hand, limited studies have been done using the second approach to prevent rapid proteolytic inactivation. Therefore, we aim to further explore the possibility of using synthetic materials to improve the therapeutic effects of native GLP-1 in this study.

One common problem that GLP-1 and GLP-1 analogs face is the short circulation half-life from rapid renal clearance due to their low molecular weights. The conjugation of natural or synthetic materials has shown to improve the pharmacokinetic (PK) properties of GLP-1 analogs. Conjugation of different lengths of poly(ethylene glycol) (PEG) or polysaccharides have increased the half-life from 1.5 ~ 5 minutes to 12.1 ~ 30.3 hours when injected subcutaneously in rodents[140,141]; integration of human serum albumin or fragment crystallizable region (Fc) has also increased the half-life to 8.5 ~ 38.2 hours in rodents[142–144]. Yet, the addition of materials could sacrifice the activities of the GLP-1 and GLP-1 analogs. The conjugation of polymers (such as PEG) or human serum albumin has been reported to dramatically reduce the potencies of GLP-1 analogs due to unwanted interactions between the bulk conjugate and the peptide, and steric hindrances of the bulk conjugate[140–142,145]. Furthermore, some synthetic materials, such as PEG, have been demonstrated to be immunogenic and vulnerable to pre-existing anti-PEG antibodies[56,146]. Therefore, it is ideal to use synthetic alternatives that would not affect peptide activity and are low immunogenic for peptide conjugation.

Zwitterionic polymer poly(carboxybetaine) (pCB) has been demonstrated to be efficacious in protecting biologics from undesired interactions in the biological environment and in improving the PK properties of the biologics[87,88,147]. Due to their super-hydrophilic nature, the conjugation of pCB polymers has demonstrated to retain protein stability and bioactivity[86,90,148]. Moreover, studies have shown that pCB polymers induce little to no anti-pCB antibodies even when

conjugated to highly immunogenic proteins[87–89,91]. In this study, we develop a bioconjugate of native GLP-1 with a super-hydrophilic zwitterionic polymer pCB. We first investigate the secondary structure and activity of the native GLP-1 after the conjugation of pCB. The PK properties of the bioconjugate, and its ability to provide glycemic control are next evaluated. We aim to demonstrate the potential of using pCB-conjugated native GLP-1 for prolonged glycemic control (**Figure 2.1**).

2.2 Materials and Methods

2.2.1 *Materials*

Glucagon Like Peptide-1 (GLP-SH, HGEGTFTSDVSSYLEGQAAKEFIAWLVKGR-SH) was purchased from GenScript (Piscataway, USA). Poly(carboxybetaine) (pCB) was synthesized as reported previously[92]. In brief, 3-acrylamido-N-(2-(tert-butoxy)-2-oxoethyl)-N,N-dimethylpropan-1-aminium (t-Butyl CBAAm) and chain transfer agent (CTA) were synthesized. pCB polymer was next prepared by a combination of reversible addition fragmentation chain transfer (RAFT) polymerization, aminolysis, acid deprotection and amine-to-thiol conversion steps utilizing the t-Butyl CBAAm and CTA prepared earlier. N-β-maleimidopropyl-oxysuccinimide ester (BMPS) was from TCI American. Amicon Ultra centrifugal filter units were purchased from EMD Millipore (Billerica, MA). Pierce 660 nm Protein Assay was purchased from Thermo Fisher Scientific (Waltham, MA). Fetal bovine serum (FBS), Gibco RPMI 1640 (ATCC modification) medium, and RPMI 1640 medium (none ATCC modification) were all purchased from Thermo Fisher Scientific (Waltham, MA). RIN-m5F cells were purchased from ATCC (Manassas, VA). Alexa Fluor™ 555 NHS Ester (Succinimidyl Ester) was purchased from Thermo Fisher Scientific (Waltham, MA).

2.2.2 *Preparation of pCB-Conjugated GLP-1 (GLP1-pCB)*

pCB (72 mg) were first dissolved in phosphate-buffered saline (PBS) pH 7.6 at 36 mg/mL, slowly mixed with 7.23 μM BMPS/DMSO (100 μL of 20 mg/mL), and reacted for 40 minutes at room temperature. The reaction mixture was then purified through centrifugal filters with a molecular cut-off at 10 kDa through multiple washes using PBS pH 7.35. GLP-1 (5 mg) were first dissolved in deionized water at 12.5 mg/mL (400 μL). The GLP-1 solution was then mixed with maleimide-modified pCB at 1.725 mg/mL (400 μL + 2500 μL) in PBS pH 7.35 by slowly dripping droplets while stirring, and reacted for 2 hours at room temperature. Reaction mixture was then transferred to 4 ^{o}C fridge and reacted overnight. Reaction mixture was then purified and collected through the ENrich Size Exclusion Chromatography 650 column (10 mm x 300 mm,) using NGC 10 Quest Chromatography System (Bio-rad). The concentration of GLP1-pCB was determined through Pierce 660 nm Protein Assay. Products from each step of the conjugation procedure were determined using ^{1}H-NMR (300.10 MHz, D_2O) and the Agilent Technologies 1260 Infinity binary high performance liquid chromatography (HPLC) system with Waters Ultrahydrogel 1000 column (7.8 mm x 300 mm).

2.2.3 *Structural Analysis of GLP1-pCB*

The GLP1-pCB and GLP-1 were characterized by circular dichroism. A Jasco J-720 spectropolarimeter was used to measure the far-UV spectra of the proteins diluted to a concentration range of 20 - 200 μM in 20 mM sodium phosphate buffer, pH 7. The mean residue ellipticity was measured from 190 - 250 nm in a 0.1 cm path length quartz cuvette at 25 °C. All spectra were accumulated with standard sensitivity.

2.2.4 *In vitro Insulinotropic Activity Assay*

The insulinotropic activity of GLP-1 and GLP1-pCB were evaluated by static incubation of RIN-m5F cells. Cells were seeded in 10% FBS/Gibco RPMI 1640 (ATCC modification) medium in Corning Costar Flat Bottom cell culture plate, 96 well at a density of 1.5×10^5 cells/well, and grown overnight at 37 °C, under 5% CO_2. Acute tests for insulin release upon contact with samples were preceded by 2-hour pre-incubation at 37 °C, under 5% CO_2 in glucose-free/serum-free RPMI 1640 medium (none ATCC modification). Test incubation was performed in the presence of 2 mM glucose (Thermo Fisher Scientific) and samples in serum-free RPMI 1640 medium at the final concentration from 10^{-12} to 10^{-6} M. After 30 minutes of incubation, the supernatant of each well was collected and centrifuged at 1,000 × g for 5 minutes at 10 °C. The insulin content was analyzed forthwith by using rat insulin ELISA kit (Thermo Fisher Scientific). Concentration–response curves were analyzed by using a non-linear curve fitting computer program (GraphPad Prism, San Diego, CA, USA), which yielded EC_{50} (concentration producing half-maximal response) and E_{max} (maximal effect) values.

2.2.5 *Pharmacokinetic Studies*

All animal experiments in this study adhered to federal guidelines and were approved by the University of Washington Institutional Animal Care and Use Committee. GLP1-pCB was first tagged with Alexa Fluor™ 555 with NHS ester. GLP1-pCB was dissolved in 1 mL of PBS pH 7.6 at 2 mg/mL, Alexa Fluor™ 555 was dissolved in 100 μL DMSO at 20 mg/mL. The Alexa Fluor™ 555/DMSO mixture was then slowly mixed with the GLP1-pCB solution by dripping droplets while stirring, reacted for 2 hours at room temperature. Reaction mixture was then transferred to 4 °C fridge and reacted overnight. Reaction mixture was then purified and collected through

multiple buffer exchanges (PBS pH 7.4) using 30 kDa MWCO Amicon Ultra centrifugal filter units.

Male C57BL/6 mice (5 – 8 weeks old, n = 12) received subcutaneous injections of 1 mg/kg Alexa Fluor™ 555-labeled GLP1-pCB conjugate at time 0 h. Blood samples were collected from tail vein at 6, 30, 54, 78, 102, 126, 150 h post-administration. Serum samples were prepared from the blood samples by centrifuging at 11,000 rmp for 10 minutes. The concentrations of GLP1-pCB were determined by the fluorescence intensity (excitation at 552 nm, emission at 576 nm) measured with a microplate reader (BioTek, Cytation 5). Pharmacokinetic parameters were determined through PKSolver[149].

2.2.6 *Pharmacodynamic Studies with Intraperitoneal Glucose-Tolerance Test*

Male C57BL/6 mice (5 – 8 weeks old, n = 144) received subcutaneous injections of pharmaceutical grade saline, 1 mg/kg of GLP-1, or 1 mg/kg of GLP1-pCB conjugate at time 0 h. At different time points, including 6, 30, 54, 78, 102,126, and 150 h, 6 animals were challenged with IPGTT. Each animal has only been challenged once throughout the whole experiment. For each IPGTT challenge, animals were first fast for 6 hours. After the fast, they were given an intraperitoneal injection of sterilized pharmaceutical grade glucose at 2 g/kg. Blood glucose levels were measured at time 0, 20, 40, 60, 80, 100, and 120 min after the glucose challenge with a self-monitoring blood glucose meter (Advocate, Redi-Code^{+}, 2 – 5 μL of blood samples). The blood glucose levels were plotted over time, and the $AUC_{0\text{-}120}$ was obtained using GraphPad Prism7. No animals were excluded due to complications.

2.2.7 *Statistical Analysis*

Results are reported as mean ± SD. Two-tailed Student's *t*-test was used to compare two small sets of quantitative data.

2.3 Results and Discussion

2.3.1 *Conjugation of pCB polymer onto GLP-1*

The structure-activity relationship of GLP-1 has been well investigated and several amino acid residues on the N-terminus have been identified to be critical for receptor binding and activation[150]. Previous studies on the site-specific conjugation of PEG onto GLP-1 have demonstrated that the N-terminus of GLP-1 is essential for receptor activation[140]. Though the conjugation of PEG close to the N-terminus can mitigate the proteolytic inactivation of GLP-1 by DDP-IV, the potency of GLP-1 was greatly reduced[140,145]. Hence, in this study, a zwitterionic polymer pCB was conjugated *via* thiol-maleimide "click chemistry" to the C-terminus of GLP-1 modified with a cysteine residue to ensure a site-specific conjugation (**Figure 2.2A**). Considering that the renal filtration cutoff size for globular proteins is 50–70 kDa[151,152], we synthesized a 66 kDa pCB polymer for the conjugation. We hypothesized that the increased hydrodynamic volume from the conjugation of 66 kDa pCB could prevent the filtration of GLP-1 in the kidney. A two-step conjugation process was performed and the success of each step was evaluated through nuclear magnetic resonance spectroscopy (^{1}H-NMR). During the first step of adding the N-β-maleimidopropyl-oxysuccinimide ester linker (BMPS) onto pCB, the spectrum of the product (labeled as pCB-maleimide) would show the peak specific for maleimide. After the conjugation of GLP-1, the peak for maleimide was no longer present, indicating the success of the process (**Figure 2.2B**). The final product of conjugating pCB onto GLP-1 was further evaluated through gel

permeation chromatography (GPC). The left shift of the peak compared to pCB alone indicated the success of producing pCB-conjugated GLP-1 (denoted as GLP1-pCB) (**Figure 2.2C**). Additionally, GLP-1 was poorly dissolved in phosphate-buffered saline before the conjugation of pCB; GLP1-pCB experienced no issues dissolving back into any water-based solution.

2.3.2 *Secondary Structure Analysis*

When attaching a high-molecular-weight polymer onto a fairly small peptide, it is of particular concern whether the secondary structure of the peptide would be affected, which can affect the activity of the peptide. Although PEG has been considered to be inert and is widely used in many different biotherapeutics applications, recent studies have revealed that PEG interacts with peptides or proteins which could cause the loss in activity or stability[153,154]. It is important to identify polymeric materials that would not interfere with the structure of the peptide. We evaluated the secondary structures of GLP-1 and GLP1-pCB using circular dichroism spectroscopy (**Figure 2.3A**). GLP-1 is a peptide consisted of two α-helix structures[130], GLP1-pCB showed no significant differences in structure compared to GLP-1, while pCB showed no structure at all. This result has further suggested that pCB can be considered a good candidate for peptide conjugation due to the minimum interferences of the peptide from the polymer.

2.3.3 *Potency and Efficacy Analysis through In vitro Insulinotropic Activity Assay*

We next investigated the activity GLP1-pCB through *in vitro* insulin secretion assay as GLP-1 augments insulin release with a glucose-dependent manner. The activity of GLP1-pCB was evaluated through analyzing its potency and efficacy. Potency denotes the amount of GLP-1 or GLP1-pCB needed to produce a half-maximal response (EC_{50}), which is inversely proportional to the binding affinity of the peptide to its receptor; while the relative efficacy (E_{max}) is the maximal

insulin release that GLP1-pCB produces compared to GLP-1 irrespective of concentration, and is related to the activation of receptors[155]. Rat pancreatic/islet RIN-m5F cells were incubated with different concentrations of GLP1-pCB or GLP-1 with the presence of glucose to determine the concentration of a peptide that gives the EC_{50}. GLP-1 showed an EC_{50} value of 1.08 nM, consistent with what was previously reported[130,141,145,150], whereas GLP1-pCB showed an EC_{50} value of 7.24 nM (**Figure 2.3B** and **Table 2.1**). The decrease in the potency of the GLP1-pCB was expected, as large 66 kDa pCB inevitably brings some steric hindrance. In comparison, the site-specific mono-PEGylated GLP-1 with a similar molecular weight of 50 kDa only remained an EC_{50} of 1870 nM, corresponding to 0.03% of the unconjugated peptide[140]. Similarly, when GLP-1 was conjugated to a human serum albumin (66 kDa) through a short PEG linker, the potency of GLP-1 was reduced by 3–4 orders of magnitude[142]. Even though there was a decrease in potency, E_{max} of GLP1-pCB was 98.8% with respective to GLP-1 set as 100%, suggesting the conjugation of pCB would not affect the activation of GLP-1 receptors, but only the binding affinity. We hypothesize that pCB draws water away from the relatively hydrophobic peptide, allowing the peptide and the receptor to interact by shifting the equilibrium, which maintains the potency and efficacy of GLP-1. Furthermore, as suggested before, it is hypothesized that the minimized nonspecific interactions between pCB and the GLP-1 receptor due to the super-hydrophilic nature of the zwitterionic polymer can further facilitate the interaction between the peptide and its receptors[90].

2.3.4 *Pharmacokinetic Profile*

The short circulation half-life of GLP-1 and GLP-1 analogs due to their small sizes is one major challenge for clinical use. The conjugation of natural or synthetic materials has improved the PK profiles of GLP-1. PEG polymers with different lengths or polysaccharides have increased the half-life of GLP-1 analogs to 12.1 ~ 30.3 hours from 1.5 ~ 5 minutes with a single subcutaneous

injection[140,141]; the integration of human serum albumin or Fc has also increased the half-life to 8.5 ~ 38.2 hours in rodents[142–144,156]. With pCB having a molecular weight similar to that of human serum albumin, we next investigated the PK properties of GLP1-pCB. Fluorescent-labeled GLP1-pCB was given subcutaneously with a dosage of 300 nmol/kg (equivalent to 1 mg/kg of GLP-1). Concentrations of GLP1-pCB is expressed as the amount of fluorescent-labeled GLP-1 detected in the serum. Concentrations of GLP1-pCB at different time points were fitted into a two-compartment model to analyze the PK profile (**Figure 2.4** and **Table 2.2**). GLP1-pCB had a much longer circulation half-life ($T_{1/2\beta}$ = 43.0 h) than that of GLP-1, and with a maximum serum concentration observed (C_{max}) of 1427.1 ng/mL at T_{max} = 13.4 h (time of maximum concentration observed). The $T_{1/2\beta}$ was comparable to other modifications of GLP-1 reported previously ($T_{1/2\beta}$ = 12.1 ~ 38.2 h), while C_{max} was slightly better than other modifications of GLP-1 reported previously (C_{max} = 684 ~ 1022 ng/mL)[140,141]. These results indicated that more GLP1-pCB was able to enter the systemic blood stream and maintain a prolonged circulation profile. It has been reported that protein therapeutics and nanoparticles with a molecular weight more than 16 kDa administered subcutaneously exhibit limited direct transportation into the blood capillaries upon administration and enter the systemic circulation *via* an indirect route, through the lymphatic absorption[157–159]. It is therefore suggested that the conjugation of pCB could effectively facilitate GLP-1 entering the systemic circulation by protecting GLP-1 from degradation and clearance when passing through the lymphatic system. This could possibly due to the prevention of non-specific interaction with the environment owing to the superhydrophilicity of pCB.

2.3.5 *Pharmacodynamic Profile through Intraperitoneal Glucose-Tolerance Test*

As GLP1-pCB showed good activity *in vitro* and improved circulation half-life *in vivo*, we last evaluated its pharmacodynamic (PD) profile through the intraperitoneal glucose-tolerance test

(IPGTT) (**Figure 2.5**). C57BL/6 mice were subcutaneously injected with a single dose of 300 nmol/kg (equivalent to 1 mg/kg of GLP-1) of GLP-1, GLP1-pCB, or saline (negative control) at time 0. IPGTTs were performed once on each mouse at different time points: 6, 30, 54, 78, 102, 126, and 150 hours after sample injection. Mice were fasted for 6 hours before the IPGTT, when the mice were challenged with an intraperitoneal injection of glucose at 2 g/kg. Blood glucose levels were monitored for 120 minutes after glucose challenge (**Figure 2.5A**). For the group of mice that only received saline as the control, there was an elevation of blood glucose level to ~350 mg/dL, 20 minutes after the challenge. The glucose level eventually returned to baseline after two hours. The group that received a single dose of GLP-1was able to keep the glucose level close to baseline on the same day challenge, but failed to maintain the glucose level during the second IPGTT challenge (at the 30-hour time point). GLP1-pCB, on the other hand, was able to keep blood glucose level below 300 mg/dL when challenged up to 126 hours after a single injection (**Figure 2.5B** to **H**). The loss of activity after 150 hours could due to the low concentration of GLP1-pCB remained in the blood stream. The area under the curve ($AUC_{0\text{-}120}$) further illustrated the differences of the accumulative blood glucose level for up to 7 days (**Figure 2.5I**). These results showed the GLP1-pCB exerted activity for up to 6 days, suggesting pCB could provide protection for GLP-1 from proteolytic cleavages in the blood stream and provide prolonged glycemic control.

2.4 CONCLUSIONS

In this study, we developed a bioconjugate GLP1-pCB consists of the native GLP-1 peptide with a zwitterionic polymer pCB. We first demonstrated that the conjugation of pCB onto the peptide did not alter the secondary structure of GLP-1, and the GLP1-pCB conjugate possessed

good efficacy and potency *in vitro*. GLP1-pCB had a prolonged circulation half-life and exerted activity up to 6 days after a single subcutaneous injection. The conjugation of pCB provides a potential solution for the fast clearance and rapid inactivation of GLP-1, which shows promise for providing long-term glycemic control for treating T2DM.

2.5 TABLES

Table 2.1. *In vitro* potency and relative efficacy of GLP-1 and GLP1-pCB.

	Potency EC_{50} (nM)	[1]Relative E_{max} (%)
GLP-1	1.08 ± 1.17	100%
GLP1-pCB	7.25 ± 1.12	98.8%

[1]Relative E_{max}: Maximum insulin release relative to GLP-1 as 100%

Table 2.2. Pharmacokinetics profile of GLP1-pCB.

$T_{1/2\beta}$ (h)	T_{max} (h)	C_{max} (ng/mL[1])	$AUC_{0-\infty}$ (ng/mL[1]·h)
43.0	13.4	1427.1	72931.1

[1]ng/mL: the concentrations of GLP1-pCB is expressed as the amount of GLP-1 detected in the serum. 10 ng/mL of GLP-1 detected is equivalent to 3 nmol/mL of GLP1-pCB in the serum.

2.6 FIGURES

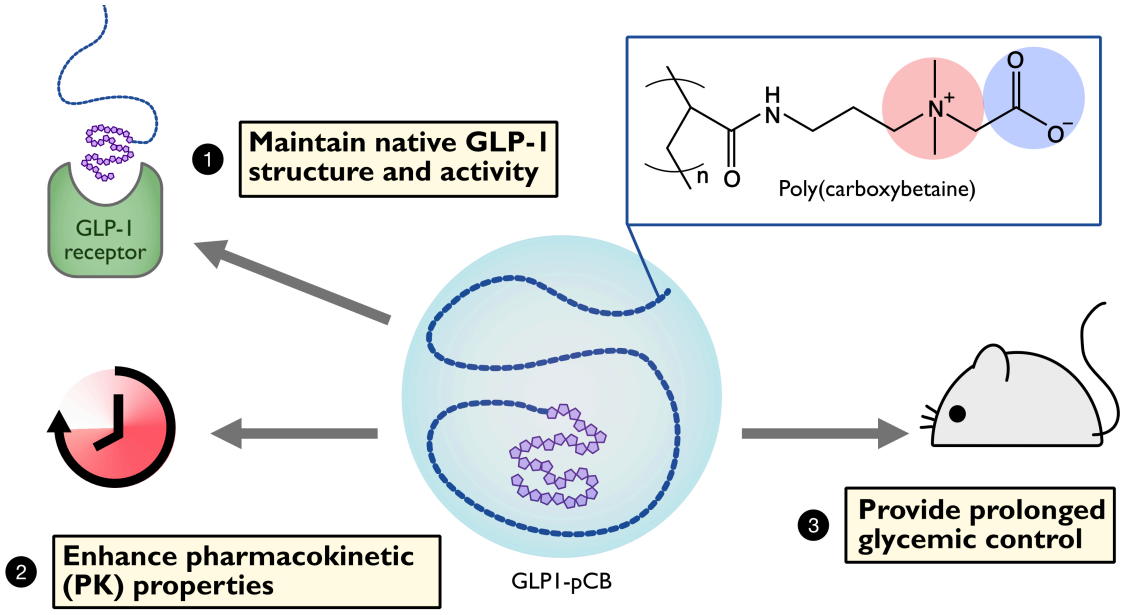

Figure 2.1. Advantages of the conjugation of a pCB polymer onto native GLP-1.

Through the conjugation of zwitterionic poly(carboxybatine) polymer onto native glucagon-like peptide-1, the bioconjugate GLP1-pCB has three potential advantages: (1) maintains the secondary structure and activity of GLP-1, (2) enhances the pharmacokinetic properties in vivo, and (3) provides prolong glycemic control in a mouse study.

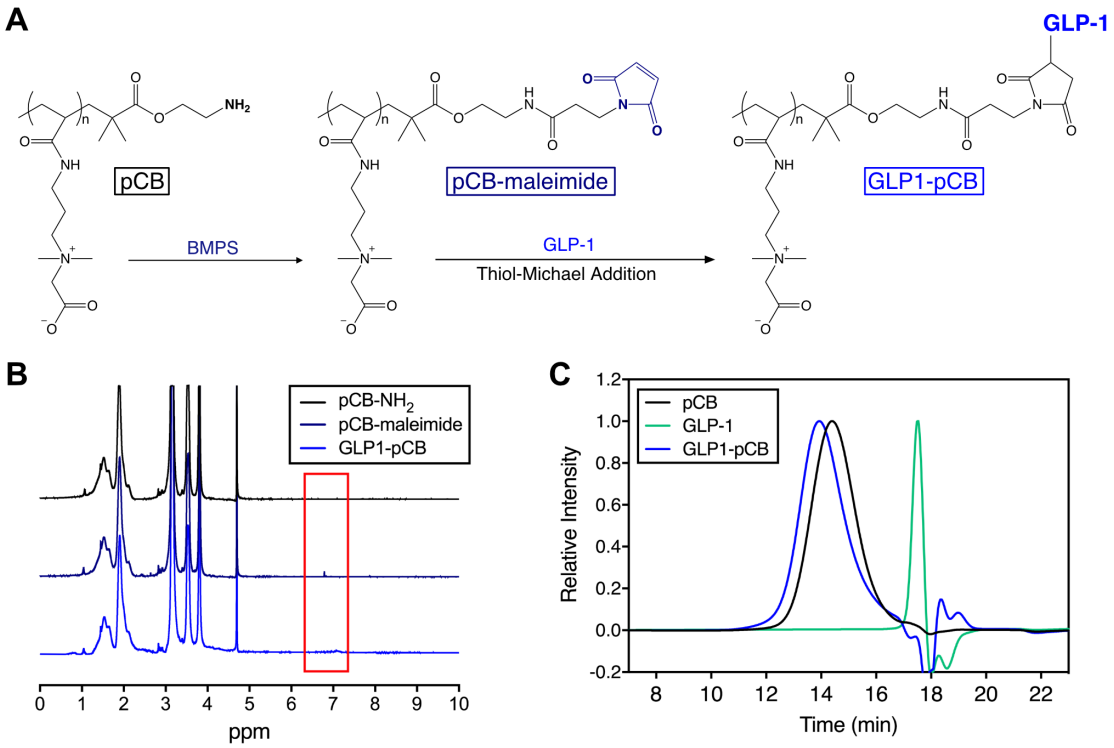

Figure 2.2. Synthetic scheme and characterizations of GLP1-pCB.

A. Synthetic scheme for pCB conjugation onto GLP-1. **B.** Nuclear magnetic resonance spectroscopy (^{1}H-NMR) profile of each conjugation step. The appearance of the small peak indicates the successful addition of the maleimide, while the disappearance indicates the successful conjugation onto GLP-1. **C.** Gel permeation chromatography (GPC) traces of GLP1-pCB. The left-shift of GLP1-pCB peak of suggests the success of conjugation as GLP1-pCB is larger than pCB alone.

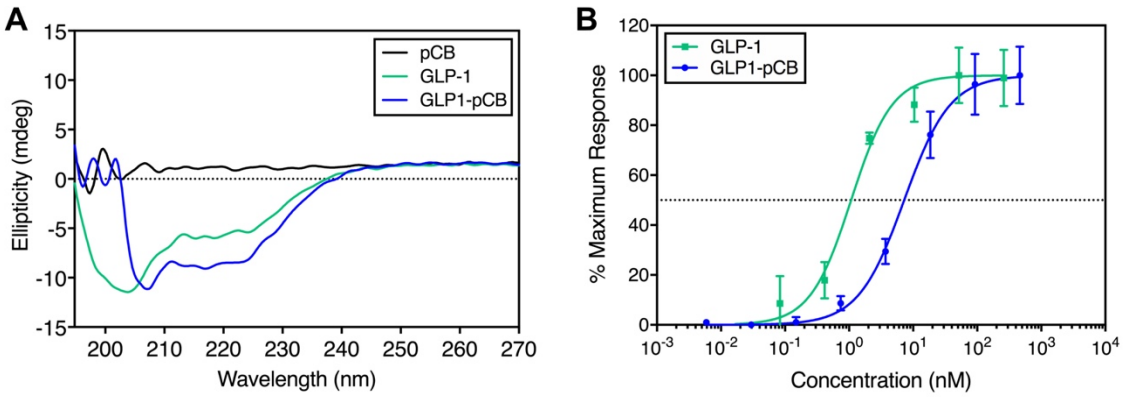

Figure 2.3. Circular dichroism spectroscopy and *in vitro* insulinotropic activity assay.

A. Circular dichroism (CD) spectroscopy of pCB, GLP-1, and GLP1-pCB. GLP1-pCB maintains the secondary structure of GLP-1. **B.** *In vitro* insulinotropic activity of GLP-1 and GLP1-pCB. Properties of both are summarized in Table 1.

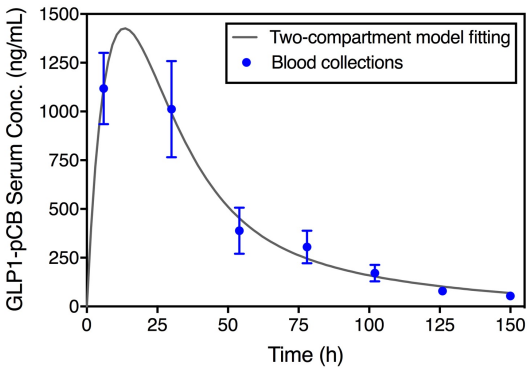

Figure 2.4. Circulation profile of a single subcutaneous injection of GLP1-pCB.

The concentrations of GLP1-pCB is expressed as the amount of fluorescent-labeled GLP-1 detected in the serum.

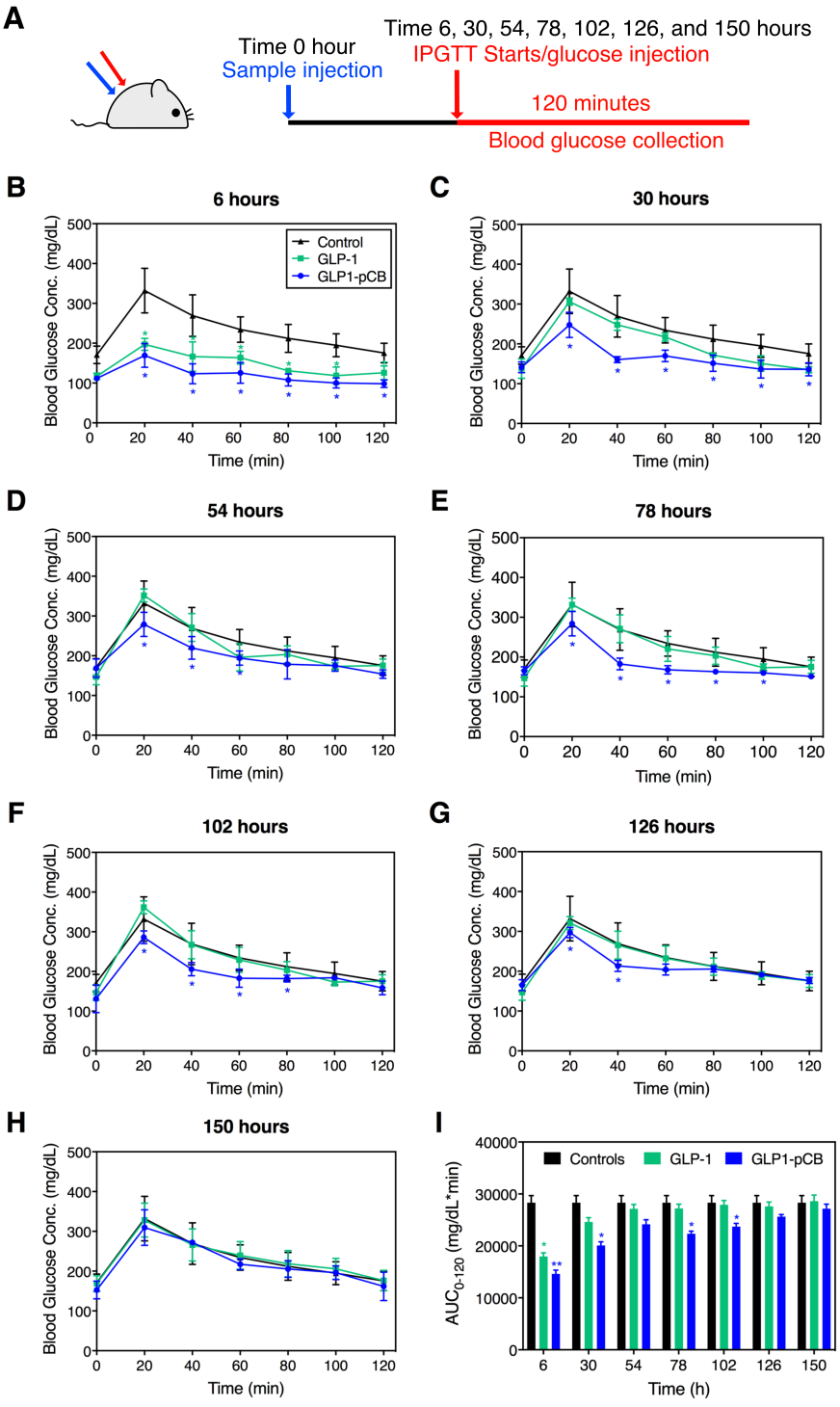

Figure 2.5. Intraperitoneal glucose-tolerance test (IPGTT) of GLP-1 and GLP1-pCB.

A. Experimental design for the IPGTT. Mice were first subcutaneously injected with a single dose of 300 nmol/kg GLP-1, GLP1-pCB, or saline (labeled as Control) at time 0 h. IPGTTs were then conducted on animals with an intraperitoneal injection of glucose (2 g/kg) at different time points: 6, 30, 54, 78, 102, 126, and 150 h post-sample injection. Blood glucose levels were then monitored for 120 minutes during each IPGTT. **B.-H.** Blood glucose profiles of IPGTT at different time points after sample injection. **I.** Accumulative blood glucose $AUC_{0\text{-}120}$ (area under the curve) profiles of IPGTT. The AUC was calculated based on the blood glucose profiles from B.-H. *$p < 0.05$, **$p < 0.01$

Chapter 3. Enhanced Pulmonary Systemic Delivery of Protein Drug *via* Zwitterionic Polymer Conjugation

Pulmonary delivery of protein drugs into the systemic circulation is highly desirable as the lung provides a large absorption surface area and a more favorable environment for biologics compared to other delivery routes. However, pulmonary systemic delivery of proteins presents several challenges such as poor protein stability and limited bioavailability, especially for large proteins (molecular weight > 50 kDa), which exhibit an average bioavailability of 1% to 5% when delivered *via* the pulmonary route. Here, we demonstrated that with the conjugation of zwitterionic poly(carboxybetaine) (pCB) polymer, the bioavailability of organophosphate hydrolase (OPH) was significantly increased from 5% to 53%. OPH conjugated with pCB delivered through intubation-assisted intratracheal instillation (IAIS) into the lung exhibited improved pharmacokinetic properties and prophylactic efficacy against organophosphate poisoning, showing its application potential. Zwitterionic polymer conjugation provides the possibility for a favorable, non-invasive delivery of biological therapeutics into the systemic circulation.

3.1 INTRODUCTION

Biological therapeutics, such as proteins and peptides, have been gaining increased interest for the past decades due to their specificity and effectiveness in treating difficult medical conditions[160–162]. Non-invasive systemic protein drug delivery *via* the pulmonary route has always been fantasized and explored since the 1950s owing to the large surface area of the lung for absorption, high epithelial permeability compared with the gastrointestinal tract, and favorable

environment for biologics compared to the hostile conditions associated with oral delivery[163–165]. However, the progress in pulmonary delivery of biologics has been fairly limited.

Many efforts had been made to understand the barriers in the lung and to improve the efficiency of pulmonary systemic delivery[163,166–168]. Recent studies have revealed that two main obstacles have hindered the progress of pulmonary systemic delivery of proteins: (1) poor protein stability in the lung environment[169–171], and (2) limited absorption due to the size and molecular weight of the protein[163,169,170]. Exogenous proteins in the lung environment could undergo undesired endogenous protein absorption, denaturation, then aggregation. Subsequently, aggregated proteins in the lung lose their activities and are, then, marked by macrophages for clearance through phagocytosis and intercellular enzymatic degradation[172,173]. Moreover, the size or molecular weight of the protein is one of the main causes for limited systemic actions. While small peptides can "leak" into the systemic bloodstream, delivering large proteins (molecular weight > 50 kDa) into the systemic circulation through the lung remains a major challenge due to their low bioavailability, ranging from 1% to 5%[100,101,171,174]. As alveolar macrophages are one of the barriers that prevent the transport of large proteins from the airway lumen into the bloodstream, the depletion of alveolar macrophages using liposome-encapsulated dichloromethylene diphosphonate could result in several-fold enhancement in the systemic absorption of large proteins[175,176]. Despite their improvement of absorption, the potential harm to the lung using these "proactive" approaches may not be overlooked. Hence, a "passive" delivery approach which would not interfere or interact with the lung environment but would improve absorption is highly desirable.

Organophosphorus hydrolase (OPH) is an enzymatic protein has received much attention as an advanced prophylactic against organophosphate (OP) nerve agents or insecticides due to its

catalytic activity and broad substrate specificity when compared to other OP bioscavengers[102,104,177–183]. Moreover, because of the unpredictable and urgent needs for the protection of warfighters at the frontline, bioscavengers delivery methods that are easy, quick, and efficacious are much desired. Pulmonary delivery of bioscavengers to the lung has hence been studied to create a pulmonary bioshield[183–186]. Yet, no studies on the systemic pharmacokinetic properties of pulmonary-delivered bioscavengers have been reported. Herein, this work focuses on the systemic delivery of OPH *via* the pulmonary route for bioscavenging and for broader applications in protein therapeutics.

Zwitterionic poly(carboxybetaine) (pCB), derived from natural occurring glycine betaine, has been demonstrated to possess superior hydration capability in forming a "water shield" and provide non-specific binding resistance when coated on surfaces[187–189]. In recent years, conjugation of pCB polymer onto particle surfaces have further been shown to avoid non-specific interactions with the environment, reduce macrophage uptake[190,191], and ameliorate protein immunogenicity when delivered directly into the systemic blood stream[87–89], demonstrating the great potential of employing pCB polymer for improving protein therapeutics. In this study, we demonstrate that the conjugation of zwitterionic pCB polymer can help stabilize and protect proteins from the lung environment, and increase the absorption of proteins through the barriers in the lung, thus, penetrating into the bloodstream. We envision that pulmonary systemic delivery of biotherapeutics can be achieved for various medical applications with the help of zwitterionic polymer conjugation in the future (**Figure 3.1**).

3.2 Materials and Methods

3.2.1 *Materials*

Zwitterionic polymers, 5, 10, and 20 kDa pCB, were produced as previously reported (chemical structure shown in **Figure 3.2**)[92]. In brief, 3-acrylamido-N-(2-(tert-butoxy)-2-oxoethyl)-N,N-dimethylpropan-1-aminium (t-Butyl CBAAm) and chain transfer agent (CTA) were synthesized. pCB polymer was next prepared by a combination of reversible addition fragmentation chain transfer (RAFT) polymerization, aminolysis, acid deprotection and amine-to-thiol conversion steps utilizing the t-Butyl CBAAm and CTA prepared earlier. Wild-type OPH (A0A060GZX0) used in this study was originally derived from Brevundimonas diminuta, and expressed following a published protocol[89]. N-α-maleimidoacet-oxysuccinimide ester (AMAS, Sigma-Aldrich), 2-Iminothiolane hydrochloride (Traut's reagent, Sigma-Aldrich), N-hydroxysulfosuccinmide (sulfo-NHS, Sigma-Aldrich) and N-(3-Dimethylaminopropyl)-N'-ethylcarbodiimide hydrochloride (EDC, Sigma-Aldrich) were used in the process of polymer conjugation. Paraoxon-ethyl (Sigma-Aldrich) was used in the study of protective efficacy. Amicon Ultra centrifugal filter units were purchased from EMD Millipore (Billerica, MA). Pierce 660 nm Protein Assay was purchased from Thermo Fisher Scientific (Waltham, MA).

3.2.2 *pCB Polymer Conjugation*

OPH (10 mg, 2.5 mg/mL in 0.02 M PB, 0.1 mM Co^{2+}, 1% w/v stabilizer, pH 7.4) were first reacted with AMAS (0.775 mg prepared as 20 mg/mL in DMSO) for 40 minutes at room temperature in order to activate the lysines on the protein. 400 mg of 5, 10, 20 kDa pCB polymer end groups (dissolved in 0.02 M PB, pH 7.4) were activated with 5.5 mg of Traut's reagent (prepared as 20 mg/mL in DI water) for 2 to 3 hours at room temperature. Activated OPH and pCB were mixed

together, reacted for 2 hours at room temperature. The reaction was then transferred to 4ºC, overnight. The reaction was stopped the next day by multiple buffer (0.02 M PB, 0.1 mM Co^{2+}, pH 7.4) exchange through centrifugal columns, washing excess unreacted polymers and proteins. OPH solution is kept at the concentration of 2.5 mg/mL or above.

3.2.3 *Structural Analysis of pCB-conjugated OPH*

The PCB-conjugated OPH and OPH were characterized by circular dichroism. A Jasco J-720 spectropolarimeter was used to measure the far-UV spectra of the proteins diluted to a concentration range of 50 - 100 μg/mL in 20 mM sodium phosphate buffer, 0.1 mM Co^{2+}, pH 7. The mean residue ellipticity was measured from 190 - 270 nm in a 0.1 cm path length quartz cuvette at 25 °C. All spectra were accumulated with standard sensitivity.

3.2.4 *Analysis of Surface Charge Change through Cation Exchange*

A Capto S cation exchange column (4.7 ml, 0.77 × 10 cm, GE Healthcare) was used for this study. Cation exchange was carried out using a loading buffer of 50 mM sodium acetate, pH 5.5, with an increasing NaCl gradient from 0 to 1 M during elution.

3.2.5 *Enzyme Kinetics Measurement*

Paraoxon-ethyl was used as the substrate to perform enzyme kinetics measurement. The OPH test samples were diluted to 50 ng/mL in 50 mM HEPES buffer (pH 8.5), and the substrate was dissolved in the same buffer at a range of concentrations from 0.1 to 2 mM. To perform the test, 100 μL of the above OPH sample dilution was added to a 96-well plate, followed by adding 100 μL substrate solution. Upon mixing, the absorption change at 405 nm was monitored using a plate reader (BioTek Cytation 3). The enzyme kinetics parameters were calculated using Michaelis–Menten equation.

3.2.6 *Intubation-Assisted Intratracheal Instillation (IAIS)*

All experiments using rats as the animal model adhered to federal guidelines, and were approved by the University of Washington Institutional Animal Care and Use Committee. IAIS was conducted with the immense help of Small Animal Intubation Kit (Kent Scientific Corporation). Female Sprague-Dawley rats were first for anesthetized for 10 minutes using 5% Isoflurane. Animals were then placed on a platform designed for intubation. Fiber optic cable connected with LED light through trans-tracheal illuminator was leading a 16 G catheter into the tracheal. Fiber optic cable was then removed from the catheter, leaving the catheter in the tracheal. Samples dissolved in 100 μL pharmaceutical grade phosphate-buffered saline (PBS) with 0.1 mM Co^{2+} were filled in a 1 mL syringe then attached to the 16 G catheter and injected into the lung (instillation).

3.2.7 *Pharmacokinetic Studies*

Female Sprague-Dawley rats (200 – 300 g, n = 6) were administered with dosage of 2.5 mg/kg OPH or OPH-pCB *via* IAIS. Plasma concentration profiles of OPH and OPH-pCB were determined through collection of blood samples. Blood samples were collected in Microtainer (BD) at 2, 4, 6, 8, and 24 hours after IAIS administration *via* tail vein. Blood samples were then centrifuged at 11,000 rpm for 10 minutes. Plasma were then collected and frozen in -20^{o}C for future analysis. The OPH or OPH-pCB conjugate content in plasma was estimated by activity assay using paraoxon as the substrate at a concentration of 2 mM. The enzyme activity was converted into the concentration using a standard curve. The activities were measured with a microplate reader (BioTek, Cytation 5). The concentration-time profiles and pharmacokinetic parameters were then determined utilizing PKSolver following instructions[149].

Bioavailability of pulmonary-delivered native OPH and OPH-pCB conjugates were calculated based on the definition of bioavailability

$$Bioavailability = 100 \cdot \frac{AUC_{IAIS} \cdot D_{IV}}{AUC_{IV} \cdot D_{IAIS}}$$

where AUC_{IV} and D_{IV} of native OPH were suggested in Liu et al[88]. *AUC*: area under the curve delivered by intravenous injection (IV) or intubation-assisted intratracheal instillation (IAIS); *D*: dose administered by IV or IAIS.

3.2.8 *Prophylactic Efficacy Study*

Female Sprague-Dawley rats (200 – 300 g, n = 72) were administered with dosage of 2.5 mg/kg OPH or OPH-pCB *via* IAIS at time 0. Animals were then challenged with various dosage of paraoxon based on the median lethal dose (paraoxon IV LD_{50}, 0.24 mg/kg[192]). Paraoxon was prepared by dissolved in 100 μL pharmaceutical grade PBS and was delivered *via* IAIS as mentioned before. Paraoxon was delivered 4 or 24 hours after the administration of OPH or OPH-pCB. Each animal received a single dosage of Paraoxon. For the 4-hour study, test Paraoxon dosages were 2X (2 times), 3X, 4X, or 5X IV LD_{50}. For the 24-hours study, Test Paraoxon dosages were 1X, 2X or 3X IV LD_{50}. Animals were then being observed after poisoning for over 30 minutes. Survival rates were calculated using GraphPad Prism7 based on the total number of animals in the same group.

3.2.9 *Lung Histology Analysis*

Three female Sprague-Dawley rats (200 – 300 g) were administered with dosage of 2.5 mg/kg OPH-pCB 5k *via* IAIS. Three other untreated, healthy female rats were used as negative controls. One week after administration, animals were sacrificed and their lung were collected. Sectioning

and H&E staining were performed by University of Washington Histology and Imagining Core (HIC). Lung sections were analyzed under 100× magnification using a microscope (Nikon Eclipse 80i).

3.2.10 *Statistical Analysis*

Unpaired two-tail Welch's *t* test was used to compare two small sets of quantitative data from pharmacokinetics, with $P < 0.01$ being considered as statistically significant.

3.3 Results and Discussion

3.3.1 *Synthesis and Characterization of OPH-pCB Conjugates*

Large proteins modified with zwitterionic pCB polymer have previously been demonstrated to possess enhanced pharmacokinetic properties, reduce protein immunogenicity, and avoid non-specific interactions with the environment when delivered directly into the systemic blood stream[87–89,91]. Moreover, nanoparticles with a hydrodynamic diameter less than 6 nm and a zwitterionic surface have shown to enter the blood stream quickly from the alveolar airspaces upon instillation[193]. Therefore, we conjugated pCB polymers onto the surface of OPH to form a super-hydrophilic protective layer, while maintaining a small hydrodynamic diameter for the overall construct. OPH was first conjugated with three pCB polymers with the molecular weights of 5, 10, and 20 kDa (reaction scheme shown in **Figure 3.2**). Three OPH-pCB conjugates, OPH-pCB 5kDa (denoted as OPH-pCB 5k for the rest of the studies), OPH-pCB 10kDa (OPH-pCB 10k), and OPH-pCB 20 kDa (OPH-pCB 20k), were evaluated by gel permeation chromatography (GPC) and dynamic light scattering to determine the diameters of the conjugates. With the increasing molecular weight of the pCB polymer conjugated, OPH-pCB conjugates eluted out in the order as

expected: with OPH-pCB 20k being the first, OPH-pCB 10k, OPH-pCB 5k, and OPH being the last (**Figure 3.3A**). While OPH protein had an average diameter of 7.25 nm, the average diameters for OPH-pCB 5k, OPH-pCB 10k, and OPH-pCB 20k, were 12.57, 18.98, and 24.37 nm, respectively (**Figure 3.3B**). Moreover, the surface charge of OPH changed after conjugation as the OPH-pCB conjugate behaved differently from native OPH during the cation exchange process (**Figure 3.4**).

3.3.2 *Synthesis and Characterization of OPH-pCB Conjugates*

Next, we investigated whether the conjugation would affect the native structure and catalytic properties of OPH. Circular dichroism (CD) spectroscopy was performed on OPH and OPH-pCB conjugates. OPH consists of a majority of α-helices, as seen from our analysis. The conjugation of pCB polymer did not alter the tertiary structure of OPH as α-helices were maintained in all OPH-pCB constructs (**Figure 3.5A**). With the integrity of the conjugates confirmed, we next evaluated the catalytic efficiency of OPH-pCB conjugates. Enzyme kinetics were studied using paraoxon-ethyl as the substrate. The Michaelis constants (K_m) were 0.3 and 0.43 mM for native OPH and OPH-pCB conjugates, respectively. The catalytic efficiency (k_{cat}/K_m) was determined to be 4.61×10^7, 6.34×10^7, 5.47×10^7, and 5.42×10^7 s^{-1} M^{-1} for OPH, OPH-pCB 5k, OPH-pCB 10k, and OPH-pCB 20k, respectively (**Figure 3.5B**). The slight increase in the catalytic efficiencies could be due to the stabilization of OPH after pCB polymer conjugation.

3.3.3 *Pharmacokinetics and Bioavailability Profile of OPH-pCB Conjugates*

The pharmacokinetics of pulmonary-delivered native and conjugated OPH was studied using Sprague-Dawley rats as animal model. Both native and conjugated OPH were delivered through intubation-assisted intratracheal instillation (IAIS). Native OPH had a peak concentration

of 83 ng/mL, 4 hours after the administration, while the peak concentration of OPH-pCB 5k conjugates could be as high as 352 ng/mL. Furthermore, OPH was no longer detectable in the systemic circulation after 24 hours, while the concentration of OPH-pCB conjugates were around 50 ng/mL or above after 24 hours, suggesting that the conjugation of pCB polymer was able to provide enhanced OPH stability and facilitate the translocation of the protein from the lung into the systemic bloodstream (**Figure 3.6**). However, as the size of OPH-pCB conjugates increased, entry into the systemic bloodstream was reduced, with OPH-pCB 5k entering the most and OPH-pCB 20k the least due to the natural size-dependent limitation of the lung barrier[194]. Based on these findings, we have chosen OPH conjugated with 5 kDa pCB polymer for the rest of the study.

We further analyzed the pharmacokinetic properties of the OPH-pCB 5k conjugate in detail. When administered a dosage of 2.5 mg/kg, the circulation half-life of OPH was greatly increased after the conjugation of pCB polymer, from 2.7 to 12.4 hours. The peak concentration of OPH-pCB 5k conjugate was 4.7-folds higher than that of OPH while the $AUC_{0-\infty}$ (area under the curve) increased by 9.8-folds. The bioavailability of OPH was further calculated for both native OPH and OPH-pCB 5k conjugate. Bioavailability is an indicator for drug absorption and the fraction of an administered dose of unchanged drug that reaches the systemic circulation when compared to intravenous injection. The bioavailability of the OPH significantly increased after conjugation, from 5.1% to 53.4% (**Table 3.1**). The more than 10-fold increase in bioavailability and improved pharmacokinetic properties of OPH after pCB conjugation could be explained by its neutral-charged nature and super-hydrophilicity. Native OPH is overall positively-charged in physiological environment (pH 7.4 – 7.5), which could quickly absorb endogenous protein in the lung onto its surface and form aggregates, thus has an restricted behavior or even get taken up by alveolar macrophages[195,196]. The conjugation of zwitterionic pCB polymer onto the surface of OPH

could mask its positive residues. Furthermore, the super-hydrophilic nature of pCB polymer could provide a layer of "water-shield" around OPH which helps stabilize OPH in the lung environment by preventing protein aggregation and alveolar macrophage uptake. Moreover, upon administration, both native OPH and OPH-pCB conjugate would need to travel through the bronchi and bronchioles before reaching the alveoli to enter the bloodstream. The bronchi and bronchioles are coated with a viscous layer of mucus which entraps and removes particles[171]. While negatively-charged mucin proteoglycans would bind to positively-charged OPH with avidity, particles with net neutral surface have shown minimal hinderance when traveling through mucus by avoiding electrostatic adhesive interactions[197–199]. The "water-shield" provided by the super-hydrophilicity pCB polymers could further reduce the hydrophobic entrapment to mucus, resulting in more OPH-pCB conjugates reaching the alveoli and hence the improved pharmacokinetic properties.

3.3.4 *Prophylactic Efficacy of OPH-pCB 5k Against Organophosphate Poisoning*

To explore the prophylactic efficacy of OPH-pCB conjugate, a study of OPH against organophosphate poisoning was conducted. Due to its enhanced pharmacokinetic profile, OPH-pCB 5k was selected for this study. The experimental design is shown in **Figure 3.7A**. OPH and OPH-pCB 5k at a dosage of 2.5 mg/kg were first delivered into the lung through IAIS at time 0. Animals were then challenged with various dosages of paraoxon based on the median lethal dose (paraoxon IV LD_{50}, 0.24 mg/kg[192]). Animals were challenged at 4 hours and 24 hours after the dose of OPH or OPH-pCB. The 24-hour mark for challenge was chosen in attempt to illustrate the differences in protective efficacy due to the significant difference in the blood concentration, while both OPH and OPH-pCB 5k had a peak concentration in blood at the 4-hour mark. Right after the administration of paraoxon, animals were observed for signs of intoxication, such as tremors,

respiratory depression, and mortality. Survival rates were calculated based the percentage of animals that survived in the same group. The groups that received native OPH were only able to provide protection up to 50% of the animals when challenged with a paraoxon dosage of 3 times the IV LD_{50} (3X IV LD_{50}), 4 hours after the administration of the native bioscavenger (**Figure 3.7B**). When challenged with the dosage of 2X IV LD_{50} (normal lethal dosage), OPH was no longer capable of providing protection to animals after 24 hours (**Figure 3.7C**). This was expected since OPH was no long detectable in the blood after 24 hours. Animals administered with OPH-pCB 5k, on the other hand, were able to withstand the challenge up to the dosage of 4X IV LD_{50}, 4 hours after the administration of the pCB polymer-conjugated bioscavenger. With the remaining concentration of OPH-pCB 5k after 24 hours, animals all survived the challenge of 2X IV LD_{50}. All animals that survived showed no signs of distress 24 hours after the challenge. This result demonstrates the distinctive difference in the level of protection OPH-pCB conjugate from OPH. With the conjugation of zwitterionic polymer, it is promising that a single administration of the bioscavenger *via* the lung could have the potential of providing complete protection for at least 24 hours. The extended time of protection could greatly reduce potential damage caused by nerve agents in warfighters on the battlefield.

3.4 CONCLUSIONS

In this study, we demonstrated that the conjugation of pCB polymer could help stabilize a protein, provide protection in the complex environment, and facilitate the protein to enter the systemic circulation *via* the pulmonary route. More importantly, the bioavailability of protein (larger than 50 kDa) delivered *via* the pulmonary route was significantly increased from 5% to 53%. This is the first time that one has greatly increased the bioavailability of large protein drugs delivered into the systematic circulation through the lung without the addition of “proactive”

substances. This delivery method is efficacious as further demonstrated through the enhanced protective efficacy against organophosphate poisoning using OPH as the model drug. Thus, this study has shown great potential of utilizing the pCB polymer for the future systemic delivery of biologics *via* the pulmonary route and would create a great incentive to use biological therapeutics as common treatments.

3.5 TABLES

Table 3.1. Pharmacokinetics and bioavailability profile of OPH and OPH-pCB 5k.

	$t_{1/2}\beta$ (h)	C_{max} (ng/mL)	T_{max} (h)	$AUC_{0-\infty}$ (ng/mL•h)	Bioavailability (%)
OPH	2.7	72.25	3.75	732.03	5.1
OPH-pCB 5k	12.37	340.77	4.06	7170.90	53.4

$t_{1/2}\beta$: elimination half-life; C_{max}: maximum serum concentration; T_{max}: the time take to reach C_{max}; $AUC_{0-\infty}$: area under the curve from time 0 to infinite

3.6 FIGURES

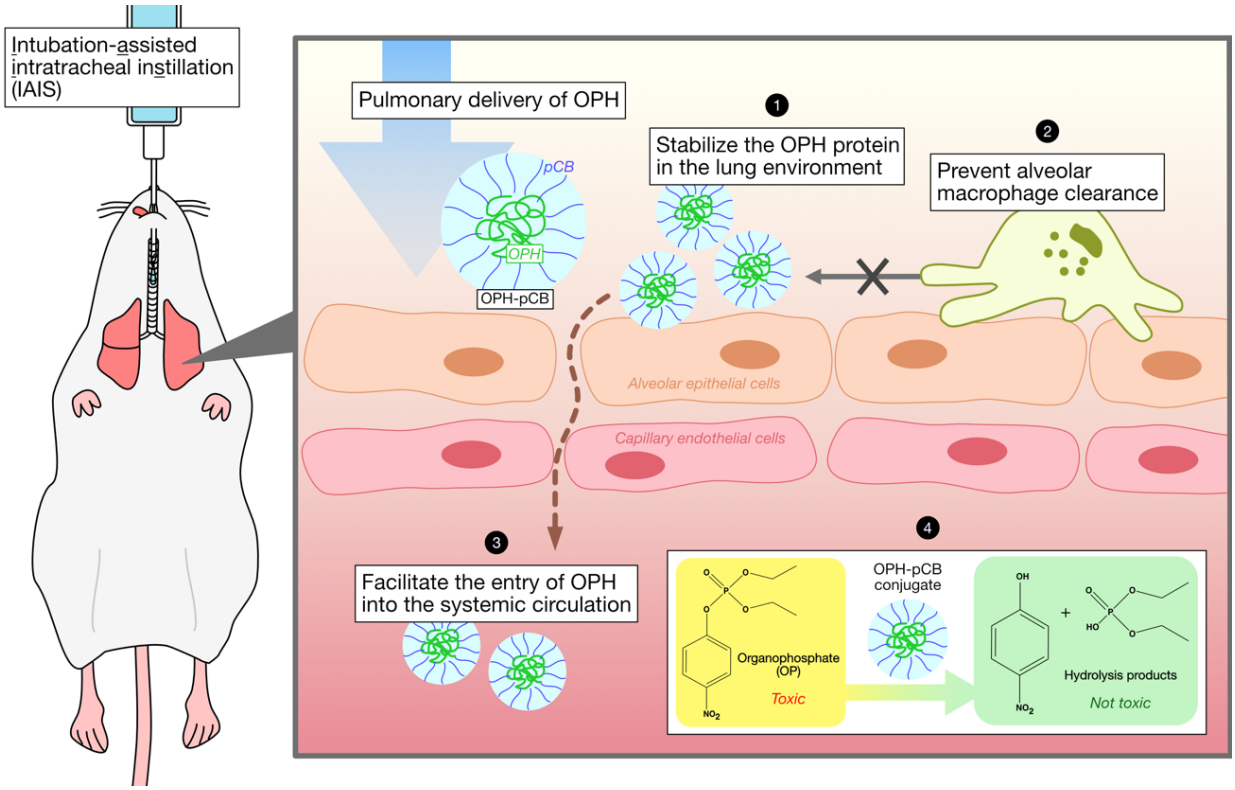

Figure 3.1. Schematic illustration of systemic delivery of poly(carboxybetaine) (pCB) polymer conjugated organophosphate hydrolase (OPH) *via* the pulmonary route.

Schematic illustration of systemic delivery of poly(carboxybetaine) (pCB) polymer conjugated organophosphate hydrolase (OPH) via the pulmonary route. The conjugation of pCB polymer: (1) helps stabilize OPH in the lung environment, maintaining OPH activity, (2) prevents uptake and clearance from alveolar macrophages, and (3) facilitates the entry of OPH into the systemic circulation with enhanced pharmacokinetic properties. Furthermore, (4) OPH-pCB conjugates can hydrolyaze toxic organophophate (OP) into non-toxic products to prevent OP poisoning. Through the conjugation of zwitterionic polymers, future biotherapeutics could be delivered into the systemic circulation *via* the pulmonary route.

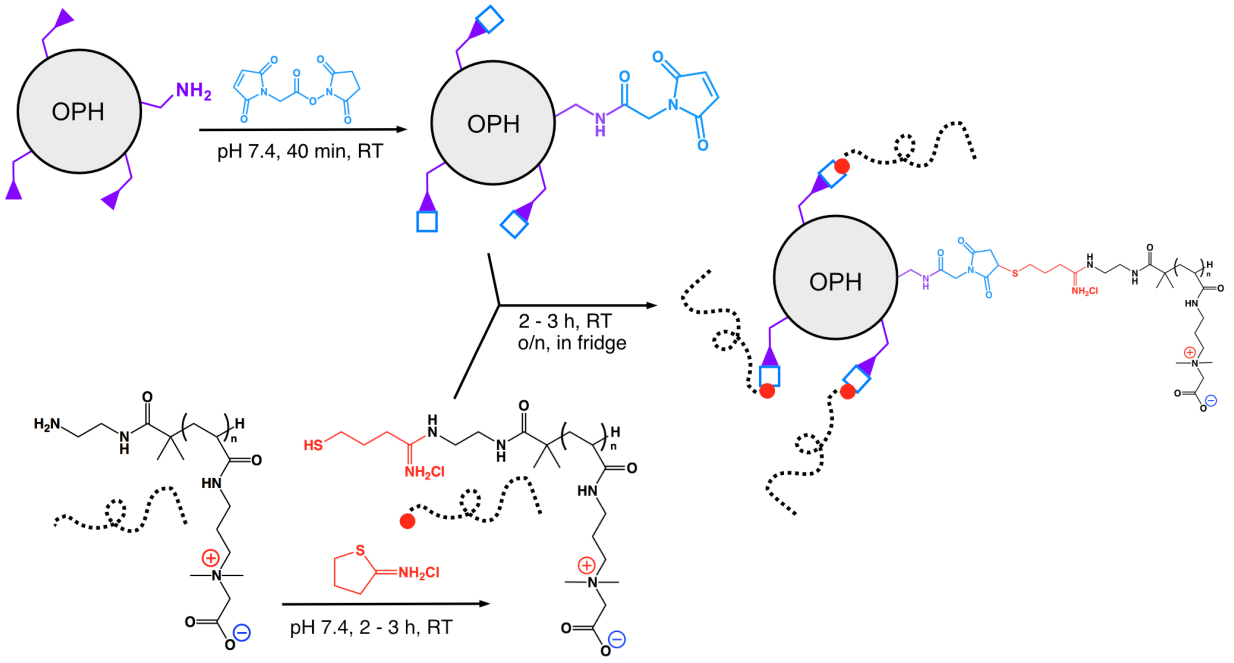

Figure 3.2. Reaction scheme of pCB polymer conjugation onto OPH.

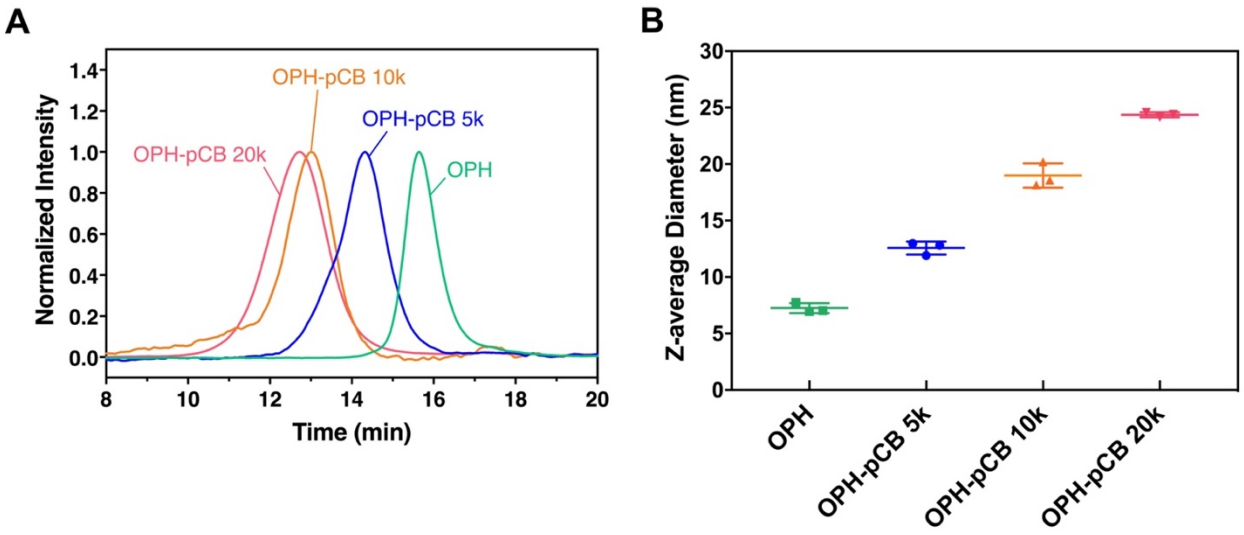

Figure 3.3. Gel permeation chromatography traces and dynamic light scattering results.

Gel permeation chromatography (GPC) traces of native OPH and three OPH-pCB conjugates. The OPH-pCB conjugates eluted out in the expected order as indicated by the left-shifts of all conjugates to native OPH. **B.** Hydrodynamic diameter of OPH and OPH-pCB conjugates measured through dynamic light scattering (DLS), shown with means and standard deviations.

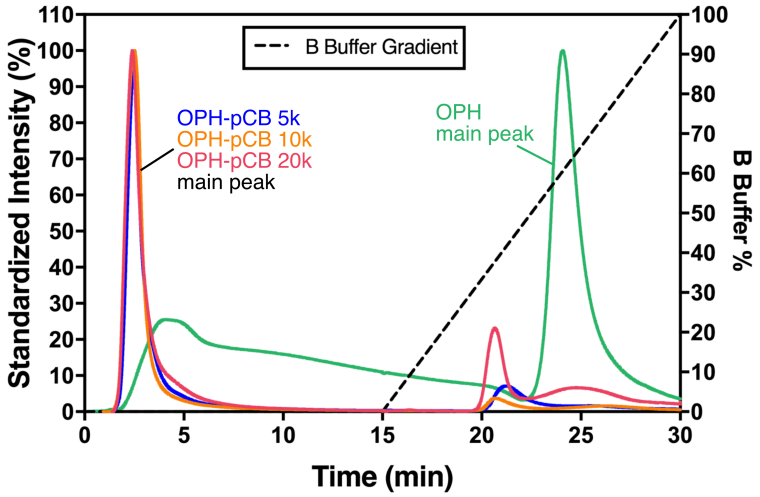

Figure 3.4. Cation exchange profiles of native OPH and three OPH-pCB conjugates.

Majority of the OPH-pCB conjugates did not bind to the column, as they flowed through the column before applying the NaCl gradient (labeled as the OPH-pCB 5k/10k/20k main peak). Majority of the native OPH bound to the column during the first phase and was eluted out after applying the salt gradient (labeled as the OPH main peak). This indicated that the surface charge of OPH had been modified due to the conjugation of pCB polymers. Buffers used for this study: A buffer - 50 mM sodium acetate, pH 5.5; B buffer - 50 mM sodium acetate, 1 M NaCl, pH 5.5.

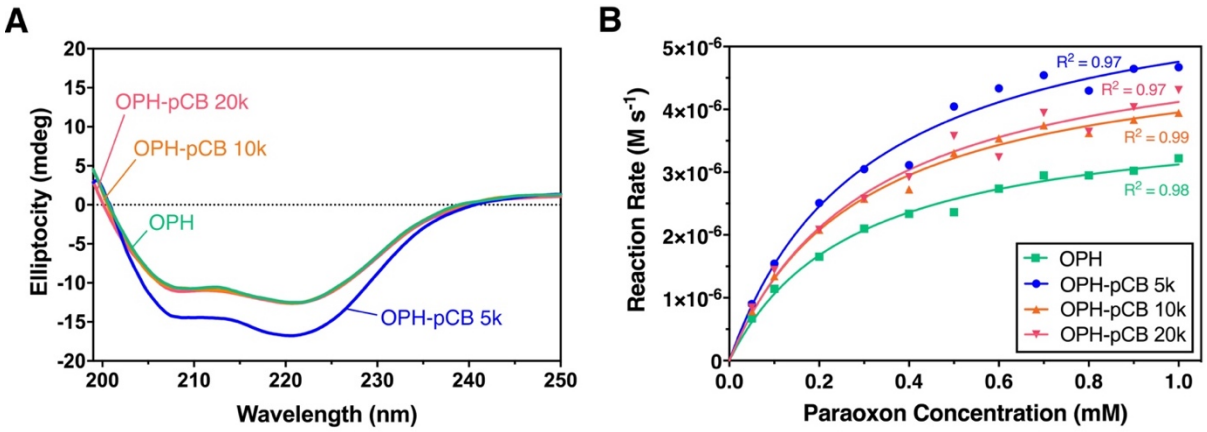

Figure 3.5. Circular dichroism spectroscopy and enzyme kinetics profiles.

A. Circular dichroism (CD) spectroscopy of native and OPH-pCB conjugates. α-helices were maintained after conjugation. **B.** Enzyme kinetics profiles of OPH and three OPH-pCB conjugates.

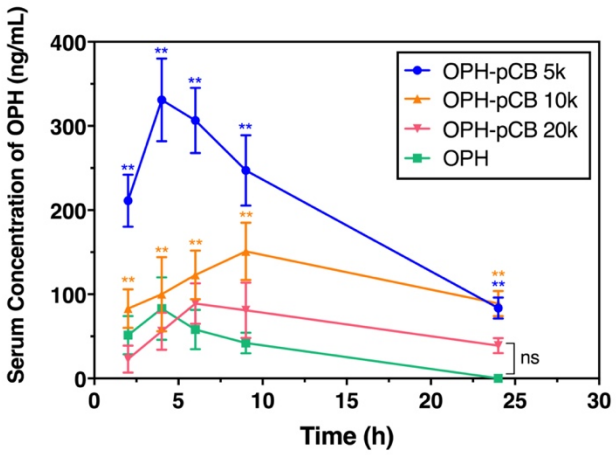

Figure 3.6. Serum concentration profiles of OPH and three OPH-pCB conjugates *via* IAIS administration.

Blood serum was collected at various time points from the tail vein to determine the concentrations of OPH and OPH-pCB conjugates in the systemic blood stream. Unpaired Welch's *t* test was used to compare each OPH-pCB conjugates sets to native OPH sets. ns, not significant. *$P < 0.05$, **$P < 0.01$, ***$P < 0.001$.

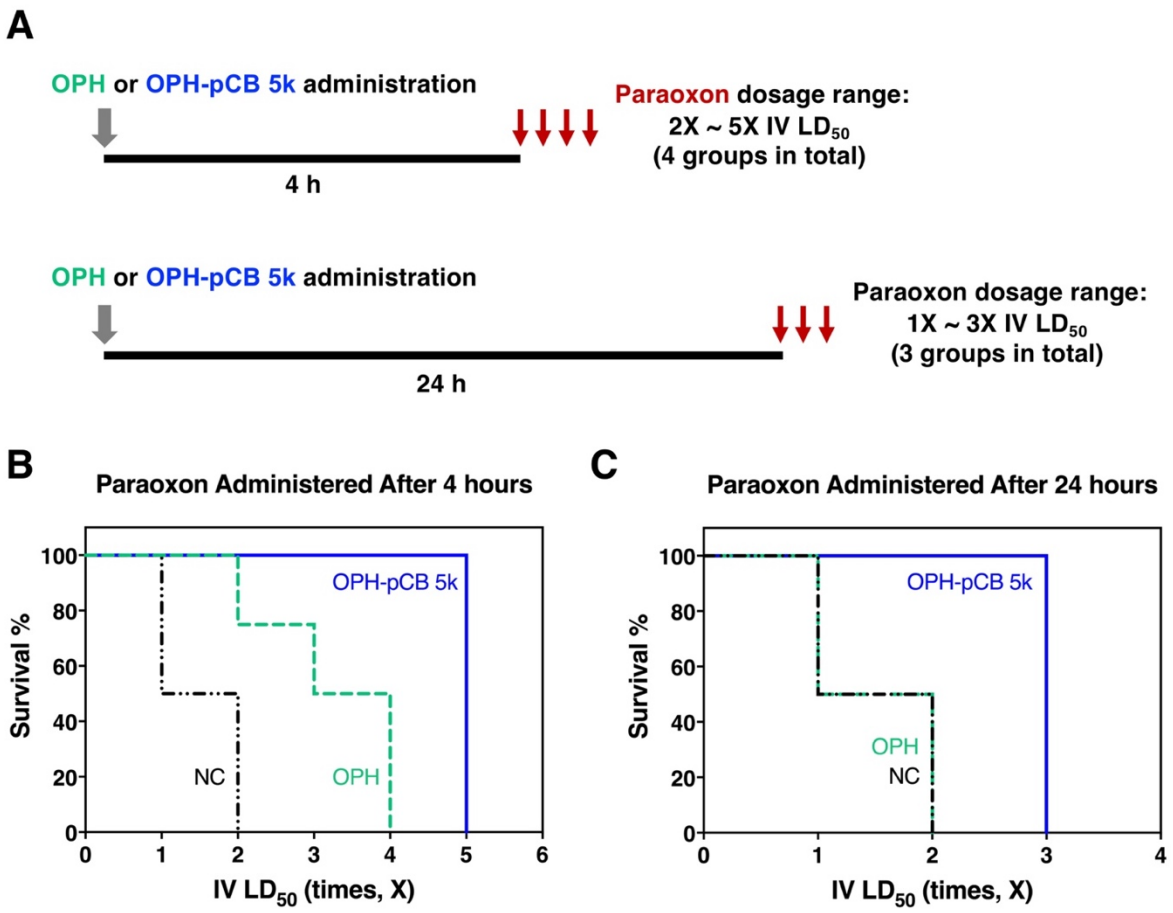

Figure 3.7. Prophylactic efficacy study against organophosphate poisoning.

A. Experimental design of the prophylactic efficacy of OPH and OPH-pCB 5k against organophosphate poisoning (paraoxon-ethyl). Both OPH and OPH-pCB 5k were administered *via* IAIS at time 0 h to different groups. After 4 hours and 24 hours, animals were challenged with various dosages of paraoxon through IAIS. The 4-hour mark was chosen due to the peak concentration for both OPH and OPH-pCB 5k were at 4 hours. The 24-hour mark for challenge was chosen in attempt to illustrate the differences in protective efficacy due to the significant difference in the blood concentration of OPH and OPH-pCB 5k. **B.** Survival rates of paraoxon

challenge at the 4-hour mark. **C.** Survival rates of paraoxon challenge at the 24-hour mark. *n = 6* in all groups. NC: Negative controls.

Chapter 4. Hight Strength and Fibrous Capsule-resistant Zwitterionic Elastomers

The high mechanical strength and long-term resistance to the fibrous capsule formation are two major challenges for implantable materials. Unfortunately, these two distinct properties do not come together and instead compromise each other. Here we report a unique class of materials by integrating two weak zwitterionic hydrogels into an elastomer-like high-strength pure zwitterionic hydrogel *via* "swelling" and "locking" mechanisms. These Zwitterionic-Elastomeric-Networked (ZEN) hydrogels are further shown to efficaciously resist the fibrous capsule formation upon implantation in mice for up to one year. Such materials with both high mechanical properties and long-term fibrous capsule-resistance have never been achieved before. This work not only demonstrates a new class of durable and fibrous capsule-resistant materials, but also provides design principles for zwitterionic elastomeric hydrogels.

4.1 INTRODUCTION

Synthetic hydrogels have long been attractive materials to mimic biological tissues for medical applications such as tissue scaffolding[26,200–203]. There are two main criteria for achieving this goal: excellent mechanical properties and long-term resistance to the fibrous capsule formation induced by the foreign body reaction. However, these properties generally do not coexist in the same material and compromise each other, as the former requires hydrophilicity while the latter hydrophobicity[204,205]. While *in vitro* protein adsorption, cell adhesion, and cytotoxicity are commonly used to evaluate biomaterials, they are far from the challenges involving fibrous capsule-resistance in complex living systems. The ability of the material not to trigger the fibrous capsule formation after implantation for a long period is particularly challenging. It is well known

that nearly all synthetic materials trigger the foreign body reaction and fibrous capsule formation within one month upon materials implantation[19,93,206,207]. While many efforts have been made to mitigate this foreign body reaction through materials geometry or chemical modification[203,208], super-hydrophilic zwitterionic hydrogels are particularly promising for solving this issue[85–87,93,204,206,209–212]. In our early studies, zwitterionic poly(carboxybetaine) (pCB) hydrogels were shown to avoid capsule formation for three months after subcutaneous implantation in mice, which was the longest time a biomaterial had mitigated this response[93,206]. However, the mechanical properties of those zwitterionic hydrogels were rather weak, due to their super-hydrophilic characteristics. A simple solution to increase the mechanical properties of materials is to add a hydrophobic component, but which increases protein adsorption and induces fibrous capsule formation. In parallel, significant progress has been made to strengthen the mechanical properties of various hydrogels[112,213–219]. While these hydrogels are shown to have low protein adsorption and cell adhesion, they are still far from long-term fibrous capsule-resistance. Thus, our objective in this study is to develop a high-strength pure zwitterionic elastomer with excellent long-term fibrous capsule-resistance.

Here we present a Zwitterionic-Elastomeric-Networked (ZEN) hydrogel (**Figure 4.1**), realized by integrating two weak zwitterionic hydrogels, poly(carboxybetaine) (pCB) and poly(sulfobetaine) (pSB). In this pCB/pSB ZEN hydrogel, pCB is the minor component, forming a tightly crosslinked network to create elasticity, while pSB is the major component, forming a loosely crosslinked network to provide viscosity[112]. Notably, the pCB network possesses a high swellability which could integrate a significant amount of the pSB network, while the pSB network "locks" the entire hydrogel *via* strong inter- and intra-molecular electrostatic interactions. The new mechanism of combining the excellent swellability and the "locking" effect allows us to achieve

ZEN hydrogels with high mechanical strengths from only pure zwitterionic constituents. We have further demonstrated that three parameters (the type, combination, and composition of zwitterionic constituents) are the key to achieve ZEN hydrogels. The pCB/pSB ZEN hydrogel was demonstrated to resist fibrous capsule formation after subcutaneous implantation in mice for up to one year.

4.2 Materials and Methods

4.2.1 *Materials*

[2-(Methacryloyloxy)ethyl]dimethyl-(3-sulfopropyl)ammonium hydroxide (SB, 95%) and 2-hydroxyethyl methacrylate (HEMA, 97%) were obtained from Sigma-Aldrich (Milwaukee, WI), purification was carried out to remove inhibitor before use. 3-[3-(Acrylamidopropyl)dimethylammonio]propionate (CB) and trimethylamine N-oxide (TMAO) monomer were synthesized following our previous reports[220,221]. N,N'-Methylenebisacrylamide (MBAA, ≥ 98%), 2-hydroxy-2-methylpropiophenone (photoinitiator 1173, 97%), ammonium persulfate (APS, ≥ 98%), N,N,N',N'-tetramethylethylenediamine (TEMED, 99%), fibrinogen from human plasma (≥ 80% clottable protein), *o*-phenylenediamine (OPD, ≥ 98%) and phosphate buffered saline (PBS, 10 mM phosphate, 138 mM sodium chloride, 2.7 mM potassium chloride, pH 7.4) were purchased from Sigma-Aldrich (Milwaukee, WI). Horseradish peroxidase (HRP) conjugated anti-fibrinogen was purchased from Alpha Diagnostic International (San Antonio, TX). Human serum with CPD, pooled and mixed gender was purchased from Biochemed Services (Winchester, VA). Pierce™ LDH Cytotoxicity Assay Kit and Pierce™ BCA Protein Assay Kit were purchased from Thermo Fisher Scientific (Bothell, WA). Rat pancreas/islet of Langerhans RIN-m5F cell line was purchased from ATCC (Manassas, VA), and mouse dendritic cell line DC

2.4 was a generous gift from Dr. K. L. Rock (University of Massachusetts Medical Center, Worcester, MA).

4.2.2 *Preparation of Hydrogels*

All the poly(CB)/poly(SB) (pCB/pSB) hydrogels were prepared following a two-step sequential free-radical polymerization method. In general, take the synthesis of pCB/pSB Zwitterionic-Elastomeric-Networked (ZEN) hydrogel for example, the ZEN hydrogel is consisted of the formation of the pCB minor-component network followed by the construction of the pSB major-componentnetwork. In the first step, the zwitterionic minor-component network (ZMN1) pCB hydrogel was synthesized by a photo polymerization using 1 m (molality) of CB monomer, 4 mol% of crosslinker and 0.1 mol% of photoinitiator 1173 (molar percentages both were relative to the CB monomer) in the transparent sheet mold or the tubular rod mold under the ultraviolet (UV) irradiation with a wavelength of 302 nm and a power of 6 watt for 6 h under the nitrogen atmosphere. In the second step, the prepared pCB ZMN1 hydrogels were immersed into the precursor solution of the zwitterionic major-component network (ZMN2) containing 4 m of SB monomer, 0.1 mol% of MBAA crosslinker and 0.01 mol% of photoinitiator 1173 (molar percentages were both relative to the SB monomer) overnight. The fully swollen ZMN1 hydrogels containing the precursor for ZMN2 were further polymerized by UV irradiation with a wavelength of 302 nm and 6 watt power for 6 h under the nitrogen atmosphere. After this two-step synthesis, the as-prepared pCB/pSB ZEN hydrogel was immersed in water for at least one day with at least three water replacements until it reached the swelling equilibrium. All other different two-zwitterionic-network hydrogels were prepared following the same method but with different zwitterionic components and composition ratios. Hereafter, the two-zwitterionic-network hydrogels were named as pA/pB [x_1-y_1-z_1/x_2-y_2-z_2] where A and B were the abbrevations of the

zwitterionic monmer used to form ZMN1 and ZMN2, respectively; x_i, y_i and z_i (i=1, 2) were monomer molality (m), crosslinker and initiator concentration (mol% respect to corresponding monomer) of ZMNi, respectively.

For parent zwitterionic hydrogels preparation, the pCB hydrogel was prepared following the same protocol of pCB ZMN1 hydrogel as above. The pSB hydrogel was synthesized by a photo polymerization using 4 m of SB monomer, 0.1 mol% of MBAA crosslinker and 0.01 mol% of photoinitiator 1173 (molar percentages were both relative to the SB monomer) in a transparent sheet mold under the UV irradiation with a wavelength of 302 nm and 6 watt power for 6 h under the nitrogen atmosphere. The parent hydrogels were respectively named as pCB [1-4-0.1] and pSB [4-0.1-0.01] similar as described above, where x, y and z for [x-y-z] represent the molar monomer concentration (molality, m), crosslinker (mol% respect to monomer), and initiator concentration (mol% respect to monomer), respectively. For the pHEMA hydrogel, 1 m of HEMA monomer, 4 mol% of MBAA crosslinker, 0.1 mol% of iniator APS and 0.1 mol% of accelerator TEMED (molar percentages were both relative to the HEMA monomer) were mixed in ethanol/water (1:1, v/v) solution and then injected into the sheet mold to polymerize at 37 °C for 24 h. The as-prepared pHEMA hydrogel was then allowed to swell in deionized water for at least two days with water replacements until all the ethanol was removed and the hydrogel turned transparent. All other as-prepared hydrogels were also equilibrated in deionized water or PBS before use.

4.2.3 *Equilibrium Swelling Ratio and Equilibrium Water Content Test*

The equilibrium swelling ratios (ESR) of equilibrated hydrogels to their as-prepared state were evaluated *via* a dimension measurement method. The diameters (r_1) and heights (h_1) of as-prepared two-zwitterionic-network hydrogels fabricated from ZMN1 disks with a fixed dimension

of Φ5 mm × 0.5 mm were measured. The as-prepared hydrogels were then soaked in deionized water for two days for completely swelling and the diameters (r_2) and heights (h_2) of their corresponding equilibrated state were measured. The ESRs were calculated as follows:

$$ESR = \frac{r_2^2 \times h_2}{r_1^2 \times h_1} \times 100\%$$

The equilibrium water contents (EWC) of equilibrated hydrogels were measured through a gravimetric method. Hydrogel disks (10 mm in diameter and 1 mm in thickness) were allowed to swell in deionized water until reaching equilibrium at 37 °C. The equilibrated samples were taken out and their wet masses (M_w) were measured after the removal of excess water on the surface by rolling them on the filter paper. The samples were then snap-frozen in liquid nitrogen and lyophilized for 2 days until a complete dryness and their dry masses (M_d) were measured. The EWCs were calculated as follows:

$$EWC = \frac{M_w - M_d}{M_w} \times 100\%$$

Each measurement was performed in triplicate (independent replicates).

4.2.4 *Compressive and Tensile Test*

Hydrogels were allowed to reach swelling equilibrium in deionized water for one day at room temperature before testing. The compressive property of hydrogels was tested on a universal testing machine (Instron 5543A, Instron Corp., Norwood, MA) with a 10 kN load cell at room temperature. Biopsy punch was used to punch equilibrated hydrogels into 5 mm-diameter and 2 mm-thickness cylinders. The crosshead speed was set at 1 mm/min and the test limit of compressive strain was set at 99% to protect the machine. The tensile property of hydrogels was

tested on a universal testing machine (WDW-05, Si Pai Inc., China) with a 500 N load cell at room temperature. The equilibrium sheet samples were cut into dumbbell shape with a length of 30 mm, a gauge length of 12 mm, a width of 2 mm and a thickness of 1 mm and the crosshead speed was set at 50 mm/min. Each measurement was performed at least in triplicate (independent replicates).

4.2.5 *Fibrinogen Adhesion Test by Enzyme-Linked Immunosorbent Assay*

Human fibrinogen adhesion test of hydrogels was performed in 24-well tissue culture polystyrene (TCPS) plates utilizing an enzyme-linked immunosorbent assay (ELISA) method following our previous reports[205,222] (*7, 35*). Prior to the experiment, all the tested hydrogels were equilibrated in PBS and then cut into uniform disks (5 mm in diameter and 1 mm in thickness) with the biopsy punch. Each sample disk was first incubated in 1 mL of fibrinogen solution (1 mg/mL, freshly prepared in PBS) at 37 °C for 1.5 h. Before being transferred into new wells, the samples were rinsed with 5 × 2 mL PBS to remove dissociative fibrinogen. 1 mL of HRP conjugated anti-fibrinogen solution (1 μg/mL, in PBS) was then added in each well followed by incubation at room temperature for 1.5 hours. All the samples were then transferred to new wells after another 5 washes with PBS. 1 mL of OPD solution (1 mg/mL, with 0.1 M citrate phosphate, pH 5.0) containing 0.03% hydrogen peroxide was added. After 15 min of incubation at room temperature, the enzymatic reaction was stopped by adding 1 mL of 1N HCl. The absorbance values at 492 nm of all the samples were recorded by a plate reader (Cytation 3, BioTek, Winooski, VT) and were normalized to that of TCPS (96-well, control). Each measurement was performed in quadruplicate (independent replicates).

4.2.6 *Serum Fouling test by BCA Assay*

Human serum fouling of the hydrogels was evaluated *via* the BCA method. Pre-equilibrated hydrogel disks in PBS (5 mm in diameter and 1 mm in thickness) were suspended into 400 μL of undiluted human pooled serum in 24-well TCPS plates with one disk per well followed by incubation at 37 °C for 2 h. Before being transferred into new wells, all the samples were rinsed with 1 mL of PBS five times to remove the dissociative proteins. A BCA assay was then directly carried out to determine the amount of proteins adsorbed on the hydrogel and the absorbance values at 562 nm of all the samples were recorded by a plate reader and were normalized to that of TCPS (96-well, control). Each measurement was performed in triplicate (independent replicates).

4.2.7 *Platelet Adhesion Analysis by Lactate Dehydrogenase Assay*

Platelets used for adhesion analysis were freshly collected from the blood of two 11- to 13-week-old female Sprague Dawley (SD) rats. Fresh blood collected in Becton Dickinson (Franklin Lakes, NJ) plasma tube (75 USP units of sodium heparin [spray coated]) was then immediately centrifuged at 200 g for 10 min to get platelet rich plasma (PRP). The residue was further centrifuged at 2000 g for 20 min to obtain platelet poor plasma (PPP). PRP and PPP were gently remixed and the final platelet density was adjusted to 2×10^8 mL^{-1}. Pre-equilibrated hydrogel disks in PBS (5 mm in diameter and 1 mm in thickness) were placed in 24-well TCPS plates with one disk per well, immersed with 400 μL of final platelet solution and incubated at 37 °C for 3 h. After incubation, the disks were rinsed with 1 mL of PBS five times and then transferred into new wells. The number of adhered platelets was determined by the lactate dehydrogenase (LDH) assay. For LDH assay, the rinsed samples were soaked in 24-well TCPS plates with one disk per well, 300 μL PBS and 10 μL 10 × lysis buffer and incubated at 37 °C, 5% CO_2 for 45 minutes. 50 μL reaction

mixtures were then added into each well and incubated at room temperature for 30 minutes in the dark. To stop the reaction, 50 μL stop solution was added to each well and mixed by gentle pipetting. Finally 200 μL of the mixture was taken out from each well and the absorbance at 490 nm and 680 nm was measured by a platelet reader. The LDH activity was determined by subtracting the absorbance value of 680 nm from that of the 490 nm. Data were normalized to that of TCPS (96-well, control). Each measurement was performed in triplicate (independent replicates).

4.2.8 *Cell Adhesion Assay*

Rat pancreatic β cells [RIN-m5F] and murine DC 2.4 dendritic cells were selected for the cell adhesion assay of the hydrogels. In brief, PBS pre-equilibrated and UV sterilized hydrogels disks (5 mm in diameter and 1 mm in thickness) were placed individually into the wells of a 96-well plate. RIN-m5F (suspended in ATCC-formulated RPMI-1640 Medium with 10% FBS) or DC 2.4 cells (suspended in RPMI-1640 with 10% FBS, 1X L-glutamine, 1X non-essential amino acids, 1X HEPES buffer solution, and 0.0054X β-mercaptoethanol) were seeded onto the hydrogels at a density of 1×10^5 cells/mL or 5×10^4 cells/mL, respectively, and allowed to grow for 24 h at 37 °C in a humidified atmosphere with 5% CO_2. The medium was then removed and the hydrogels were gently washed with PBS and re-immersed with PBS. For optical imaging, cells adhesion and cellular morphology on the samples were observed at 200 × magnification using a microscope (Nikon Eclipse 80i). For quantitative analysis of adhered cells, the samples were gently transferred to new wells and then the LDH assay was carried out following the protocol as described above. All the data were normalized to that of TCPS (96-well, control). Each measurement was performed in triplicate (independent replicates).

4.2.9 *Hydrogel sterilization by Autoclaving*

The pCB/pSB ZEN hydrogels were sterilized *via* a standard autoclaving method. As-prepared ZEN hydrogels were soaked in water or PBS until equilibrium and then sterilized at 121 °C for 30 min together with corresponding soaking solutions. The sterilized hydrogels were then cooled to room temperature for further use or test. Hydrogels experienced one to three rounds of such heating-cooling autoclaving sterilization process were named as ZEN-R1, ZEN-R2 and ZEN-R3, respectively. The subsequent protein and cell adhesion tests of autoclaved ZEN hydrogels all followed the protocols described as above.

4.2.10 *In vivo Implantation of ZEN Hydrogels*

6 to 8-week-old male C57BL/6 mice were purchased from Charles River Labs. All the animal experiments were operated according to the federal guidelines and were approved by the University of Washington Institutional Animal Care and Use Committee (IACUC). Subcutaneous implantation experiments were carried out to evaluate the foreign body reaction and fibrous capsule formation of pCB/pSB ZEN hydrogels. pHEMA hydrogels implantation were selected as positive controls according to our previous study (*8*). Negative controls were set by skin tissues of mice that did not undergo any surgeries or other experiments. ZEN hydrogel (1 cm × 1 cm and 1 cm × 3 cm in dimension) and pHEMA hydrogel (1 cm × 1 cm in dimension) sheets were sterilized by autoclaving (121 °C for 30 min in PBS) and UV (for 30 min), respectively, prior to implantation to prevent bacterial infection. The animal surgery was performed under anesthesia and aseptic conditions. In brief, each mouse was subcutaneously implanted with two ZEN or two pHEMA hydrogels symmetrically on the back, with one hydrogel on each side. The two hydrogel samples in all mice did not overlap throughout the whole study. Mice were anesthetized using 3% isoflurane and shaved. The area where the incision would be made was sterilized using Iodine and 70%

ethanol. A longitudinal incision (no longer than 2 cm) was made on the central dorsal surface using surgical scissors to provide access to the subcutaneous space. Subcutaneous pockets on either side of the incision were created with a blunt forceps for the implantation of the hydrogel samples. After implantation, the incisions were closed using wound nylon sutures. Mice were monitored until recovery from anesthesia and housed for 1 week, 4 weeks, 12 weeks or 1 year before retrieving samples. For each experiment group/condition, three different mice were implanted with hydrogel samples or not (as negative control) to provide statistical significance in the histological studies (n = 3). The researchers did not subjectively select starting materials or animals. No animals were lost before reaching their assigned endpoints.

4.2.11 *Hydrogels Retrieval and Histological Analysis*

1 week, 4 weeks, 12 weeks or 1 year after implantation, mice were euthanized by CO_2 asphyxiation. The hydrogel samples together with the adjacent skin tissue were excised by cutting along the edge of the hydrogels. Negative controls were set by skin tissues of mice that did not undergo any surgeries or other experiments. The retrieved skin samples were then fixed in 4% paraformaldehyde for at least 2 days and then embedded in paraffin. Each retrieved skin tissue was sectioned with a thickness of 4 μm and mounted onto slides for histological staining. The inflammatory response was examined by staining with hematoxylin & eosin (H&E), in which cell nuclei would appear dark purple and cell cytoplasm pink. The fibrous capsule formation was stained using Masson's trichrome staining, which stains collagen blue, cell cytoplasm red and cell nuclei black. Each stained slide was examined at 100 × magnification using a Leica DMIL Inverted Phase Contrast Microscope and images were captured from at least three different sites alongside the interface between the subcutaneous skin tissue and the hydrogel. Examination and quantification of histological sections were done by three independent researches with at least

three random images/fields per sample and per animal. Researchers were blinded to sample identity. The collagen densities of the subcutaneous skin tissues from different mice were analyzed with corresponding Masson's trichrome staining histological images (as described above) *via* the ImageJ software. In this study, the area proportion of the collagen (where stained with blue) was defined as the collagen density of the selected area. For each image, the collagen densities were continuously collected in the subcutaneous skin tissue within 50 μm at 10-μm increments starting from the interface with the hydrogel sample (for negative control, starting from the internal surface adjacent to the back of the mouse). Each calculating area was in rectangular (10 μm × 100 μm in dimension) and was parallel to the interface. The starting calculating area was randomly selected alongside the interface for each image. Each skin tissue sample was analyzed in triplicate from three different corresponding histological images. For testing the dry weight and compressive strength of retrieved ZEN hydrogels, hydrogels were first slightly washed by deionized water after retrieval. Biopsy punch was then used to punch hydrogels into 5 mm-diameter disks. Compressive testing followed the same procedure as described above. Dry weights were measured after lyophilization. Each measurement was carried out in triplicate.

4.2.12 *Statistical Analysis*

All data are expressed and presented as means and standard deviation (SD). Statistical analyses were performed with OriginPro 8.5 software. A two-tailed Student's *t*-test was used for all statistical analyses. $P < 0.01$ was considered statistically significant.

4.3 Results and Discussion

4.3.1 *Mechanical Properties of ZEN Hydrogels*

Conventional hydrogels for medical applications, such as poly(ethylene glycol) (PEG) and poly(2-hydroxyethyl methacrylate) (pHEMA), have relatively weak mechanical properties, with compressive fracture stresses ranging from 0.6 to 3 MPa[112,213,223]. Traditional zwitterionic hydrogels, such as pCB, pSB, and poly(2-methacryloyloxyethyl phosphorylcholine) (pMPC), are quite weak as well, having a limit around 3 MPa[85,204]. In contrast, the pCB/pSB ZEN hydrogel was able to be smoothly compressed to a strain of 99% with a fracture stress of 22.3 MPa, and remained its original shape upon release (**Figure 4.1B**, **C**, and **Figure 4.2**). Similarly, the pCB/pSB ZEN hydrogel exhibited a large tensile strain of 169.9% with a fracture stress close to 1 MPa (**Figure 4.1D** and **E**), which is comparable to that of biological tissues such as blood vessels[205,224]. The tensile curve of the pCB/pSB ZEN hydrogel behaved in an elastomeric manner without obvious stress yielding. Moreover, the pCB/pSB ZEN hydrogel could be fabricated into many shapes, and was able to hold extensive deformation before returning to their original geometry (**Figure 4.1F** to **H**).

4.3.2 *Design Principles of ZEN Hydrogels*

To elucidate the universal design principles of the ZEN hydrogels, we studied the structure-property relationship between the two zwitterionic networks, pCB and pSB. First, we carried out an orthogonal compressive test of a series of hydrogels consisting of three different pCB networks and seven pSB networks, each varying in monomer concentrations and crosslinker ratios (**Figure 4.3A** to **C**). The monomer, crosslinker, and initiator concentrations resulting in the optimal compressive fracture stress for the pCB/pSB hydrogel were 1-4-0.1 (monomer-crosslinker-

initiator) for the pCB network and 4-0.1-0.01 for the pSB network. This indicated the importance of combining a higher-crosslinked (4 mol%) pCB network to provide elasticity, with a lower crosslinking density (0.1 mol%) in the pSB network to provide viscosity. Crosslinking density of the pSB network lower than 0.1 mol% would contribute to a fragile pCB/pSB hydrogel regardless of the composition of pCB network. The mass percentages of the pSB and pCB components corresponding to the optimal mechanical strength were 95% and 5%, respectively, which made pSB the major component and pCB the minor component (**Figure 4.3D**). A significant amount of the pSB component was able to be integrated due to the high swellability of the pCB component. Moreover, The critical "locking" effect was observed after the pCB/pSB ZEN hydrogel was immersed in water for swelling to equilibrium (**Figure 4.3E**). The volume of the equilibrated pCB/pSB ZEN hydrogel increased only slightly (~ 9%) from its as-prepared state, while its parent pCB hydrogel (1-4-0.1, monomer-crosslinker-initiator) had a large volume increase of about 500%. Under the same orthogonal study (**Figure 4.3F**), we observed other pCB/pSB formulations to also exhibit only small increases in volume, with equilibrium water contents (EWCs) kept around 60% ~ 66%. This suggested the "locking" effect to be universal in the pCB/pSB hydrogel system when pSB was the major-component network.

The first series of structure-property experiments above showed that the high strength of the pCB/pSB ZEN hydrogel was derived from an optimal elasticity/viscosity ratio of the two networks, which was achieved through the two key concepts: the high swellability of the pCB minor-component network, and a "locking" effect generated by the pSB major-component network. To demonstrate the importance of these two key concepts, we next compared other minor-component/major-component combinations of the two zwitterionic networks: pCB/pCB, pSB/pCB and pSB/pSB. We first conducted an orthogonal compressive test for pCB/pCB

hydrogels to examine the effect when pSB is not the major-component network (**Figure 4.4A**, **D**, **E**, and **Figure 4.5**). As expected, without pSB as the "locking" major-component network, all pCB/pCB hydrogels exhibited a large volume increase after reaching equilibrium in water (**Figure 4.4F**), resulting in weak mechanical properties. The highest fracture stress among all pCB/pCB combinations was only one fifth that of the pCB/pSB ZEN hydrogel. In the pSB/pCB system (**Figure 4.4B**, **D**, **E**, and **F**) where pSB being the minor-component network, there was also no "locking" effect, as the hydrogel increased 120% of its original size after reaching equilibration, resulting in a fracture stress only around 1 MPa. On the other hand, in the pSB/pSB system (**Figure 4.4C**, **D**, **E**, and **F**), the "locking" effect was observed as expected, along with a small increase in equilibrated volume around 7.9%. Even though all the pSB/pSB hydrogels exhibited improved mechanical strength when compared to traditional pSB hydrogels — with the optimal pSB/pSB (1-4-0.1/4-0.1-0.01) formulation having a compressive fracture stress around 10 MPa — the maximum compressive fracture stress was only half of that of the pCB/pSB ZEN hydrogel. This could be due to the inferior swellability of pSB as the minor-component network, resulting in a lower mass percentage of the major-component network (less than 85%) which affected the mechanical strength of the pSB/pSB hydrogels. Together, these results confirm the essential design principles of the ZEN hydrogels: having a minor-component network with high swellabiltiy and a major-component network with the "locking" effect are critical to realize ZEN hydrogels with an optimal elasticity/viscosity ratio. The ZEN hydrogels could also be achieved when other super-hydrophilic zwitterionic materials such as poly(trimethylamine N-oxide) (pTMAO)[220] with high swellability were used as the minor-component network and pSB as the major-component network with the "locking" effect, further resonating with the two key concepts of making the ZEN hydrogels (**Figure 4.6**).

4.3.3 *Long-term Subcutaneous Implantation of ZEN Hydrogels in Mice*

After elucidating the principles behind the high strength of the ZEN hydrogels, we continued to examine how living tissues respond to the presence of pCB/pSB ZEN hydrogels upon implantation. While many polymeric hydrogels, such as those based on PEG and pHEMA, have been developed for tissue engineering and regenerative medicine[207], they frequently elicit fibrous capsule formation upon subcutaneous implantation[225,226]. This is the result of triggering the foreign body reaction, a physiological response towards synthetic materials initiated by non-specific protein adsorption onto implant surfaces, followed by cell adhesion and the subsequent formation of fibrous tissue around the implants[19,93,204,206]. This "capsule" acts as an impermeable barrier that impedes nutrient and signal transport, often culminating in implant failure[207]. As non-specific protein adsorption and cell adhesion are the initial steps in this response, we first challenged the pCB/pSB ZEN hydrogel with *in vitro* exposure to fibrinogen, undiluted human serum, rat-derived platelet-rich plasma, and two adherent cell lines (rat pancreatic β cells [RIN-m5F] and murine DC 2.4 dendritic cells). The results were compared to those of pCB, pSB, and pHEMA hydrogels (**Figure 4.7** and **Figure 4.8**). We found the pCB/pSB ZEN hydrogel to maintain excellent non-fouling properties (**$P < 0.01$) similar to its parent zwitterionic hydrogels, pCB and pSB, but the pHEMA hydrogel was unable to prevent non-specific protein adsorption and cell adhesion as effectively ($^{\#\#}P < 0.01$). The pCB/pSB ZEN hydrogel also exhibited excellent stability after sterilization — even after three rounds of routine autoclaving cycles (121°C, 30 minutes each), the pCB/pSB ZEN hydrogel retained its non-fouling properties against proteins, platelets, and cells (**$P < 0.01$) (**Figure 4.9**).

Encouraged by the unique combination of strength, durability, and non-fouling properties exhibited by the pCB/pSB ZEN hydrogel, we last explored its long-term *in vivo* fibrous capsule

resistance upon implantation. Both pCB/pSB ZEN and pHEMA hydrogel samples were subcutaneously implanted on the back of immunocompetent C57BL/6 mice for up to one year. Skin tissues in contact with the hydrogel samples were collected from mice at various time intervals (1, 4, 12 weeks, and 1 year) to evaluate potential fibrous capsule formation. Positive controls were skin tissues collected from mice that were implanted with pHEMA hydrogels[93], while negative controls were collected from mice that did not undergo any surgeries or other experiments. All skin tissues were further treated with hematoxylin & eosin (H&E) and Masson's trichrome staining for histological analysis. One week after implantation, basophilic discoloration and obvious cell accumulation were observed at the tissue interface in direct contact with pHEMA hydrogels, indicating an acute inflammatory response (**Figure 4.10A**). As inflammation is known to trigger recruitment of collagen-secreting fibroblasts to encapsulate and isolate the foreign material[19,207], it was not surprising to observe the formation of an initial collagen layer in these mice after one week (**Figure 4.10B** and **C**, $^{**}P < 0.01$). By the fourth week of pHEMA hydrogel implantation, a dense and mature collagenous capsule had formed, which further thickened after one year (**Figure 4.10B** and **C**).

In contrast, few to no cells were observed at the interface between tissue and implanted pCB/pSB ZEN hydrogels after one week (**Figure 4.10A**), similar to that of the negative controls, suggesting they elicited little or no acute inflammation — a phenomenon derived from excellent non-fouling properties[19,85,206]. Remarkably, over the entire span of this study, skin tissues adjacent to pCB/pSB ZEN hydrogels showed neither signs of inflammation (**Figure 4.11**) nor any dense fibrous capsule formation, but instead a loose subcutaneous structure similar to that of the negative control skin tissues (**Figure 4.10B** and **C**). Furthermore, the pCB/pSB ZEN hydrogel samples maintained their shape and were highly durable, with no obvious degradation

and loss in mechanical properties after one full year of implantation (**Figure 4.10D** and **E**). This suggests that ZEN hydrogel materials are enable to maintain long-term fibrous capsule-resistance and durability *in vivo*.

4.4 CONCLUSIONS

In summary, we report here a Zwitterionic-Elastomeric-Networked "ZEN" hydrogel exhibiting a unique combination of mechanical strength and long-term fibrous capsule-resistance. The key feature of a ZEN hydrogel is its composition from two different pure zwitterionic networks — a tightly-crosslinked minor-component network that possesses high swellability, and a loosely-crosslinked major-component network that exhibits critical "locking" effect. We found the pCB/pSB ZEN hydrogel to exhibit excellent elasticity under extensive deformation, mitigate the fibrous capsule formation, and remain stable without degradation or loss of mechanical strength when implanted subcutaneously for up to one year in mice. We envision the durability and fibrous capsule-resistance of ZEN hydrogels to provide a new route to long-standing ambitions of implantable materials.

4.5 FIGURES

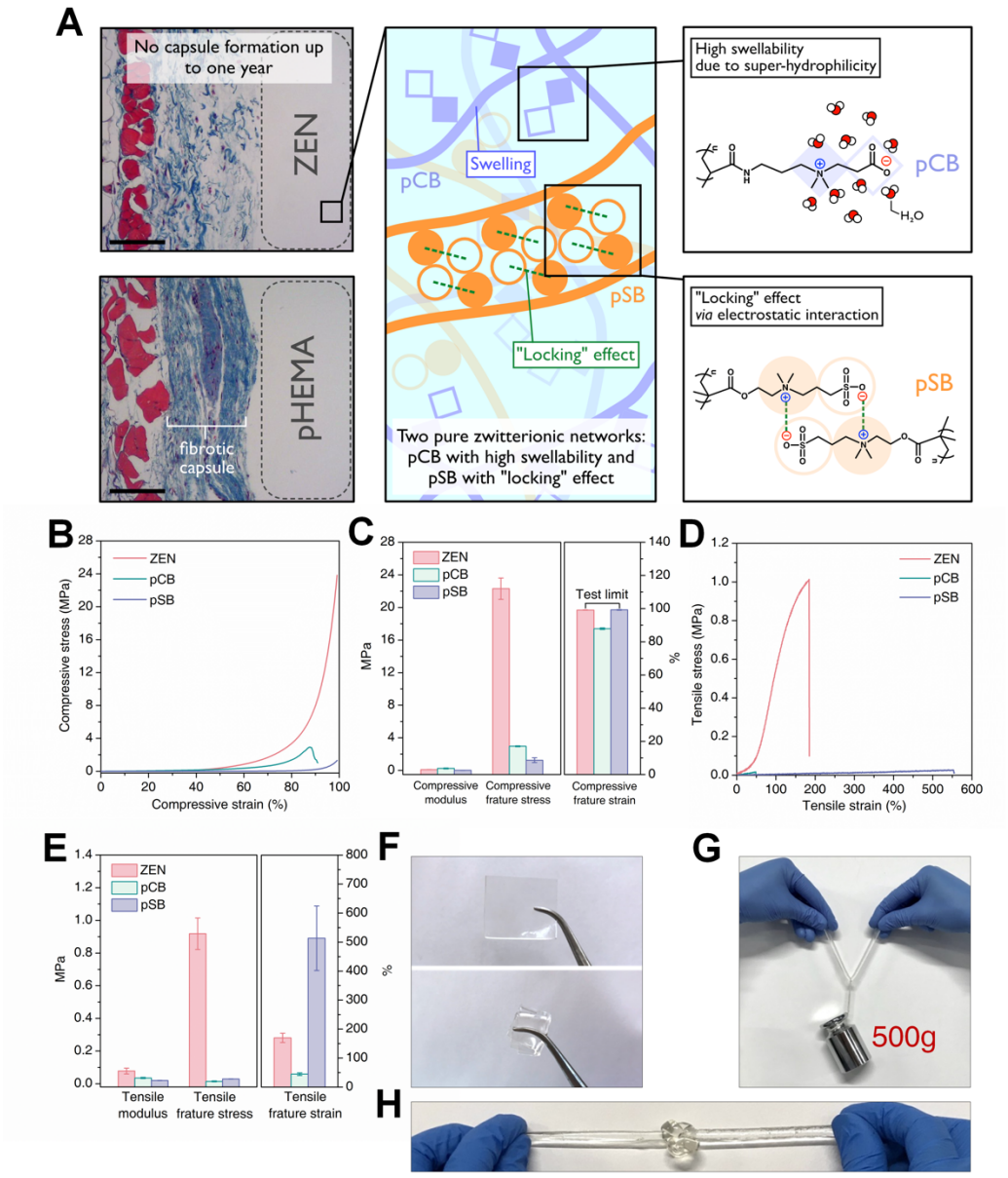

Figure 4.1. pCB/pSB ZEN hydrogels with high mechanical properties.

A. Schematic illustration of the design principles of the high-strength pCB/pSB ZEN hydrogel. Left, Masson's trichrome staining results for skin tissues of mice with hydrogels subcutaneous implantation for one year. Skin tissue of mice that implanted with pHEMA hydrogel was set as

positive control with fibrous capsule formation. Scale bars represent 100 μm. **B.-E.** Representative uniaxial compressive curves (**B**), compressive modulus, fracture stress and fracture strain (**C**), representative tensile curves (**D**), and tensile modulus, fracture stress and fracture strain (**E**) of the pCB/pSB ZEN, pCB [1-4-0.1], and pSB [4-0.1-0.01] hydrogels. **F.** The pCB/pSB ZEN hydrogel sheet can be stretched, twisted, and folded repeatedly without any visible damage observed. **G.-H.** The pCB/pSB ZEN hydrogel rope with a cross-section diameter of 6 mm can hold a weight of 500 grams (**G**), and can tie knots without breaking (**H**). Note that *x*, *y* and *z* for [*x*-*y*-*z*] represent the molar monomer concentration, crosslinker (mol% respect to monomer), and initiator concentration (mol% respect to monomer), respectively.

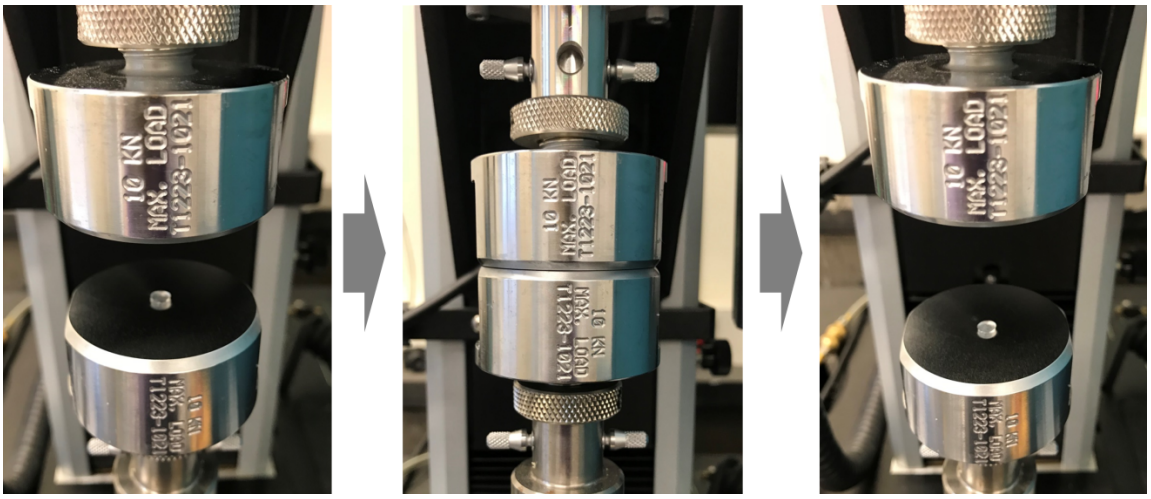

Figure 4.2. Representative images of the pCB/pSB ZEN hydrogel disk under a universal uniaxial compressive test.

The sample disk kept its original shape and appearance after being released from a compressive test to the testing limit of the tester when two anvils almost touched.

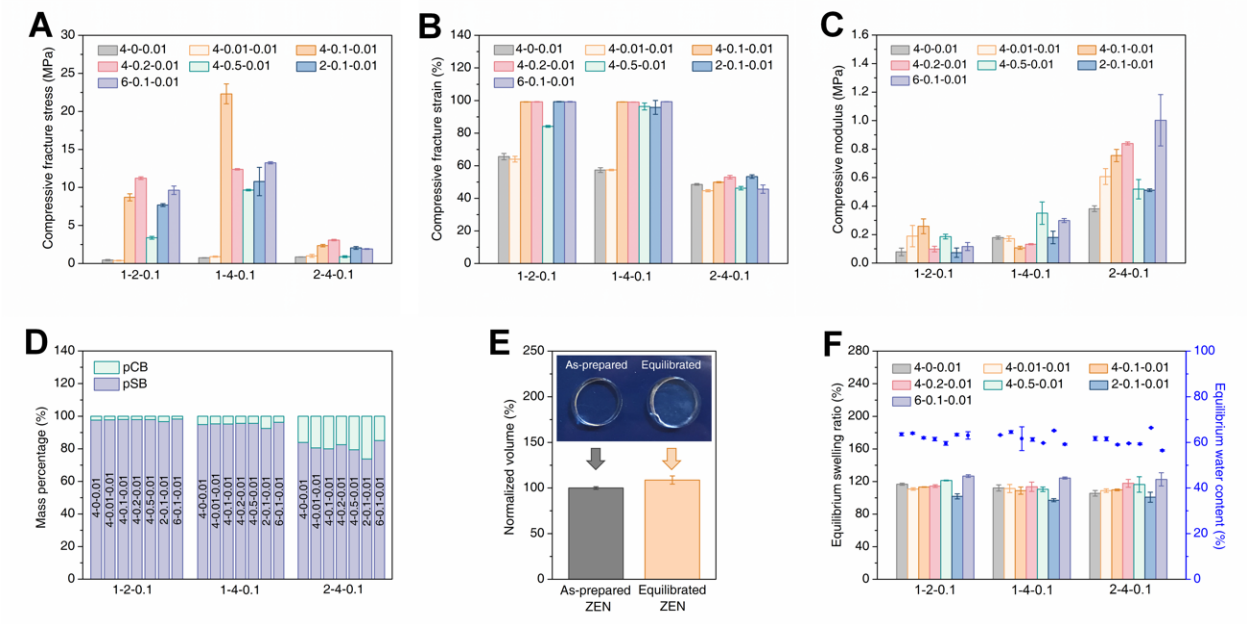

Figure 4.3. Mechanical and swelling properties of a series of pCB/pSB hydrogels.

A.-D. Compressive fracture stress (**A**), compressive fracture strain (**B**), compressive modulus (**C**), and component mass percentage (**D**) of a series of pCB/pSB hydrogels with combinations of three pCB network (1-2-0.1, 1-4-0.1, and 2-4-0.1) and seven pSB network (4-0-0.01, 4-0.01-0.01, 4-0.1-0.01, 4-0.2-0.01, 4-0.5-0.01, 2-0.1-0.01, and 6-0.1-0.01) component ratios. (**E**) Volume change of the pCB/pSB ZEN hydrogel before and after reaching equilibrium in water. The volume of the equilibrated pCB/pSB ZEN hydrogel was normalized to the corresponding as-prepared ZEN hydrogel. (**F**) Equilibrium swelling ratios and equilibrium water contents of a series of pCB/pSB hydrogels with combinations of three pCB network and seven pSB network component ratios. Note that *x*, *y*, and *z* for *x*-*y*-*z* represent the molar monomer concentration, crosslinker (mol% respect to monomer), and initiator concentration (mol% respect to monomer) of corresponding network, respectively.

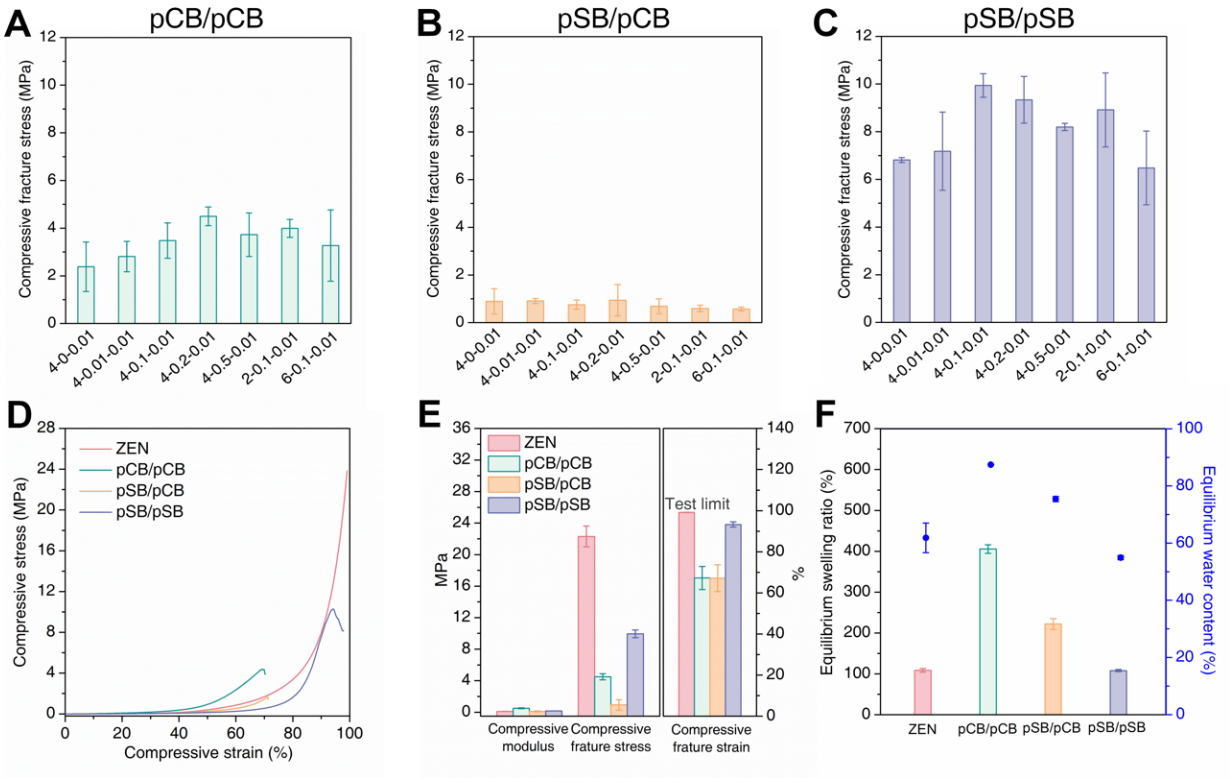

Figure 4.4. Essential design principles of the ZEN hydrogels.

A minor-component network with high swellabiltiy and a major-component network with the "locking" effect are the essential design principles of the ZEN hydrogels. **A.-C.** Compressive fracture stress of pCB/pCB (**A**), pSB/pCB (**B**), and pSB/pSB hydrogels (**C**). The minor-component network of these hydrogels was made according to the composition of 1-4-0.1. The major-component network was made according to seven different compositions as indicated on the x-axis. *x*, *y*, and *z* for *x*-*y*-*z* represent the molar monomer concentration, crosslinker (mol% respect to monomer), and initiator concentration (mol% respect to monomer) of corresponding network, respectively. **D.-F.** Representative compressive curves (**D**) compressive modulus, fracture stress and fracture strain (**E**), and equilibrium swelling ratios and equilibrium water contents (**F**) of the pCB/pSB ZEN, pCB/pCB, pSB/pCB, and pSB/pSB hydrogels. The pCB/pSB ZEN and pSB/pSB

hydrogels were made according to the composition of 1-4-0.1/4-0.1-0.01, while pCB/pCB and pSB/pCB hydrogels were made according to the composition of 1-4-0.1/4-0.2-0.01. Note that x, y, and z for x_1-y_1-z_1/x_2-y_2-z_2 represent the molar monomer concentration, crosslinker (mol% respect to monomer), and initiator concentration (mol% respect to monomer) for the two component networks, respectively.

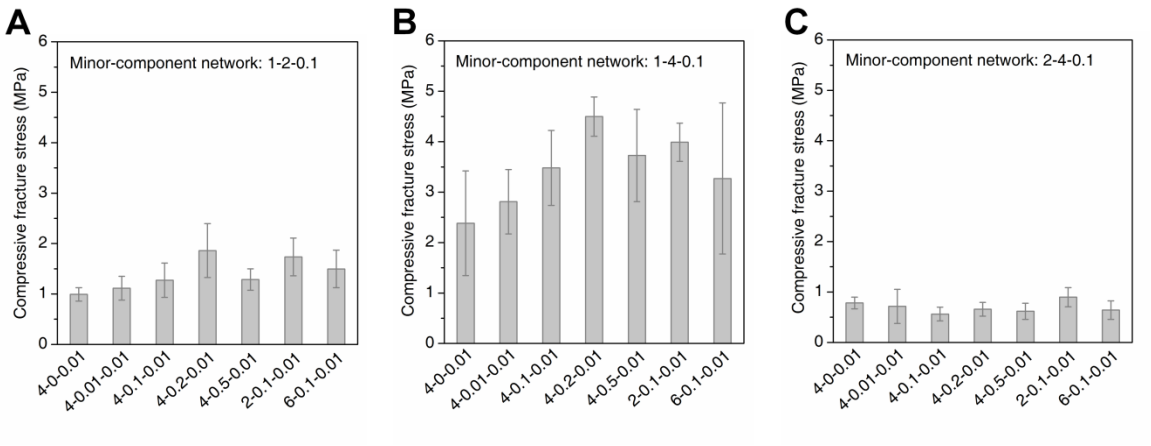

Figure 4.5. Compressive fracture stress of a series of pCB/pCB [minor-component/major-component network] hydrogels.

The minor-component networks were made according to the composition of (**A**) 1-2-0.1, (**B**) 1-4-0.1, and (**C**) 2-4-0.1, respectively. The major-component networks were made according to seven different compositions as indicated in the x-axis. Note that *x*, *y* and *z* for *x*-*y*-*z* represent the molar monomer concentration, crosslinker (mol% respect to monomer), and initiator concentration (mol% respect to monomer), respectively.

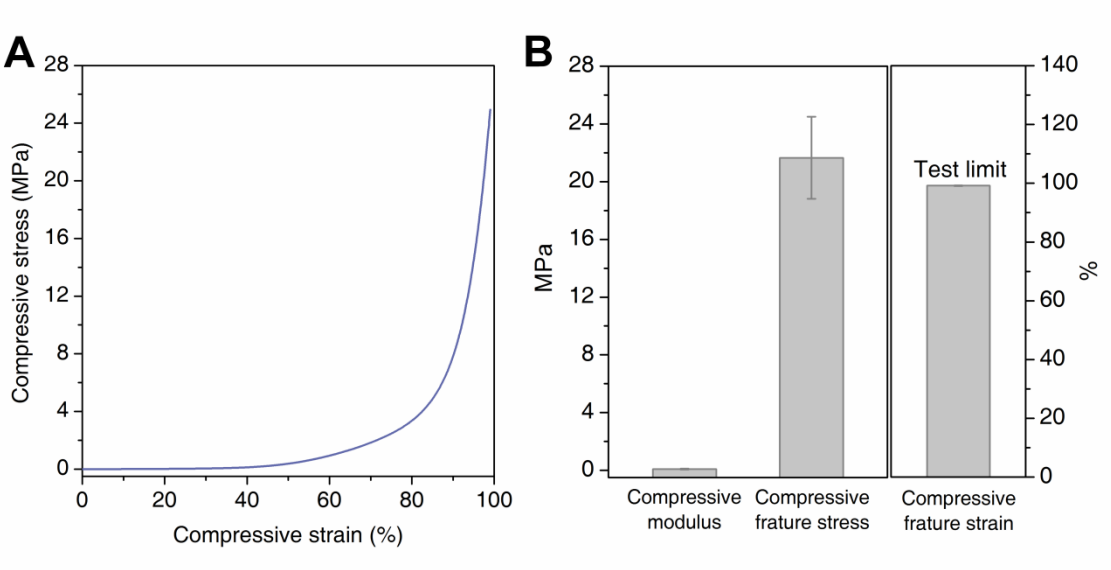

Figure 4.6. The compressive behavior of the pTMAO/pSB ZEN hydrogel.

The pTMAO/pSB ZEN hydrogel was made according to the composition of 1-4-0.1/4-0.1-0.01. Note that *x*, *y*, and *z* for x_1-y_1-z_1/x_2-y_2-z_2 represent the molar monomer concentration, crosslinker (mol% respect to monomer), and initiator concentration (mol% respect to monomer) for the two component networks, respectively. **A.** Representative compressive curve and **B.** Compressive modulus, fracture stress and fracture strain of pTMAO/pSB hydrogel.

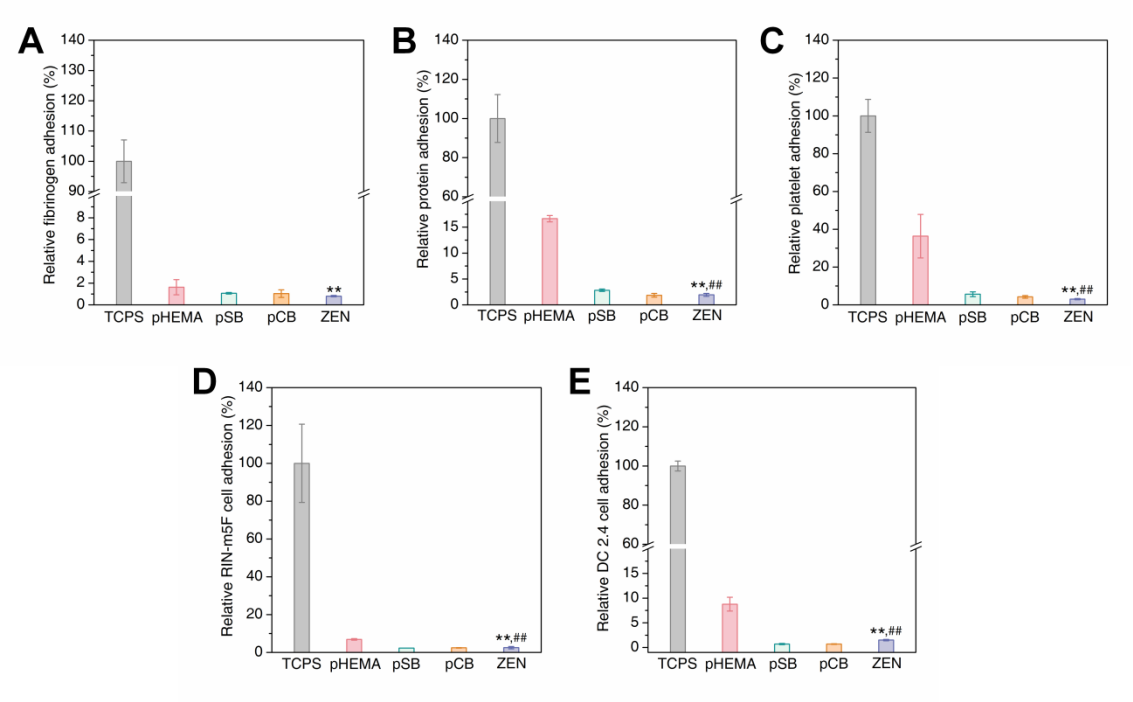

Figure 4.7. Biofouling tests of different material surfaces.

Relative (**A**) human fibrinogen protein, (**B**) undiluted human serum proteins adsorption, (**C**) rat platelets, (**D**) RIN-m5F cells, and (**E**) DC 2.4 cells adhesion onto the tissue culture polystyrene (TCPS) and different hydrogel surfaces. All the data were normalized with respect to TCPS. $^{**}P < 0.01$ *vs.* TCPS, $^{\#\#}P < 0.01$ *vs.* pHEMA.

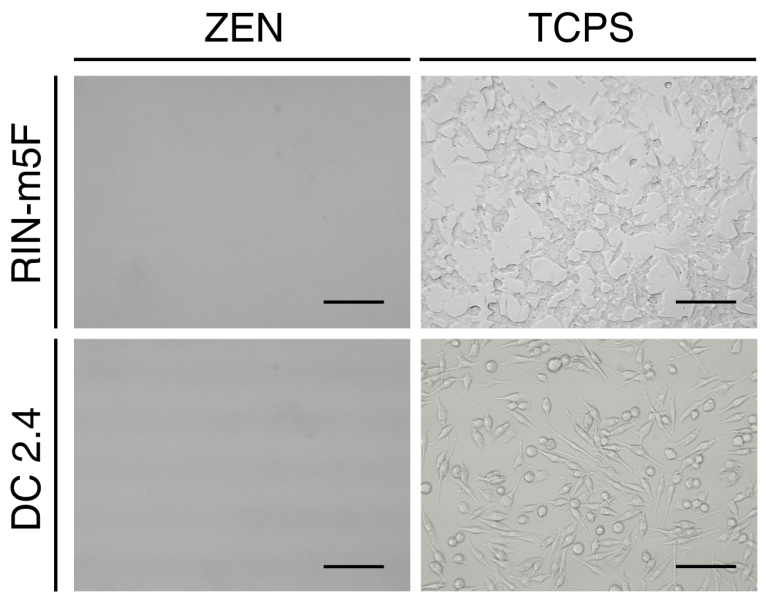

Figure 4.8. Cells adhesion on different material surfaces.

Optical images of RIN-m5F cells and DC 2.4 cells adhered onto tissue culture polystyrene (TCPS) and the pCB/pSB ZEN hydrogel surfaces. Scale bars represent 50 μm.

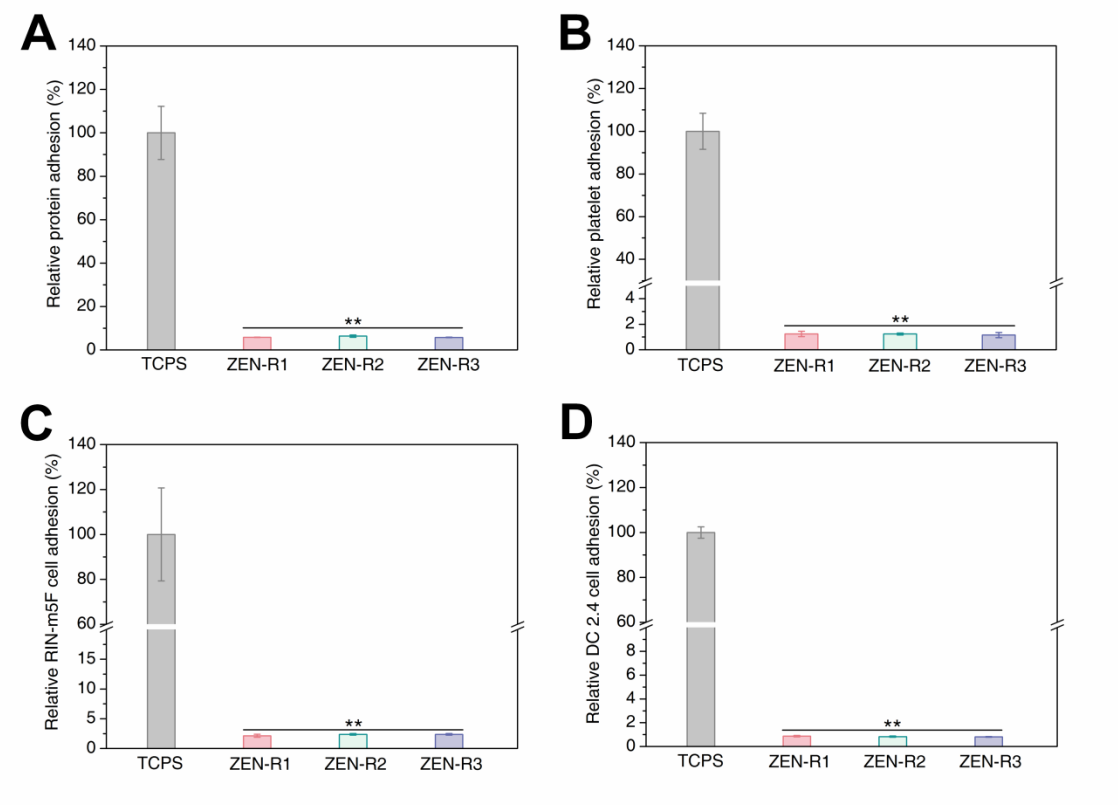

Figure 4.9. Biofouling tests of ZEN hydrogel surfaces after autoclaving sterilization.

Relative (A) undiluted human serum proteins, (B) rat platelets, (C) RIN-m5F cells, and (D) DC 2.4 cells adhesion onto the tissue culture polystyrene (TCPS) and the pCB/pSB ZEN hydrogel surfaces after one to three rounds of autoclaving sterilization. Each round of autoclaving sterilization is indicated as ZEN-R1, ZEN-R2, and ZEN-R3, respectively. All the data were normalized with respect to TCPS. $^{**}P < 0.01$ *vs.* TCPS.

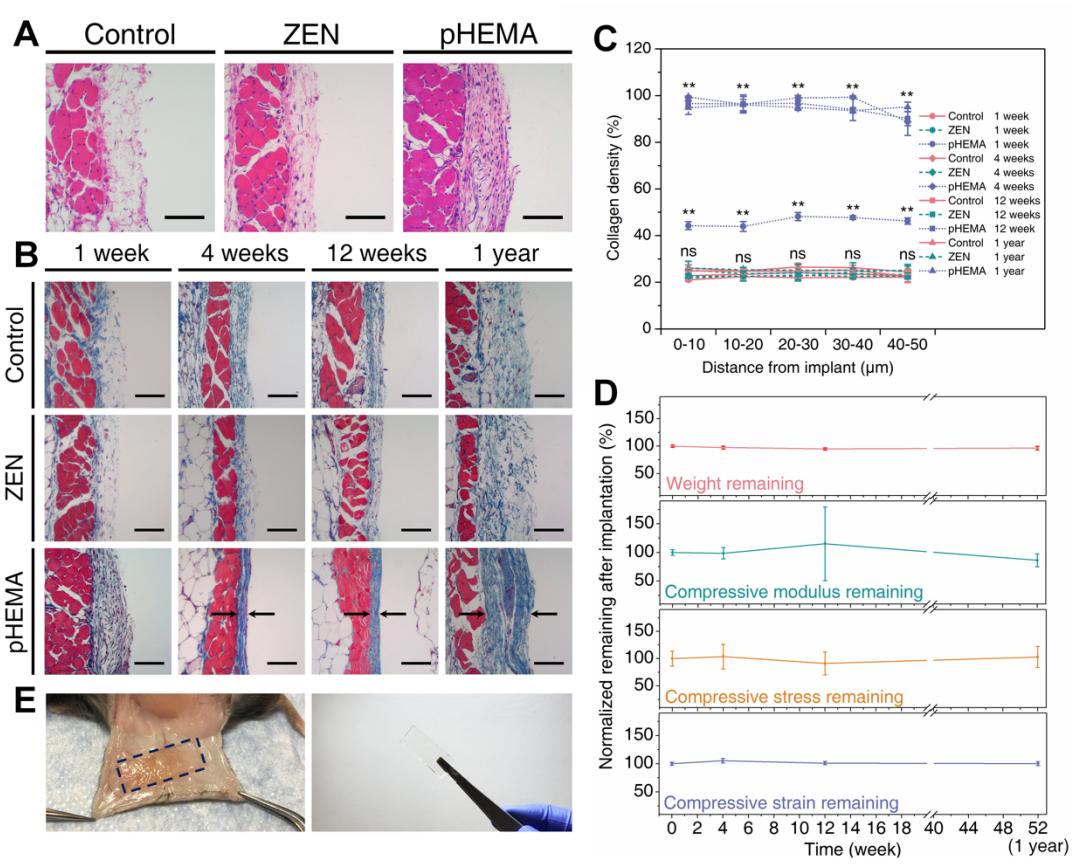

Figure 4.10. pCB/pSB ZEN hydrogels present long-term fibrous capsule-resistance and durability after subcutaneous implantation in mice up to one year.

A.-B. H&E staining for skin tissues in contact with the ZEN and pHEMA hydrogels after one week of implantation (**A**). The basophilic discoloration and increased cell counts (stained dark purple) at the interface in contact with pHEMA hydrogels indicates the accumulation of cells into the interface. Masson's trichrome staining for skin tissues with different hydrogel samples after implantation for 1, 4, 12 weeks, and 1 year (**B**). Black arrows indicate the fibrous capsule. Positive controls were skin tissues collected from mice that were implanted with pHEMA hydrogels, while negative controls were collected from mice that did not undergo any surgeries or other experiments. Scale bars represent 100 μm. $n = 3$ for all the implantation experiments (three mice

per experiment group/condition, two hydrogel samples per mouse for ZEN or pHEMA hydrogels implantation). (**C**) Collagen density in the skin tissues adjacent to the hydrogel samples after implantation for 1, 4, 12 weeks, and 1 year. Data were collected in the skin tissues within 50 μm from the interface (at 10-μm increments). $^{**}P < 0.01$ *vs.* control, *ns* = no statistical difference *vs.* control. (**D**) Normalized dry weight and compressive strength (compressive modulus, stress and strain) remaining of the ZEN hydrogels during the implantation for one year. All data were normalized to that of the original ZEN hydrogels before implantation (0 week). (**E**) Representative images of the implanted mice and retrieved ZEN hydrogels after one year implantation.

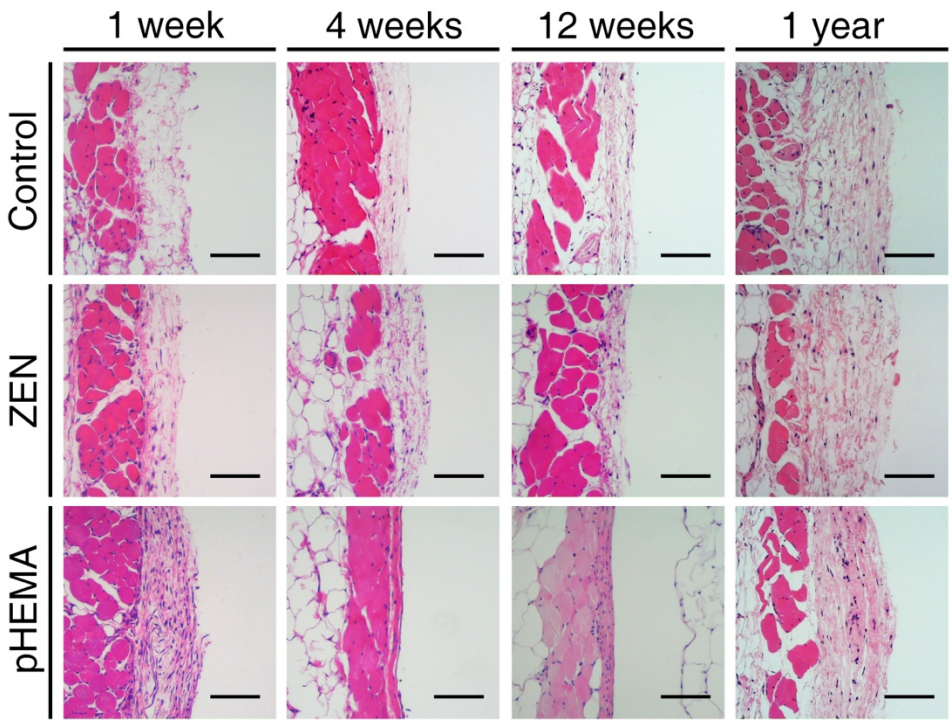

Figure 4.11. H&E staining for mouse skin tissues.

H&E staining for mouse skin tissues with different hydrogel samples after subcutaneous implantation in mice for 1, 4, 12 weeks, and 1 year. Positive controls were skin tissues collected from mice that were implanted with pHEMA hydrogels, while negative controls were collected from mice that did not undergo any surgeries or other experiments. $n = 3$ for all the implantation experiments (three mice per experiment group/condition, two hydrogel samples per mouse for ZEN or pHEMA hydrogels implantation). Scale bars represent 100 μm. The basophilic discoloration and increased cell counts (stained dark purple) at the tissue in contact with pHEMA hydrogels indicates the accumulation of cells into the interface.

Chapter 5. Conclusions and Future Work

5.1 Current Conclusions

Biotherapeutics are highly attractive in medicine due to their high potency uniquely paired with high specificity. The major drawbacks of this class of therapeutics, however, are poor stability in complex biological environments upon administration, suboptimal circulation half-lives due to rapid renal clearance, and potential immunogenicity due to its foreignness to the human body. As a result, biotherapeutics have relatively short therapeutic half-lives and low bioavailability when delivered through alternative routes. Implantable devices with complex functionalities bring unprecedented solutions to help improve the quality of life. However, hydrogel-based devices often lack mechanical endurances, and the majority of these devices suffer from the induction of the foreign body reaction which greatly shortens their life expectancies. Therefore, suitable mechanical properties and their ability to mitigate the foreign-body reaction are the crucial requirements for these implantable devices. Zwitterionic pCB polymers have been demonstrated to exhibit their excellent biocompatibility for the applications of biotherapeutics and hydrogels, showing great potential for solving these unmet issues.

In this dissertation, we have developed platforms for biological drug delivery and implantable devices utilizing zwitterionic polymers to provide excellent solutions for the field of medicine. In the first part (Chapter 2 and Chapter 3), we developed a biological drug delivery platform for both small peptides and large protein drugs, in order to improve their pharmacokinetic properties. In Chapter 2, we conjugated a pCB polymer with a molecular weight of 66 kDa on to the native GLP-1 to protect the degradation of the native peptide from peptidases and to prolong the circulation half-life of the native GLP-1 and protect it from the degradation of peptidases. The

conjugation of a pCB polymer did not alter the structure of the native GLP-1 while the activity and potency of the peptide were maintained. The pCB-conjugated GLP-1 was able to provide glycemic control in mice for up to 6 days, which was achieved by the significantly improved circulation half-life (from minutes to 43 hours). The conjugation of pCB provides a potential solution for the fast clearance and rapid inactivation of the native GLP- 1, which shows promise for providing long-term glycemic control for treating T2DM.

In Chapter 3, we enhanced the entry of larger proteins into the systemic bloodstream through non-invasive pulmonary systemic delivery. From this study, pCB polymers stabilized bioscavenger Organophosphate hydrolase (OPH) when first delivered to the lung, then further facilitated the protein entering the bloodstream. The conjugation of pCB polymers greatly improved the bioavailability of OPH *via* pulmonary delivery, from 5% to 50%. The efficacy of OPH was also enhanced as animals given pCB-conjugated OPH (OPH-pCB) were able to withstand up to 5 times the median lethal dose (LD_{50}) on the same day of organophosphate poisoning. 24 hours after the delivery of OPH-pCB, animals also survived when given a dose that was three times the LD_{50}, while animals given native OPH all did not survive at the lethal dose (2X LD_{50}), as expected. The prevention of organophosphate poisoning through simple inhalation of OPH showed promising capability for protecting our warfighters under potential threats, and further demonstrated the capability of utilizing this zwitterionic polymer-based, non-invasive pulmonary protein drug delivery platform for more applications.

In Chapter 4, we designed a new class of zwitterionic hydrogels, the zwitterionic-elastomeric-networked (ZEN) hydrogels, which significantly improved their mechanical properties for the application of implantable devices in Chapter 4. The ZEN hydrogels were developed following the central principle of having a highly cross-linked but high in swelling

hydrogel as the minor network, and having a loosely cross-linked but strong intermolecular/intramolecular interaction hydrogel as the major network. The ZEN hydrogels also showed the "lock" effect, where the size and shape of the hydrogel would not change even after reaching equilibrium in water-based solutions, which is crucial for maintaining shape and mechanical properties after implanted in patients. The ZEN hydrogels were also able to withstand multiple rounds of autoclave sterilization, making it easy to be prepared for surgery. Lastly, we investigated its potential in resisting the foreign-body reaction *in vitro* and *in vivo*. The "non-fouling" property of the ZEN hydrogels avoided the non-specific adsorption of proteins and cells, showing promise for preventing the initiation of the foreign body response. The ZEN hydrogels was then shown to be highly biocompatible as no fibrous capsule elicited from foreign body reaction was formed even after one year of implantation. The ZEN hydrogels also showed good stability *in vivo*, as no loss in weight or mechanical properties was observed after long-term implantation. Therefore, the development of high strength, pure ZEN hydrogels which can resist fibrotic capsule formation shows promise for future applications in implantable devices, such as tissue engineering and regenerative medicine.

As a summary of the studies mentioned above, we have demonstrated the capacity of using zwitterionic pCB polymers as platforms for peptide therapeutics, non-invasive pulmonary systemic delivery of large biotherapeutics, and implantable devices. Zwitterionic polymers have shown their great strengths continuously in the fields of biotherapeutics and implantable materials, due to their non-immunogenic nature and ability to resist the foreign body reaction. This dissertation further provided new solutions to unmet challenges through the implementations of zwitterionic polymers.

5.2 FUTURE DIRECTIONS

The conjugation of high molecular weight polyethylene glycols (PEG) has been widely used to extend the half-life of protein therapeutics[48–52]. A new class of biotherapeutics, nucleic acid aptamers, are starting to emerge and are facing similar issues: degradation by nuclease and the rapid filtration by the kidney. Nucleic acid aptamers are short, single-stranded DNA or RNA molecules that are selected for binding to a specific target. RNA aptamers were first discovered in 1990 when several groups isolated the first RNA aptamers through the evolutionary processes[227–230]. Aptamers bind to the target molecules (typically soluble or cell-bound proteins) with high affinity and specificity. Therefore, they are an attractive alternative to therapeutic antibodies or peptide ligands. Aptamers possess many enticing features. They are small in size and flexible in structure, allowing them to interact with smaller targets that are considered inaccessible for antibodies. Compared with the delicate and expensive *in vivo* screening for antibody generation, aptamers can be isolated within days via a cost-efficient *in vitro* selection procedure. Lastly, aptamers are considered to be non-immunogenic, when recombinant antibodies might potentially trigger immune responses in patients. However, the development of commercial effective therapeutic aptamers has lagged, when compared with therapeutic antibodies[231–233]. Two main challenges that aptamers face are the degradation by nuclease and the rapid filtration by the kidney. Many modifications have been done to help improve the pharmacokinetic properties of aptamer-based therapeutics. Besides the sugar modifications (2'-fluoro, 2'-amino, 2'-*O*-methyl) for increasing nucleases resistance, PEGylation has been frequently used for prolonging the therapeutic half-life of the aptamers[234–236].

REG1 is an antithrombotic system consisting of an active anticoagulant (pegnivacogin) and a complementary control agent (anivamersen) that neutralizes the anticoagulant effect.

Pegnivacogin targets Factor IXa to prevent blood coagulation. Anivamersen, a complementary oligonucleotide, hybridizes with an inactivates pegnivacogin to quickly reverse the anticoagulation effect[237–239]. REG1 had begun the phase III clinical trial when the trial was terminated early due to severe allergic reactions in 1% of the patients enrolled[61]. The allergic reactions, however, were caused by the pre-existing anti-poly(ethylene glycol) antibodies (anti-PEG antibodies)[59,240]. As PEGylation is used more and more commonly to extend the half-life of biologics, pre-existing anti-PEG antibodies have started to gain more concern as reported that up to 44% of the population could have pre-existing anti-PEG antibodies[56–58,241–244]. Therefore, a novel aptamer delivery platform is desperately needed for the future of therapeutic aptamers.

The goal of this study will be to (1) develop a "pre-existing anti-PEG antibodies" animal model and (2) use zwitterionic pCB polymers to replace PEG and enhance the pharmacokinetics of the aptamer 9.3t (the original pegnivacogin). One study has previously developed two models to mimic the pre-existing anti-PEG antibodies in animals[245]: one is through two injections of PEGylated proteins - the first one is for initial exposure and the second one is for boosting. The other one is simply the infusion of commercialized anti-PEG antibodies. However, both methods were not ideal since the two injections of the PEGylated proteins might not be strong enough to induce enough anti-PEG antibodies, and the foreign anti-PEG antibodies infused could suffer from fast clearance, resulting in an inaccurate representation of the model. Therefore, we aim to develop a reliable model by adopting the dosage regimen of Pegloticase, a PEGylated uricase. More than 40% of the patients receiving Pegloticase became responders after four months of treatments due to the generation of anti-PEG antibodies[54]. We plan to first administer multiple weekly dosages of PEGylated uricase, and by monitoring the concentration and subtypes of the antibodies specific to PEG weekly, we will determine when the model is mature for further studies. Furthermore, a

previous study on the pharmacokinetic model has indicated the concentration of anti-PEG antibodies as low as 500 ng/mL could induce accelerated clearance of PEGylated nanoparticles[246]. We will also consider the anti-PEG antibodies concentration during our evaluation. pCB-conjugated uricase will also follow the same procedure, the generation of anti-pCB antibodies will also be evaluated. However, based on our previous studies, we are expecting no anti-pCB antibodies generated[87–89,91]. We will next develop a pCB conjugate of the aptamer, and study the *in vitro* enzyme assays, clotting assays, and antidote assays to determine the potency of the conjugate. The circulation half-life and the efficacy of the conjugate will be first evaluated in animals without any pre-treatment. Lastly, the conjugates would be challenged in the developed pre-existing antibody animal model to study the effect of the anti-PEG/pCB antibodies.

In this study, we aim to demonstrate that zwitterionic pCB polymers are an ideal alternative for biotherapeutics modification utilizing the case of pegnivacogin, and to provide aptamers with a new zwitterionic platform for future therapeutic applications.

BIBLIOGRAPHY

1. Miller, K. L. & Lanthier, M. Innovation in biologic new molecular entities: 1986–2014. *Nat. Rev. Drug Discov.* **14**, 83–83 (2015).
2. Ghilardi, N., Pappu, R., Arron, J. R. & Chan, A. C. 30 Years of Biotherapeutics Development—What Have We Learned? *Annu. Rev. Immunol.* **38**, 249–287 (2020).
3. Usmani, S. S. *et al.* THPdb: Database of FDA-approved peptide and protein therapeutics. *PLoS One* **12**, e0181748 (2017).
4. Wilson, C. J. Rational protein design: developing next-generation biological therapeutics and nanobiotechnological tools. *Wiley Interdiscip. Rev. Nanomedicine Nanobiotechnology* **7**, 330–341 (2015).
5. Duncan, R. The dawning era of polymer therapeutics. *Nat. Rev. Drug Discov.* **2**, 347–360 (2003).
6. Teo, A. J. T. *et al.* Polymeric Biomaterials for Medical Implants and Devices. *ACS Biomater. Sci. Eng.* **2**, 454–472 (2016).
7. Weber, J. S. & Mulé, J. J. Cancer immunotherapy meets biomaterials. *Nat. Biotechnol.* **33**, 44–45 (2015).
8. Kopeček, J. Hydrogel biomaterials: A smart future? *Biomaterials* **28**, 5185–5192 (2007).
9. Caló, E. & Khutoryanskiy, V. V. Biomedical applications of hydrogels: A review of patents and commercial products. *Eur. Polym. J.* **65**, 252–267 (2015).
10. Li, W. A. & Mooney, D. J. Materials based tumor immunotherapy vaccines. *Curr. Opin. Immunol.* **25**, 238–245 (2013).
11. Chew, S. A. & Danti, S. Biomaterial-Based Implantable Devices for Cancer Therapy. *Adv. Healthc. Mater.* **6**, 1600766 (2017).
12. Kontermann, R. E. Half-life extended biotherapeutics. *Expert Opin. Biol. Ther.* **16**, 903–915 (2016).
13. Krishna, M. & Nadler, S. G. Immunogenicity to Biotherapeutics – The Role of Anti-drug Immune Complexes. *Front. Immunol.* **7**, (2016).
14. Kuriakose, A., Chirmule, N. & Nair, P. Immunogenicity of Biotherapeutics: Causes and

Association with Posttranslational Modifications. *J. Immunol. Res.* **2016**, 1–18 (2016).

15. Kontermann, R. E. Strategies for extended serum half-life of protein therapeutics. *Curr. Opin. Biotechnol.* **22**, 868–876 (2011).
16. Zaman, R. *et al.* Current strategies in extending half-lives of therapeutic proteins. *J. Control. Release* **301**, 176–189 (2019).
17. Anderson, J. M. Inflammatory Response to Implants. *ASAIO J.* **34**, 101–107 (1988).
18. Kastellorizios, M., Tipnis, N. & Burgess, D. J. Foreign Body Reaction to Subcutaneous Implants. in *Advances in Experimental Medicine and Biology* **865**, 93–108 (2015).
19. Anderson, J. M., Rodriguez, A. & Chang, D. T. Foreign body reaction to biomaterials. *Semin. Immunol.* **20**, 86–100 (2008).
20. Ward, W. K. A Review of the Foreign-body Response to Subcutaneously-implanted Devices: The Role of Macrophages and Cytokines in Biofouling and Fibrosis. *J. Diabetes Sci. Technol.* **2**, 768–777 (2008).
21. Ratner, B. D. Biomaterials: Been There, Done That, and Evolving into the Future. *Annu. Rev. Biomed. Eng.* **21**, 171–191 (2019).
22. Langer, R. & Peppas, N. A. Advances in biomaterials, drug delivery, and bionanotechnology. *AIChE J.* **49**, 2990–3006 (2003).
23. Webber, M. J., Appel, E. A., Meijer, E. W. & Langer, R. Supramolecular biomaterials. *Nat. Mater.* **15**, 13–26 (2016).
24. Sadtler, K. *et al.* Design, clinical translation and immunological response of biomaterials in regenerative medicine. *Nat. Rev. Mater.* **1**, 16040 (2016).
25. Huebsch, N. & Mooney, D. J. Inspiration and application in the evolution of biomaterials. *Nature* **462**, 426–432 (2009).
26. Langer, R. & Tirrell, D. A. Designing materials for biology and medicine. *Nature* **428**, 487–492 (2004).
27. Chandra, P., Yoo, J. J. & Lee, S. J. Biomaterials in Regenerative Medicine. in *Translational Regenerative Medicine* 151–167 (Elsevier, 2015). doi:10.1016/B978-0-12-410396-2.00013-X
28. Anderson, J. M. Future challenges in the in vitro and in vivo evaluation of biomaterial biocompatibility. *Regen. Biomater.* **3**, 73–77 (2016).
29. Williams, D. F. Challenges With the Development of Biomaterials for Sustainable Tissue

Engineering. *Front. Bioeng. Biotechnol.* **7**, 127 (2019).

30. Hoang Thi, T. T. *et al.* The Importance of Poly(ethylene glycol) Alternatives for Overcoming PEG Immunogenicity in Drug Delivery and Bioconjugation. *Polymers (Basel).* **12**, 298 (2020).
31. Aguado, B. A., Grim, J. C., Rosales, A. M., Watson-Capps, J. J. & Anseth, K. S. Engineering precision biomaterials for personalized medicine. *Sci. Transl. Med.* **10**, eaam8645 (2018).
32. Hamburg, M. A. & Collins, F. S. The Path to Personalized Medicine. *N. Engl. J. Med.* **363**, 301–304 (2010).
33. Artzi, N. Materializing Personalized Medicine. *Adv. Mater.* **32**, 1908065 (2020).
34. Rewers, A. H. & Akturk, H. K. Ever-Increasing Insulin-Requiring Patients Globally. *IABETES Technol. Ther.* **20**, 10–13 (2018).
35. Mitragotri, S., Burke, P. A. & Langer, R. Overcoming the challenges in administering biopharmaceuticals: formulation and delivery strategies. *Nat. Rev. Drug Discov.* **13**, 655–672 (2014).
36. Leader, B., Baca, Q. J. & Golan, D. E. Protein therapeutics: a summary and pharmacological classification. *Nat. Rev. Drug Discov.* **7**, 21–39 (2008).
37. Lagassé, H. A. D. *et al.* Recent advances in (therapeutic protein) drug development. *F1000Research* **6**, 113 (2017).
38. Pisal, D. S., Kosloski, M. P. & Balu-Iyer, S. V. Delivery of Therapeutic Proteins. *J. Pharm. Sci.* **99**, 2557–2575 (2010).
39. Antosova, Z., Mackova, M., Kral, V. & Macek, T. Therapeutic application of peptides and proteins: parenteral forever? *Trends Biotechnol.* **27**, 628–635 (2009).
40. Frokjaer, S. & Otzen, D. E. Protein drug stability: a formulation challenge. *Nat. Rev. Drug Discov.* **4**, 298–306 (2005).
41. De Groot, A. S. & Scott, D. W. Immunogenicity of protein therapeutics. *Trends Immunol.* **28**, 482–490 (2007).
42. Kronenberg, S. *et al.* Current challenges and opportunities in nonclinical safety testing of biologics. *Drug Discov. Today* **18**, 1138–1143 (2013).
43. Baumann, A. Early Development of Therapeutic Biologics - Pharmacokinetics. *Curr. Drug Metab.* **7**, 15–21 (2006).

44. Sathish, J. G. *et al.* Challenges and approaches for the development of safer immunomodulatory biologics. *Nat. Rev. Drug Discov.* **12**, 306–324 (2013).
45. Ivens, I. A. *et al.* PEGylated Biopharmaceuticals. *Toxicol. Pathol.* **43**, 959–983 (2015).
46. Jevsevar, S., Kunstelj, M. & Porekar, V. G. PEGylation of therapeutic proteins. *Biotechnol. J.* **5**, 113–128 (2010).
47. Roberts, M. J., Bentley, M. D. & Harris, J. M. Chemistry for peptide and protein PEGylation. *Adv. Drug Deliv. Rev.* **64**, 116–127 (2012).
48. Harris, J. M. & Chess, R. B. Effect of pegylation on pharmaceuticals. *Nat. Rev. Drug Discov.* **2**, 214–221 (2003).
49. Champman, A. P. PEGylated antibodies and antibody fragments for improve therapy: a review. *Adv. Drug Deliv. Rev.* **54**, 531–545 (2002).
50. Webster, R. *et al.* PEGylated proteins: Evaluation of their safety in the absence of definitive metabolism studies. *Drug Metab. Dispos.* **35**, 9–16 (2007).
51. Jevsevar, S., Kunstelj, M. & Porekar, V. G. PEGylation of therapeutic proteins. *Biotechnol. J.* **5**, 113–128 (2010).
52. Alconcel, S. N. S., Baas, A. S. & Maynard, H. D. FDA-approved poly(ethylene glycol)–protein conjugate drugs. *Polym. Chem.* **2**, 1442 (2011).
53. Podobnik, B. *et al.* Conjugation of PolyPEG to Interferon Alpha Extends Serum Half-Life while Maintaining Low Viscosity of the Conjugate. *Bioconjug. Chem.* **26**, 452–459 (2015).
54. Cunha, R. N., Aguiar, R. & Farinha, F. Impact of pegloticase on patient outcomes in refractory gout: current perspectives. *Open Access Rheumatol. Res. Rev.* **Volume 10**, 141–149 (2018).
55. Schore, R. J. *et al.* Anti-Pegaspargase, Anti-Calaspargase Pegol , and Anti-Polyethelene Glycol Antibody Incidence in High Risk Acute Lymphoblastic Leukemia Patients Receiving Pegaspargase or Calaspargase Pegol and Associated Anaphylactic or Hypersensitivity Reaction Rates: Re. *Blood* **128**, 3965–3965 (2016).
56. Zhang, P., Sun, F., Liu, S. & Jiang, S. Anti-PEG antibodies in the clinic: Current issues and beyond PEGylation. *J. Control. Release* **244**, 184–193 (2016).
57. Chen, B.-M. *et al.* Measurement of Pre-Existing IgG and IgM Antibodies against Polyethylene Glycol in Healthy Individuals. *Anal. Chem.* **88**, 10661–10666 (2016).

58. Hershfield, M. S. *et al.* Induced and pre-existing anti-polyethylene glycol antibody in a trial of every 3-week dosing of pegloticase for refractory gout, including in organ transplant recipients. *Arthritis Res. Ther.* **16**, 1–11 (2014).
59. Povsic, T. J. *et al.* Pre-existing anti-PEG antibodies are associated with severe immediate allergic reactions to pegnivacogin, a PEGylated aptamer. *J. Allergy Clin. Immunol.* **138**, 1712–1715 (2016).
60. Moreno, A. *et al.* Anti-PEG Antibodies Inhibit the Anticoagulant Activity of PEGylated Aptamers. *Cell Chem. Biol.* **26**, 634-644.e3 (2019).
61. Lincoff, A. M. *et al.* Effect of the REG1 anticoagulation system versus bivalirudin on outcomes after percutaneous coronary intervention (REGULATE-PCI): a randomised clinical trial. *Lancet* **387**, 349–356 (2016).
62. Ghobril, C. & Grinstaff, M. W. The chemistry and engineering of polymeric hydrogel adhesives for wound closure: a tutorial. *Chem. Soc. Rev.* **44**, 1820–1835 (2015).
63. Mehdizadeh, M. & Yang, J. Design Strategies and Applications of Tissue Bioadhesives. *Macromol. Biosci.* **13**, 271–288 (2013).
64. Griffin, D. R., Weaver, W. M., Scumpia, P. O., Di Carlo, D. & Segura, T. Accelerated wound healing by injectable microporous gel scaffolds assembled from annealed building blocks. *Nat. Mater.* **14**, 737–744 (2015).
65. Zhu, J. & Marchant, R. E. Design properties of hydrogel tissue-engineering scaffolds. *Expert Rev. Med. Devices* **8**, 607–626 (2011).
66. Dhandayuthapani, B., Yoshida, Y., Maekawa, T. & Kumar, D. S. Polymeric Scaffolds in Tissue Engineering Application: A Review. *Int. J. Polym. Sci.* **2011**, 1–19 (2011).
67. Rosales, A. M. & Anseth, K. S. The design of reversible hydrogels to capture extracellular matrix dynamics. *Nat. Rev. Mater.* **1**, 15012 (2016).
68. Li, J. & Mooney, D. J. Designing hydrogels for controlled drug delivery. *Nat. Rev. Mater.* **1**, 16071 (2016).
69. Hoare, T. R. & Kohane, D. S. Hydrogels in drug delivery: Progress and challenges. *Polymer (Guildf).* **49**, 1993–2007 (2008).
70. Lin, C.-C. & Metters, A. T. Hydrogels in controlled release formulations: Network design and mathematical modeling. *Adv. Drug Deliv. Rev.* **58**, 1379–1408 (2006).
71. Yang, C. & Suo, Z. Hydrogel ionotronics. *Nat. Rev. Mater.* **3**, 125–142 (2018).

72. Jung, I. Y., Kim, J. S., Choi, B. R., Lee, K. & Lee, H. Hydrogel Based Biosensors for In Vitro Diagnostics of Biochemicals, Proteins, and Genes. *Adv. Healthc. Mater.* **6**, 1601475 (2017).
73. Peppas, N. A. & Van Blarcom, D. S. Hydrogel-based biosensors and sensing devices for drug delivery. *J. Control. Release* **240**, 142–150 (2016).
74. Liu, Y., He, W., Zhang, Z. & Lee, B. Recent Developments in Tough Hydrogels for Biomedical Applications. *Gels* **4**, 46 (2018).
75. Daly, A. C., Riley, L., Segura, T. & Burdick, J. A. Hydrogel microparticles for biomedical applications. *Nat. Rev. Mater.* **5**, 20–43 (2020).
76. Burdick, J. A. & Murphy, W. L. Moving from static to dynamic complexity in hydrogel design. *Nat. Commun.* **3**, 1269 (2012).
77. Gong, J. P. Why are double network hydrogels so tough? *Soft Matter* **6**, 2583 (2010).
78. Chen, Q., Chen, H., Zhu, L. & Zheng, J. Fundamentals of double network hydrogels. *J. Mater. Chem. B* **3**, 3654–3676 (2015).
79. Li, X. *et al.* Mesoscale bicontinuous networks in self-healing hydrogels delay fatigue fracture. *Proc. Natl. Acad. Sci.* **117**, 7606–7612 (2020).
80. Ashraf, M. & Foolad, M. R. Roles of glycine betaine and proline in improving plant abiotic stress resistance. *Environ. Exp. Bot.* **59**, 206–216 (2007).
81. Cao, Z., Zhang, L. & Jiang, S. Superhydrophilic Zwitterionic Polymers Stabilize Liposomes. *Langmuir* **28**, 11625–11632 (2012).
82. Cao, Z. & Jiang, S. Super-hydrophilic zwitterionic poly(carboxybetaine) and amphiphilic non-ionic poly(ethylene glycol) for stealth nanoparticles. *Nano Today* **7**, 404–413 (2012).
83. Shao, Q. & Jiang, S. Molecular Understanding and Design of Zwitterionic Materials. *Adv. Mater.* **27**, 15–26 (2015).
84. Yang, W., Xue, H., Li, W., Zhang, J. & Jiang, S. Pursuing "Zero" Protein Adsorption of Poly(carboxybetaine) from Undiluted Blood Serum and Plasma. *Langmuir* **25**, 11911–11916 (2009).
85. Jiang, S. & Cao, Z. Ultralow-Fouling, Functionalizable, and Hydrolyzable Zwitterionic Materials and Their Derivatives for Biological Applications. *Adv. Mater.* **22**, 920–932 (2010).
86. Keefe, A. J. & Jiang, S. Poly(zwitterionic)protein conjugates offer increased stability

without sacrificing binding affinity or bioactivity. *Nat. Chem.* **4**, 59–63 (2012).

87. Zhang, P. *et al.* Zwitterionic gel encapsulation promotes protein stability, enhances pharmacokinetics, and reduces immunogenicity. *Proc. Natl. Acad. Sci. U. S. A.* **112**, 12046–12051 (2015).
88. Liu, S. & Jiang, S. Zwitterionic polymer-protein conjugates reduce polymer-specific antibody response. *Nano Today* **11**, 285–291 (2016).
89. Zhang, P. *et al.* Nanoscavenger provides long-term prophylactic protection against nerve agents in rodents. *Sci. Transl. Med.* **11**, eaau7091 (2019).
90. Han, Y., Yuan, Z., Zhang, P. & Jiang, S. Zwitterlation mitigates protein bioactivity loss: In vitro over PEGylation. *Chem. Sci.* **9**, 8561–8566 (2018).
91. Li, B. *et al.* Zwitterionic nanocages overcome the efficacy loss of biologic drugs. *Adv. Mater.* **30**, e1705728 (2018).
92. Li, B. *et al.* Revealing the Immunogenic Risk of Polymers. *Angew. Chemie - Int. Ed.* **57**, 13873–13876 (2018).
93. Zhang, L. *et al.* Zwitterionic hydrogels implanted in mice resist the foreign-body reaction. *Nat. Biotechnol.* **31**, 553–556 (2013).
94. Meier, J. J. & Nauck, M. A. Glucagon-like peptide 1(GLP-1) in biology and pathology. *Diabetes. Metab. Res. Rev.* **21**, 91–117 (2005).
95. Fosgerau, K. & Hoffmann, T. Peptide therapeutics: current status and future directions. *Drug Discov. Today* **20**, 122–128 (2015).
96. Kaspar, A. A. & Reichert, J. M. Future directions for peptide therapeutics development. *Drug Discov. Today* **18**, 807–817 (2013).
97. Cho, Y. M., Merchant, C. E. & Kieffer, T. J. Targeting the glucagon receptor family for diabetes and obesity therapy. *Pharmacol. Ther.* **135**, 247–278 (2012).
98. Meier, J. J. GLP-1 receptor agonists for individualized treatment of type 2 diabetes mellitus. *Nat. Rev. Endocrinol.* **8**, 728–742 (2012).
99. Patton, J. S., Fishburn, C. S. & Weers, J. G. The lungs as a portal of entry for systemic drug delivery. *Proc. Am. Thorac. Soc.* **1**, 338–344 (2004).
100. Pfister, T. *et al.* Bioavailability of therapeutic proteins by inhalation - Worker safety aspects. *Ann. Occup. Hyg.* **58**, 899–911 (2014).
101. Patton, J. S. Mechanisms of macromolecule absorption by the lungs. *Advanced Drug*

Delivery Reviews **19**, 3–36 (1996).

102. Grimsley, J. K., Scholtz, J. M., Pace, C. N. & Wild, J. R. Organophosphorus Hydrolase Is a Remarkably Stable Enzyme That Unfolds through a Homodimeric Intermediate †. *Biochemistry* **36**, 14366–14374 (1997).
103. Nachon, F., Brazzolotto, X., Trovaslet, M. & Masson, P. Progress in the development of enzyme-based nerve agent bioscavengers. *Chem. Biol. Interact.* **206**, 536–544 (2013).
104. Efremenko, E. N. *et al.* A simple and highly effective catalytic nanozyme scavenger for organophosphorus neurotoxins. *J. Control. Release* **247**, 175–181 (2017).
105. Stuart, M. a C. *et al.* Emerging applications of stimuli-responsive polymer materials. *Nat. Mater.* **9**, 101–113 (2010).
106. Prince, E. & Kumacheva, E. Design and applications of man-made biomimetic fibrillar hydrogels. *Nat. Rev. Mater.* **4**, 99–115 (2019).
107. Hoffman, A. S. Hydrogels for biomedical applications. *Adv. Drug Deliv. Rev.* **64**, 18–23 (2012).
108. Tang, L., Liu, W. & Liu, G. High-Strength Hydrogels with Integrated Functions of H-bonding and Thermoresponsive Surface-Mediated Reverse Transfection and Cell Detachment. *Adv. Mater.* **22**, 2652–2656 (2010).
109. Chivers, P. R. A. & Smith, D. K. Shaping and structuring supramolecular gels. *Nat. Rev. Mater.* **4**, 463–478 (2019).
110. Liang, Y., Xue, J., Du, B. & Nie, J. Ultrastiff, Tough, and Healable Ionic–Hydrogen Bond Cross-Linked Hydrogels and Their Uses as Building Blocks To Construct Complex Hydrogel Structures. *ACS Appl. Mater. Interfaces* **11**, 5441–5454 (2019).
111. Gaharwar, A. K., Peppas, N. A. & Khademhosseini, A. Nanocomposite hydrogels for biomedical applications. *Biotechnol. Bioeng.* **111**, 441–453 (2014).
112. Gong, J. P., Katsuyama, Y., Kurokawa, T. & Osada, Y. Double-Network Hydrogels with Extremely High Mechanical Strength. *Adv. Mater.* **15**, 1155–1158 (2003).
113. Yasuda, K. *et al.* Biomechanical properties of high-toughness double network hydrogels. *Biomaterials* **26**, 4468–4475 (2005).
114. Liang, Z. *et al.* Double-Network Hydrogel with Tunable Mechanical Performance and Biocompatibility for the Fabrication of Stem Cells-Encapsulated Fibers and 3D Assemble. *Sci. Rep.* **6**, 33462 (2016).

115. Dondossola, E. *et al.* Examination of the foreign body response to biomaterials by nonlinear intravital microscopy. *Nat. Biomed. Eng.* **1**, 0007 (2017).
116. Klopfleisch, R. & Jung, F. The pathology of the foreign body reaction against biomaterials. *J. Biomed. Mater. Res. Part A* **105**, 927–940 (2017).
117. Sheikh, Z., Brooks, P., Barzilay, O., Fine, N. & Glogauer, M. Macrophages, Foreign Body Giant Cells and Their Response to Implantable Biomaterials. *Materials (Basel).* **8**, 5671–5701 (2015).
118. Carr, L. R., Zhou, Y., Krause, J. E., Xue, H. & Jiang, S. Uniform zwitterionic polymer hydrogels with a nonfouling and functionalizable crosslinker using photopolymerization. *Biomaterials* **32**, 6893–6899 (2011).
119. Chien, H.-W., Tsai, W.-B. & Jiang, S. Direct cell encapsulation in biodegradable and functionalizable carboxybetaine hydrogels. *Biomaterials* **33**, 5706–5712 (2012).
120. Jansen, L. E. *et al.* Zwitterionic PEG-PC Hydrogels Modulate the Foreign Body Response in a Modulus-Dependent Manner. *Biomacromolecules* **19**, 2880–2888 (2018).
121. Zhang, Z. *et al.* Zwitterionic Hydrogels: an in Vivo Implantation Study. *J. Biomater. Sci. Polym. Ed.* **20**, 1845–1859 (2009).
122. Chatterjee, S., Khunti, K. & Davies, M. J. Type 2 diabetes. *Lancet* **389**, 2239–2251 (2017).
123. Zheng, Y., Ley, S. H. & Hu, F. B. Global aetiology and epidemiology of type 2 diabetes mellitus and its complications. *Nat. Rev. Endocrinol.* **14**, 88–98 (2018).
124. International Diabetes Federation. IDF Diabetes Atlas, 9th edn. Brussels, Belgium: 2019. Available at: http://www.diabetesatlas.org (accessed Nov 18, 2019).
125. Deacon, C. F. Therapeutic strategies based on glucagon-like peptide 1. *Diabetes* **53**, 2181–2189 (2004).
126. Zander, M., Madsbad, S., Madsen, J. L. & Holst, J. J. Effect of 6-week course of glucagon-like peptide 1 on glycaemic control, insulin sensitivity, and β-cell function in type 2 diabetes: A parallel-group study. *Lancet* **359**, 824–830 (2002).
127. Müller, T. D. *et al.* Glucagon-like peptide 1 (GLP-1). *Mol. Metab.* **30**, 72–130 (2019).
128. Ahrén, B. GLP-1 for type 2 diabetes. *Exp. Cell Res.* **317**, 1239–1245 (2011).
129. Andersen, A., Lund, A., Knop, F. K. & Vilsbøll, T. Glucagon-like peptide 1 in health and disease. *Nat. Rev. Endocrinol.* **14**, 390–403 (2018).

130. Manandhar, B. & Ahn, J. M. Glucagon-like peptide-1 (GLP-1) analogs: Recent advances, new possibilities, and therapeutic implications. *J. Med. Chem.* **58**, 1020–1037 (2015).
131. Montrose-Rafizadeh, C. *et al.* High potency antagonists of the pancreatic glucagon-like peptide-1 receptor. *J. Biol. Chem.* **272**, 21201–21206 (1997).
132. Lund, A., Knop, F. K. & Vilsbøll, T. Glucagon-like peptide-1 receptor agonists for the treatment of type 2 diabetes: Differences and similarities. *Eur. J. Intern. Med.* **25**, 407–414 (2014).
133. Tomlinson, B., Hu, M., Zhang, Y., Chan, P. & Liu, Z. M. An overview of new GLP-1 receptor agonists for type 2 diabetes. *Expert Opin. Investig. Drugs* **25**, 145–158 (2016).
134. Aroda, V. R. A review of GLP-1 receptor agonists: Evolution and advancement, through the lens of randomised controlled trials. *Diabetes, Obes. Metab.* **20**, 22–33 (2018).
135. Garber, A. J. Long-acting glucagon-like peptide 1 receptor agonists: A review of their efficacy and tolerability. *Diabetes Care* **34**, S279–S284 (2011).
136. Prasad-Reddy, L. & Isaacs, D. A clinical review of GLP-1 receptor agonists: Efficacy and safety in diabetes and beyond. *Drugs Context* **4**, 212283 (2015).
137. Filippatos, T. D., Panagiotopoulou, T. V. & Elisaf, M. S. Adverse Effects of GLP-1 Receptor Agonists. *Rev. Diabet. Stud.* **11**, 202–230 (2014).
138. Wang, Y. M. C. *et al.* Evaluating and Reporting the Immunogenicity Impacts for Biological Products—a Clinical Pharmacology Perspective. *AAPS J.* **18**, 395–403 (2016).
139. Nechansky, A. & Kircheis, R. Immunogenicity of therapeutics: A matter of efficacy and safety. *Expert Opin. Drug Discov.* **5**, 1067–1079 (2010).
140. Selis, F. *et al.* Enzymatic mono-pegylation of glucagon-like peptide 1 towards long lasting treatment of type 2 diabetes. *Results Pharma Sci.* **2**, 58–65 (2012).
141. Ichikawa, M. *et al.* Glycosaminoglycan Conjugation for Improving the Duration of Therapeutic Action of Glucagon-Like Peptide-1. *ACS Omega* **3**, 5346–5354 (2018).
142. Bukrinski, J. T. *et al.* Glucagon-like Peptide 1 Conjugated to Recombinant Human Serum Albumin Variants with Modified Neonatal Fc Receptor Binding Properties. Impact on Molecular Structure and Half-Life. *Biochemistry* **56**, 4860–4870 (2017).
143. Picha, K. M. *et al.* Protein engineering strategies for sustained Glucagon-Like peptide-1 Receptor-Dependent control of glucose homeostasis. *Diabetes* **57**, 1926–1934 (2008).
144. Glaesner, W. *et al.* Engineering and characterization of the long-acting glucagon-like

peptide-1 analogue LY2189265, an Fc fusion protein. *Diabetes. Metab. Res. Rev.* **26**, 287–296 (2010).

145. Youn, Y. S. *et al.* Evaluation of therapeutic potentials of site-specific PEGylated glucagon-like peptide-1 isomers as a type 2 anti-diabetic treatment: Insulinotropic activity, glucose-stabilizing capability, and proteolytic stability. *Biochem. Pharmacol.* **73**, 84–93 (2007).
146. Garay, R. P., El-Gewely, R., Armstrong, J. K., Garratty, G. & Richette, P. Antibodies against polyethylene glycol in healthy subjects and in patients treated with PEG-conjugated agents. *Expert Opin. Drug Deliv.* **9**, 1319–1323 (2012).
147. Tsao, C. *et al.* Enhanced pulmonary systemic delivery of protein drugs via zwitterionic polymer conjugation. *J. Control. Release* **322**, 170–176 (2020).
148. Xie, J. *et al.* Simple Protein Modification Using Zwitterionic Polymer to Mitigate the Bioactivity Loss of Conjugated Insulin. *Adv. Healthc. Mater.* **6**, (2017).
149. Zhang, Y., Huo, M., Zhou, J. & Xie, S. PKSolver: An add-in program for pharmacokinetic and pharmacodynamic data analysis in Microsoft Excel. *Comput. Methods Programs Biomed.* **99**, 306–314 (2010).
150. Adelhorst, K., Hedegaard, B. B., Knudsen, L. B. & Kirk, O. Structure-activity studies of glucagon-like peptide-1. *J. Biol. Chem.* **269**, 6275–6278 (1994).
151. Brenner, B. M., Hostetter, T. H. & Humes, H. D. Glomerular permselectivity: Barrier function based on discrimination of molecular size and charge. *Am. J. Physiol. - Ren. Fluid Electrolyte Physiol.* **3**, F455–F460 (1978).
152. Waldmann, T. A., Strober, W. & Mogielnicki, R. P. The renal handling of low molecular weight proteins. II. Disorders of serum protein catabolism in patients with tubular proteinuria, the nephrotic syndrome, or uremia. *J. Clin. Invest.* **51**, 2162–2174 (1972).
153. Xu, L. *et al.* Molecular insights for the biological interactions between polyethylene glycol and cells. *Biomaterials* **147**, 1–13 (2017).
154. Wu, J. *et al.* Binding characteristics between polyethylene glycol (PEG) and proteins in aqueous solution. *J. Mater. Chem. B* **2**, 2983–2992 (2014).
155. Kenakin, T. P. Pharmacological Assay Formats. in *A Pharmacology Primer* 61–79 (Elsevier, 2009). doi:10.1016/B978-0-12-374585-9.00004-9
156. Chung, H. S., Oh, J. Y., Yoo, S. B., Lee, S. M. & Cho, H. S. The N-terminal alanine-

extended GLP-1/IgG-Fc fusion protein confers resistance to DPP-IV and reduces serum glucose level in db/db mice. *Regul. Pept.* **170**, 1–3 (2011).

157. Richter, W. F., Bhansali, S. G. & Morris, M. E. Mechanistic Determinants of Biotherapeutics Absorption Following SC Administration. *AAPS J.* **14**, 559–570 (2012).
158. McLennan, D. N., Porter, C. J. H. & Charman, S. A. Subcutaneous drug delivery and the role of the lymphatics. *Drug Discov. Today Technol.* **2**, 89–96 (2005).
159. Sykes, E. A., Dai, Q., Tsoi, K. M., Hwang, D. M. & Chan, W. C. W. Nanoparticle exposure in animals can be visualized in the skin and analysed via skin biopsy. *Nat. Commun.* **5**, (2014).
160. Krejsa, C., Rogge, M. & Sadee, W. Protein therapeutics: New applications for pharmacogenetics. *Nature Reviews Drug Discovery* **5**, 507–521 (2006).
161. Leader, B., Baca, Q. J. & Golan, D. E. Protein therapeutics: A summary and pharmacological classification. *Nature Reviews Drug Discovery* **7**, 21–39 (2008).
162. Carter, P. J. Introduction to current and future protein therapeutics: A protein engineering perspective. *Experimental Cell Research* **317**, 1261–1269 (2011).
163. Patton, J. S., Fishburn, C. S. & Weers, J. G. The lungs as a portal of entry for systemic drug delivery. *Proceedings of the American Thoracic Society* **1**, 338–344 (2004).
164. Andrade, F., Videira, M., Ferreira, D. & Sarmento, B. Nanocarriers for pulmonary administration of peptides and therapeutic proteins. *Nanomedicine* **6**, 123–141 (2011).
165. Agu, R. U., Ugwoke, M. I., Armand, M., Kinget, R. & Verbeke, N. The lung as a route for systemic delivery of therapeutic proteins and peptides. *Respiratory Research* **2**, 198–209 (2001).
166. Patton, J. S. & Byron, P. R. Inhaling medicines: Delivering drugs to the body through the lungs. *Nat. Rev. Drug Discov.* **6**, 67–74 (2007).
167. Ruge, C. C., Kirch, J. & Lehr, C. M. Pulmonary drug delivery: From generating aerosols to overcoming biological barriers-therapeutic possibilities and technological challenges. *Lancet Respir. Med.* **1**, 402–413 (2013).
168. Patton, J. S. *et al.* The particle has landed-characterizing the fate of inhaled pharmaceuticals. *J. Aerosol Med. Pulm. Drug Deliv.* **23**, S-71-S-87 (2010).
169. Depreter, F., Pilcer, G. & Amighi, K. Inhaled proteins: Challenges and perspectives. *Int. J. Pharm.* **447**, 251–280 (2013).

170. Koussoroplis, S. & Vanbever, R. Peptides and Proteins : Pulmonary Absorption. *Encycl. Pharm. Sci. Technol.* **4**, 2607–2618 (2013).
171. Murgia, X., De Souza Carvalho, C. & Lehr, C. M. Overcoming the pulmonary barrier: New insights to improve the efficiency of inhaled therapeutics. *Eur. J. Nanomedicine* **6**, 157–169 (2014).
172. Möller, W. *et al.* Deposition, retention, and translocation of ultrafine particles from the central airways and lung periphery. *Am. J. Respir. Crit. Care Med.* **177**, 426–432 (2008).
173. Röhm, M. *et al.* A comprehensive screening platform for aerosolizable protein formulations for intranasal and pulmonary drug delivery. *Int. J. Pharm.* **532**, 537–546 (2017).
174. Patton, J. S., Trinchero, P. & Platz, R. M. Bioavailability of pulmonary delivered peptides and proteins: α-interferon, calcitonins and parathyroid hormones. *J. Control. Release* **28**, 79–85 (1994).
175. Berg, J. T., Lee, S. T., Thepen, T., Lee, C. Y. & Tsan, M. F. Depletion of alveolar macrophages by liposome-encapsulated dichloromethylene diphosphonate. *J. Appl. Physiol.* **74**, 2812–2819 (1993).
176. Lombry, C., Edwards, D. A., Préat, V. & Vanbever, R. Alveolar macrophages are a primary barrier to pulmonary absorption of macromolecules. *Am. J. Physiol. - Lung Cell. Mol. Physiol.* **286**, L1002-8 (2004).
177. Cho, C. M. H., Mulchandani, A. & Chen, W. Functional analysis of organophosphorus hydrolase variants with high degradation activity towards organophosphate pesticides. *Protein Eng. Des. Sel.* **19**, 99–105 (2006).
178. Novikov, B. N., Grimsley, J. K., Kern, R. J., Wild, J. R. & Wales, M. E. Improved pharmacokinetics and immunogenicity profile of organophosphorus hydrolase by chemical modification with polyethylene glycol. *J. Control. Release* **146**, 318–325 (2010).
179. Nicolet, Y., Lockridge, O., Masson, P., Fontecilla-Camps, J. C. & Nachon, F. Crystal structure of human butyrylcholinesterase and of its complexes with substrate and products. *J. Biol. Chem.* **278**, 41141–41147 (2003).
180. Lockridge, O. Review of human butyrylcholinesterase structure, function, genetic variants, history of use in the clinic, and potential therapeutic uses. *Pharmacology and Therapeutics* **148**, 34–46 (2015).

181. Cho, C. M. H., Mulchandani, A. & Chen, W. Bacterial cell surface display of organophosphorus hydrolase for selective screening of improved hydrolysis of organophosphate nerve agents. *Appl. Environ. Microbiol.* **68**, 2026–2030 (2002).
182. Tsai, P. C. *et al.* Stereoselective hydrolysis of organophosphate nerve agents by the bacterial phosphotriesterase. *Biochemistry* **49**, 7978–7987 (2010).
183. Rahhal, T. B. *et al.* Pulmonary delivery of butyrylcholinesterase as a model protein to the lung. *Mol. Pharm.* **13**, 1626–1635 (2016).
184. Rosenberg, Y. J. & Fink, J. B. Creation of a protective pulmonary bioshield against inhaled organophosphates using an aerosolized bioscavenger. *Ann. N. Y. Acad. Sci.* **1374**, 151–158 (2016).
185. Rosenberg, Y. J. *et al.* Pulmonary delivery of an aerosolized recombinant human butyrylcholinesterase pretreatment protects against aerosolized paraoxon in macaques. *Chem. Biol. Interact.* **203**, 167–171 (2013).
186. Rosenberg, Y. J. *et al.* Pharmacokinetics and immunogenicity of a recombinant human butyrylcholinesterase bioscavenger in macaques following intravenous and pulmonary delivery. *Chem. Biol. Interact.* **242**, 219–226 (2015).
187. Leng, C., Sun, S., Zhang, K., Jiang, S. & Chen, Z. Molecular level studies on interfacial hydration of zwitterionic and other antifouling polymers in situ. *Acta Biomaterialia* **40**, 6–15 (2016).
188. Ladd, J., Zhang, Z., Chen, S., Hower, J. C. & Jiang, S. Zwitterionic polymers exhibiting high resistance to nonspecific protein adsorption from human serum and plasma. *Biomacromolecules* **9**, 1357–1361 (2008).
189. Sun, F. *et al.* Paper sensor coated with a poly(carboxybetaine)-multiple DOPA conjugate via dip-coating for biosensing in complex media. *Anal. Chem.* **89**, 10999–11004 (2017).
190. Zhang, L. *et al.* Multifunctional and degradable zwitterionic nanogels for targeted delivery, enhanced MR imaging, reduction-sensitive drug release, and renal clearance. *Biomaterials* **32**, 4604–4608 (2011).
191. Zhang, L. *et al.* Imaging and cell targeting characteristics of magnetic nanoparticles modified by a functionalizable zwitterionic polymer with adhesive 3,4-dihydroxyphenyl-l-alanine linkages. *Biomaterials* **31**, 6582–6588 (2010).
192. Villa, A. F. *et al.* Toxic doses of paraoxon alter the respiratory pattern without causing

respiratory failure in rats. *Toxicology* **232**, 37–49 (2007).

193. Choi, H. S. *et al.* Rapid translocation of nanoparticles from the lung airspaces to the body. *Nat. Biotechnol.* **28**, 1300–1303 (2010).
194. Ryan, G. M. *et al.* Pulmonary administration of PEGylated polylysine dendrimers: Absorption from the lung versus retention within the lung is highly size-dependent. *Mol. Pharm.* **10**, 2986–2995 (2013).
195. Chen, B., Lei, C., Shin, Y. & Liu, J. Probing mechanisms for enzymatic activity enhancement of organophosphorus hydrolase in functionalized mesoporous silica. *Biochem. Biophys. Res. Commun.* **390**, 1177–1181 (2009).
196. Soo Choi, H. *et al.* Renal clearance of quantum dots. *Nat. Biotechnol.* **25**, 1165–1170 (2007).
197. Ensign, L. M., Schneider, C., Suk, J. S., Cone, R. & Hanes, J. Mucus penetrating nanoparticles: Biophysical tool and method of drug and gene delivery. *Adv. Mater.* **24**, 3887–3894 (2012).
198. Shan, W. *et al.* Enhanced oral delivery of protein drugs using zwitterion-functionalized nanoparticles to overcome both the diffusion and absorption barriers. *ACS Appl. Mater. Interfaces* **8**, 25444–25453 (2016).
199. Huckaby, J. T. & Lai, S. K. PEGylation for enhancing nanoparticle diffusion in mucus. *Advanced Drug Delivery Reviews* **124**, 125–139 (2018).
200. Lee, K. Y. & Mooney, D. J. Hydrogels for Tissue Engineering. *Chem. Rev.* **101**, 1869–1880 (2001).
201. Seliktar, D. Designing Cell-Compatible Hydrogels for Biomedical Applications. *Science (80-.).* **336**, 1124–1128 (2012).
202. Billiet, T., Vandenhaute, M., Schelfhout, J., Van Vlierberghe, S. & Dubruel, P. A review of trends and limitations in hydrogel-rapid prototyping for tissue engineering. *Biomaterials* **33**, 6020–6041 (2012).
203. Green, J. J. & Elisseeff, J. H. Mimicking biological functionality with polymers for biomedical applications. *Nature* **540**, 386–394 (2016).
204. Lewis, A. L. Phosphorylcholine-based polymers and their use in the prevention of biofouling. *Colloids Surfaces B Biointerfaces* **18**, 261–275 (2000).
205. Hung, H.-C. *et al.* A Coating-Free Nonfouling Polymeric Elastomer. *Adv. Mater.* **29**,

1700617 (2017).

206. Azvolinsky, A., Schmidt, C., Waltz, E. & Webb, S. 20 years of Nature Biotechnology biomedical research. *Nat. Biotechnol.* **34**, 262–266 (2016).
207. Ratner, B. D. Reducing capsular thickness and enhancing angiogenesis around implant drug release systems. *J. Control. Release* **78**, 211–218 (2002).
208. Vegas, A. J. *et al.* Combinatorial hydrogel library enables identification of materials that mitigate the foreign body response in primates. *Nat. Biotechnol.* **34**, 345–352 (2016).
209. Ishihara, K., Ueda, T. & Nakabayashi, N. Preparation of Phospholipid Polylners and Their Properties as Polymer Hydrogel Membranes. *Polym. J.* **22**, 355–360 (1990).
210. Bai, T. *et al.* Expansion of primitive human hematopoietic stem cells by culture in a zwitterionic hydrogel. *Nat. Med.* **25**, 1566–1575 (2019).
211. Lowe, A. B. & McCormick, C. L. Synthesis and Solution Properties of Zwitterionic Polymers †. *Chem. Rev.* **102**, 4177–4190 (2002).
212. Moro, T. *et al.* Surface grafting of artificial joints with a biocompatible polymer for preventing periprosthetic osteolysis. *Nat. Mater.* **3**, 829–836 (2004).
213. Sun, J.-Y. *et al.* Highly stretchable and tough hydrogels. *Nature* **489**, 133–136 (2012).
214. Sun, T. L. *et al.* Physical hydrogels composed of polyampholytes demonstrate high toughness and viscoelasticity. *Nat. Mater.* **12**, 932–937 (2013).
215. Kamata, H., Akagi, Y., Kayasuga-Kariya, Y., Chung, U. -i. & Sakai, T. 'Nonswellable' Hydrogel Without Mechanical Hysteresis. *Science (80-.).* **343**, 873–875 (2014).
216. Zhao, X. Multi-scale multi-mechanism design of tough hydrogels: building dissipation into stretchy networks. *Soft Matter* **10**, 672–687 (2014).
217. Yuk, H., Zhang, T., Parada, G. A., Liu, X. & Zhao, X. Skin-inspired hydrogel–elastomer hybrids with robust interfaces and functional microstructures. *Nat. Commun.* **7**, 12028 (2016).
218. Zhang, Y. S. & Khademhosseini, A. Advances in engineering hydrogels. *Science (80-.).* **356**, eaaf3627 (2017).
219. Matsuda, T., Kawakami, R., Namba, R., Nakajima, T. & Gong, J. P. Mechanoresponsive self-growing hydrogels inspired by muscle training. *Science (80-.).* **363**, 504–508 (2019).
220. Li, B. *et al.* Trimethylamine N -oxide–derived zwitterionic polymers: A new class of ultralow fouling bioinspired materials. *Sci. Adv.* **5**, eaaw9562 (2019).

221. Zhang, Z. *et al.* Nonfouling Behavior of Polycarboxybetaine-Grafted Surfaces: Structural and Environmental Effects. *Biomacromolecules* **9**, 2686–2692 (2008).
222. Chen, S. & Jiang, S. An New Avenue to Nonfouling Materials. *Adv. Mater.* **20**, 335–338 (2008).
223. Lin-Gibson, S., Jones, R. L., Washburn, N. R. & Horkay, F. Structure−Property Relationships of Photopolymerizable Poly(ethylene glycol) Dimethacrylate Hydrogels. *Macromolecules* **38**, 2897–2902 (2005).
224. Konig, G. *et al.* Mechanical properties of completely autologous human tissue engineered blood vessels compared to human saphenous vein and mammary artery. *Biomaterials* **30**, 1542–1550 (2009).
225. Swartzlander, M. D. *et al.* Linking the foreign body response and protein adsorption to PEG-based hydrogels using proteomics. *Biomaterials* **41**, 26–36 (2015).
226. Fleckman, P. *et al.* Cutaneous and inflammatory response to long-term percutaneous implants of sphere-templated porous/solid poly(HEMA) and silicone in mice. *J. Biomed. Mater. Res. Part A* **100A**, 1256–1268 (2012).
227. Tuerk, C. & Gold, L. Systematic evolution of ligands by exponential enrichment: RNA ligands to bacteriophage T4 DNA polymerase. *Science (80-.).* **249**, 505–510 (1990).
228. Ellington, A. D. & Szostak, J. W. In vitro selection of RNA molecules that bind specific ligands. *Nature* **346**, 818–822 (1990).
229. Mannironi, C., Di Nardo, A., Fruscoloni, P. & Tocchini-Valentini, G. P. In Vitro Selection of Dopamine RNA Ligands †. *Biochemistry* **36**, 9726–9734 (1997).
230. Roberts, R. W. & Szostak, J. W. RNA-peptide fusions for the in vitro selection of peptides and proteins. *Proc. Natl. Acad. Sci.* **94**, 12297–12302 (1997).
231. Keefe, A. D., Pai, S. & Ellington, A. Aptamers as therapeutics. *Nat. Rev. Drug Discov.* **9**, 537–550 (2010).
232. Zhou, J. & Rossi, J. Aptamers as targeted therapeutics: current potential and challenges. *Nat. Rev. Drug Discov.* **16**, 181–202 (2017).
233. LEE, J., STOVALL, G. & ELLINGTON, A. Aptamer therapeutics advance. *Curr. Opin. Chem. Biol.* **10**, 282–289 (2006).
234. Haruta, K. *et al.* A Novel PEGylation Method for Improving the Pharmacokinetic Properties of Anti-Interleukin-17A RNA Aptamers. *Nucleic Acid Ther.* **27**, 36–44 (2017).

235. Ni, S. *et al.* Chemical Modifications of Nucleic Acid Aptamers for Therapeutic Purposes. *Int. J. Mol. Sci.* **18**, 1683 (2017).
236. E. Wang, R., Wu, H., Niu, Y. & Cai, J. Improving the Stability of Aptamers by Chemical Modification. *Curr. Med. Chem.* **18**, 4126–4138 (2011).
237. Maier, K. E. & Levy, M. From selection hits to clinical leads: progress in aptamer discovery. *Mol. Ther. - Methods Clin. Dev.* **3**, 16014 (2016).
238. Vavalle, J. P. & Cohen, M. G. The REG1 anticoagulation system: a novel actively controlled factor IX inhibitor using RNA aptamer technology for treatment of acute coronary syndrome. *Future Cardiol.* **8**, 371–382 (2012).
239. Nimjee, S. M. *et al.* A Novel Antidote-Controlled Anticoagulant Reduces Thrombin Generation and Inflammation and Improves Cardiac Function in Cardiopulmonary Bypass Surgery. *Mol. Ther.* **14**, 408–415 (2006).
240. Ganson, N. J. *et al.* Pre-existing anti–polyethylene glycol antibody linked to first-exposure allergic reactions to pegnivacogin, a PEGylated RNA aptamer. *J. Allergy Clin. Immunol.* **137**, 1610-1613.e7 (2016).
241. Garay, R. P., El-Gewely, R., Armstrong, J. K., Garratty, G. & Richette, P. Antibodies against polyethylene glycol in healthy subjects and in patients treated with PEG-conjugated agents. *Expert Opin. Drug Deliv.* **9**, 1319–1323 (2012).
242. Shiraishi, K. *et al.* Hydrophobic blocks of PEG-conjugates play a significant role in the accelerated blood clearance (ABC) phenomenon. *J. Control. Release* **165**, 183–190 (2013).
243. Yang, Q. *et al.* Analysis of Pre-existing IgG and IgM Antibodies against Polyethylene Glycol (PEG) in the General Population. *Anal. Chem.* **88**, 11804–11812 (2016).
244. Lubich, C. *et al.* The Mystery of Antibodies Against Polyethylene Glycol (PEG) - What do we Know? *Pharm. Res.* **33**, 2239–2249 (2016).
245. Hsieh, Y.-C. *et al.* Pre-existing anti-polyethylene glycol antibody reduces the therapeutic efficacy and pharmacokinetics of PEGylated liposomes. *Theranostics* **8**, 3164–3175 (2018).
246. McSweeney, M. D. *et al.* A minimal physiologically based pharmacokinetic model that predicts anti-PEG IgG-mediated clearance of PEGylated drugs in human and mouse. *J. Control. Release* **284**, 171–178 (2018).

VITA

CAROLINE TSAO

EDUCATION

2014 – 2020 University of Washington, Seattle, WA
Ph.D. in Chemical Engineering, June 2020

2014 – 2016 University of Washington, Seattle, WA
M.S. in Chemical Engineering

2009 – 2013 National Taiwan University, Taipei, Taiwan
B.S. in Life Science

Research Interests: Nanomedicine, biomaterials, immunomodulation, humoral immunity, non-invasive drug delivery systems, regenerative medicine

RESEARCH EXPERIENCE

2014 – present University of Washington, Seattle, WA
Graduate Research Assistant, Advisor: Shaoyi Jiang, Ph.D.
Dissertation: "Zwitterionic Polymer-based Platforms for Biotherapeutics and Implants"

- Development of non-invasive pulmonary systemic protein drug delivery platform utilizing zwitterionic polymers. Enhancement of bioscavenger bioavailability *via* pulmonary delivery provided prophylactic protection against nerve agents in animal studies
- Modification of native glucagon-like peptide-1 (GLP-1) with zwitterionic polymers to enhance the pharmacokinetic profile and efficacy of GLP-1 for weekly treatment of type 2 diabetes mellitus (T2DM)
- Development of high mechanical strength, elastomer-like, and biocompatible zwitterionic hydrogels which resist foreign body reaction long-term for medical implantations/tissue scaffolds in regenerative medicine/tissue engineering
- Exploration of multiple research topics: develop 3-D printing capacity of zwitterionic hydrogels, study the diffusion rate of zwitterionic nanoparticles in mucus, and develop immunomodulatory zwitterionic peptides

2013 – 2014 National Taiwan University, Taipei, Taiwan
Research Assistant, Department of Biomedical Engineering

- Pioneered in the research field of investigation of neuron development around hair follicles during late infancy utilizing immunostaining and confocal imaging

2010 – 2010 National Taiwan University, Taipei, Taiwan
Undergraduate Research Assistant, Institute of Molecular Medicine

- Investigation of the roles of adenosine diphosphate ribosylation factors-like small GTPases in vesicular trafficking and cytoskeletal modulation

TEACHING EXPERIENCE

Jane and Joseph McCarthy Award for Excellence in ChemE Graduate Student Teaching 2015-2016

Spring 2015 *Teaching Assistant*, Mass and Energy Balance
2015 – 2016 *Lecturer*, Senior Undergraduate Special Project Design
Participation in the "Hollomon Health Innovation Challenge 2016"
Fall 2016 *Teaching Assistant*, Thermodynamics I
Winter 2016 *Teaching Assistant*, Thermodynamics II
Fall 2017 *Teaching Assistant*, Quantum Mechanics
Winter 2017 *Teaching Assistant*, Thermodynamics II
Fall 2018 *Teaching Assistant*, Quantum Mechanics
Winter 2020 *Teaching Assistant*, Thermodynamics II

PUBLICATIONS

*****Equal contribution*

1. **Tsao, C.**; Zhang, P.; Yuan, Z.; Wu, K.; Hung, H.-C.; Jiang, S. "Enhanced Systemic Protein Drug Delivery *via* Pulmonary Route By Zwitterionic Polymer Conjugation." *J. Control. Release*, 2020, 322, 170-176
2. **Tsao, C.**; Yuan, Z.; Dong, D.; Zhang, P.; McMullen, P.; Niu, L.; Wu, K.; Hung, H.-C.; Li, B.; Jiang, S. "Zwitterionic Polymer Conjugation to Native Glycogen-like Peptide-1 as Potential Long-term Therapeutics for Type 2 Diabetes Mellitus." *Under revision.*
3. **Tsao, C.***, Dong, D.*; Hung, H.-C.*; Ma, J.; Niu, L; Tang, C.; Jiang, S. "Zwitterionic-Elastomeric-Networked Hydrogel as Long-term Implantable Material." *Under review.*
4. Zhang, P.; Jain, P.; **Tsao, C.**; Wu. K.; Jiang, S. "Proactively Reducing Anti-Drug Antibodies via Immunomodulatory Bioconjugation." *Angew. Chem. Int. Ed.* 2019, 58, 2433.
5. Zhang, P.; Liu, E. J.; **Tsao, C.**; Chen, Y.; Kasten, S. A.; Otto, R.; Cerasoli, D. M.; Jain, R.; Sun, F.; Li, W.; Hung, H.-C.; Yuan, Z.; Ma, J.; Corrican, T.; Bigley, A. N.; Rauschel, F. M.; Jiang, S. "Nanoscavenger Provides Long-term Prophylactic Protection Against Nerve Agents." *Sci. Transl. Med.* 2019, 11, eaau7091.

6. Li, B.; Yuan, Z.; Hung. H.-C.; Ma, J.; Jain, P.; **Tsao, C.**; Xie, J.; Zhang, P.; Lin, X.; Wu, K.; Jiang, S. "Revealing the Immunogenic Risk of Polymers." *Angew. Chem. Int. Ed.* 2018, 57, 13873.
7. Zhang, P.; Jain, P.; **Tsao, C.**; Yuan, Z.; Li, W.; Li, B.; Wu, K.; Hung, H.-C.; Lin, X.; Jiang, S. "Polypeptides with High Zwitterion Density for Safe and Effective Therapeutics." *Angew. Chem. Int. Ed.* 2018, 57, 7743.
8. Li, B.; Yuan, Z.; Zhang, P.; Sinclair, A.; Jain, P.; Wu, K.; **Tsao, C.**; Xie, J.; Hung, H.-C.; Lin, X.; Bai, T.; Jiang, S. "Zwitterionic Nanocages Overcome the Efficacy Loss of Biologic Drugs." *Adv. Mater.* 2018, 30, 1705728.
9. Hung, H.-C.; Jain, P.; Zhang, P.; Sun, F.; Sinclair, A.; Bai, T.; Li, B.; Wu, K.; **Tsao, C.**; Liu, E. J.; Sundaram, H. S.; Lin, X.; Farahani, P.; Fujihara, T.; Jiang, S. "A Coating-Free Nonfouling Polymeric Elastomer" *Adv. Mater.* 2017, 29, 1700617.
10. Zhang, P.; Jain, P.; **Tsao, C.**; Sinclair, A.; Sun, F.; Hung, H.-C.; Bai, T.; Wu, K.; Jiang, S. "Butyrylcholinesterase Nanocapsule as A Long Circulating Bioscavenger with Reduced Immune Response." *J. Control. Release*, 2016, 230, 73-78.
11. Zhang, P.; Sun, F.; **Tsao, C.**; Liu, S.; Jain, P.; Sinclair, A.; Hung, H.-C.; Bai, T.; Wu, K.; Jiang, S. "Zwitterionic Gel Encapsulation Promotes Protein Stability, Enhances Pharmacokinetics, and Reduces Immunogenicity." *P. Natl. Acad. Sci. USA*, 2015, 112, 12046-12051.

CONFERENCE PRESENTATIONS

1. **Tsao, C.**; Zhang, P.; Li, B; Jiang, S. "Zwitterionic-based Platforms for Biotherapeutics." 4th International Conference on Bioinspired and Zwitterionic Materials, June 2019 (Poster). ***Second Place Poster Prize.***
2. **Tsao, C.**; Jiang, S. "Zwitterionic Polymeric Platforms for Biologic Drug Delivery and Tissue Engineering." 2019 AIChE, Nov 2019 (Poster).

PATENTS

1. Jiang, S.; Liu, E.; McMullen, P.; **Tsao, C.**; Luozhong, S.; Corrigan, T. "Fusion products comprising mixed charge peptides." *PCT application,* Oct 2019.
2. Jiang, S.; Liu, E.; Han, Y.; McMullen, P.; **Tsao, C.**; Luozhong, S. "Compositions and methods related to the production of long-circulating and functional fusion biological moieties *in vivo*." *Provisional patent,* Oct 2019.
3. Jiang, S.; Dong, D.; Hung, H.-S.; **Tsao, C.**; Tang, C.; MacArthur, J. "Double-network Zwitterionic and Mixed Charge Hydrogels." *Provisional patent*, March 2019.

HONORS AND AWARDS

2019 Second Place Poster Prize, 4th International Conference on Bioinspired and Zwitterionic Materials

2015 Jane and Joseph McCarthy Award for Excellence in Chemical Engineering Graduate Student Teaching, Department of Chemical Engineering, University of Washington
2015 Graduate Assistance in Areas of National Need Fellow (GAANN), U.S. Department of Education
2014 Runstad Family Endowed Fellowship, University of Washington

EXTRACURRICULAR AND OUTREACH ACTIVITIES

2019	University of Washington, The Center for Teaching and Learning. *International TA Panelist*
2019	University of Washington, Dept. of Chemical Engineering. *Graduate Student Representative* 10th Annual Regional Pacific Northwest Louis Stokes Alliance for Minority Participation (LSAMP)
2017 – 2018	Material Research Society at UW Chapter. *Director of Professional Networking*
2017	University of Washington, Dept. of Chemical Engineering. *Office Manager Interview Committee*
2011 – 2014	National Taiwan University, Badminton Varsity Team. *Director of Teaching and Training*